Development of non-laminated advanced composite straps for civil engineering applications.

Andreas Urs Winistoerfer

Thesis submitted to the University of Warwick

for the degree of Doctor of Philosophy

Department of Engineering

University of Warwick

May 20, 1999

Numerous Originals in Colour

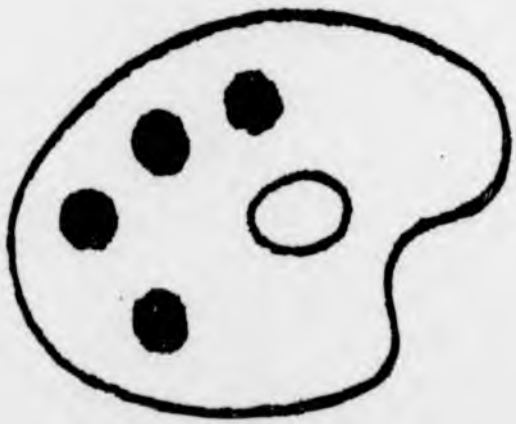

Abstract

The focus of this thesis has been the feasibility of a novel load transfer concept for a carbon fibre reinforced plastic (CFRP) tendon system using non-laminated pin-loaded straps. The principle of these straps is that, as the tensile load increases, the relative slip between the layers produces a more uniform strain distribution in the layers leading to a higher load carrying capacity than when the laminate is fully consolidated (i.e. a laminated strap). This principle has been shown to occur by observing relative displacement between individual layers and strain measurements.

Such components could be used for post strengthening purposes of existing structures. They have the potential to alleviate the current problems associated with the corrosion of externally applied steel reinforcement. Furthermore, the low density of CFRP's in combination with appropriate design procedures can provide a cost competitive solution. This advantage of choosing a non-metallic material is strengthened when whole life cycle costs are considered since composites are expected to outlive the conventional repair materials.

One objective of the project was to develop a tape material with continuous parallel fibres at low cost. At the start of the project no material available was suitable in terms of cost or quality. To drive the cost of the material down, thin lamina tapes with a thermoplastic matrix were considered. The various manufacturing processes for thermoplastic prepreg tape were reviewed and the powder impregnation process was found to meet the project's specifications. This method can produce high quality prepreg at a higher production rate compared to pultrusion with a thermosetting matrix. Sulzer Innotec Ltd. had an existing aqueous powder impregnation facility for research and development purposes. The author collaborated with the company to make specific modifications to the facility with the objective of improving material quality. This was achieved towards the end of the project, and in the thesis this material is referred to as Tape IV.

Preliminary development work was carried out throughout the duration of the project to characterise five thermoplastic materials. Two practical connection methods where developed to anchor the final outer layer in the non-laminated strap option. It was found that the clamping method was superior to the fusion bonding method; both methods will, however, find applications. A new manufacturing process for laminated pin-loaded straps was developed and is reported.

The author used MARC K6.2, a commercial finite element software, to predict the stress concentrations in the region where the strap makes contact with the steel pin. The difficulties associated with the advanced numerical modelling included contact and friction. The required results from MARC K6.2 were highly dependent on a sliding velocity parameter for which no accurate value was known. Because of the lack of rigor in the formulation of the finite element model, the stress concentrations predicted could not be used to optimise strap detailing. For completeness the MARC K6.2 modelling is described and the results reported.

To exploit the technology, research and development work will be needed, and the thesis shows where there are gaps in our knowledge and understanding.

CONTENTS

ACKNOWLEDGEMENT

The work described in this thesis was carried out at EMPA, the Swiss Federal Laboratories for Materials Testing and Research in Duebendorf, Switzerland.

Many people have supported me during my time as an external student at Warwick and I am extremely grateful for their assistance. In particular, I would like to thank my supervisors, Prof. U. Meier and Dr. J. T. Mottram, for their encouragement and invaluable guidance throughout this research project.

I could not have carried out my experimental work without the assistance of Silvano Cristofolini and the technicians in Polymers and Composites, Electronics and Metrology, Mechanical Engineering and Concrete Structures. They have all helped me on numerous occasions and have provided me with invaluable advice regarding the activities in the laboratories.

I would also like to thank Albert Vodermayer and his team at SULZER Innotec Ltd. for their support and the good collaboration during the development of the prepreg tape.

Grateful thanks is extended to Christoph Bär, Janet Lees, Ernst Lutz, Heinz Meier and Giovanni Terrasi for the good time we had in Research Group 101.

I appreciate the encouragement and support from Giovanna and my family.

DECLARATION

The author wishes to declare that, except for commonly understood and accepted ideas, or where specific reference is made to the work of others, the content of the thesis is his own investigation. This thesis has not been submitted previously, in part or in whole, to any university or institution for any degree, diploma or other qualification.

PUBLICATIONS

Winistoerfer, A. and Spescha, G. (1995). Untersuchung des mechanischen Verhaltens eines CFK/Alu-Verbundes bei Verwendung verschiedener Primer, *EMPA Research-Report No. 155'284*, Dübendorf, Switzerland, March 1995.

Meier, U. and Winistoerfer, A. (1995). Retrofitting of structures through external bonding of CFRP sheets. in L. Taerwe (Ed.), *Non-Metallic (FRP) Reinforcement for Concrete Structures*, 2nd International RILEM symposium (FRPRCS-2), Ghent, Belgium, August 23-25 1995, pp. 465 - 472.

Winistoerfer, A., Zumbuehl, R. and Deuring, M. (1995). CFK-Lamellen verstärkte Stahlbetonträger unter Brandbeanspruchung, in *Nachträgliche Verstärkung von Bauwerken mit CFK-Lamellen*, EMPA/SIA-Studientagung, SIA Dokumentation D 0128, Zürich, Switzerland, September 21 1995, pp 85-86.

Winistoerfer, A. (1995). Strangschlaufen zur nachträglichen Schubverstärkung, in *Nachträgliche Verstärkung von Bauwerken mit CFK-Lamellen*, EMPA/SIA-Studientagung, SIA Dokumentation D 0128, Zürich, Switzerland, September 21 1995, pp. 101.

Winistoerfer, A. (1996). Belastungsversuche an CFK-verstärkten Holztreppen-Elementen. *EMPA Research-Report No. 161'782*, Dübendorf, Switzerland, February 1996.

Winistoerfer, A. (1996). The optimisation of the load transfer area of pin loaded straps, in *Student Seminar, Success of Materials by Combination*, 17th international SAMPE Europe Conference, Basel, Switzerland, May 28-30 1996.

Meier, U. and Winistoerfer, A. (1998). Multilayer Traction Element in the Form of a Loop, *European Patent 0 815 329*, January 7 1998.

Winistoerfer, A. (1998). Anchorage Systems, in J. T. Mottram and G. J. Turvey (Eds.), *State-of-the-art review on design, testing, analysis and applications of polymeric composite connections*, COST C1 EUR 18172 EN, pp. 50-55.

Winistoerfer, A., Meier, U. and Mottram, J. T. (1998). The Behaviour of Non-laminated Advanced Composite Straps, in *Control of the Semi-Rigid Behaviour of Civil Engineering Structural Connections*, COST C1 International Conference, Liège, Belgium, September 17-19 1998.

Lees, J. M., Winistoerfer, A. and Meier, U. (1999). Non-laminated Pin-Loaded CFRP Straps for the Shear Enhancement of Concrete, in *Fourth International Symposium on FRP for Reinforced Concrete Structures (FRPRCS-4)*, Baltimore, USA, October 31-November 5 1999.

LIST OF FIGURES

LIST OF TABLES

NOTATION

c_m	water absorption of matrix
c_{opt}	ideal particle concentration
d_f	filament diameter
k	stress concentration factor
n_{Load}	number of load carrying members
p_i	internal pressure
r_i	inside radius
r_o	outside radius
r_p	particle radius
s	standard deviation
t	tape thickness
t_{gauge}	distance between tape surface and strain gauge
w	tape width

A	constant
B	constant
C	relative sliding velocity
$C.O.V.$	coefficient of variation
D	constant
E_1	longitudinal modulus of elasticity of composite
E_2	transverse modulus of elasticity of composite
E_3	through-thickness modulus of elasticity of composite
E_f	longitudinal modulus of fibre
E_m	modulus of elasticity of matrix
F	applied load
F_A	tensile force in one leg of strap
F_h	horizontal force
$F_{measure}$	measured load carrying capacity
F_n	normal force
$F_{predict}$	predicted load carrying capacity
F_t	tangential force
F_U	load carrying capacity
F_{U1}	lower bound load carrying capacity
F_{U2}	upper bound load carrying capacity
G_{12}	shear modulus of elasticity of composite
G_{13}	shear modulus of elasticity of composite
G_f	shear modulus of elasticity of fibre
G_m	shear modulus of elasticity of matrix
L_O	pin separation
L_p	particle spacing
N	number of specimens
N_L	number of layers
S	shear strength of composite
S_{ij}	compliance
T	twisting moment
T_f	yield of fibre

T_g	glass transition temperature
T_m	melting temperature of polymer
V_E	free volume
V_f	fibre volume fraction
X_1	strength of composite in longitudinal direction
X_2	strength of composite in transverse direction
X_3	strength of composite in through-thickness direction
X_f	longitudinal tensile strength of fibre
X_m	tensile strength of matrix

α	stiffness ratio
$\Delta_{L,creep}$	change in length due to creep
ε_1	longitudinal strain
ε_2	transverse strain
ε_3	through-thickness strain
ε_{fU}	tensile failure strain of fibre
ε_{mU}	tensile failure strain of matrix
ε_t	creep strain
ε_U	tensile failure strain of composite
γ_{12}	shear strain
γ_{13}	shear strain
γ_{23}	shear strain
φ	angle
μ	friction coefficient
v	tangential velocity
ν_{12}	Poisson's ratio
ν_{13}	Poisson's ratio
ν_{21}	Poisson's ratio
ν_{23}	Poisson's ratio
ν_{31}	Poisson's ratio
ν_m	Poisson's ratio of matrix
ρ_f	density of fibre
ρ_m	density of matrix
σ_1	longitudinal stress
σ_1^*	longitudinal stress with friction present
σ_2	transverse stress
σ_3	through-thickness stress
σ_3^*	through-thickness stress with friction present
σ_n	normal stress
σ_{Ustrap}	failure stress in strap
τ_{12}	shear stress
τ_{13}	shear stress
τ_{13}^*	shear stress with friction present
τ_{23}	shear stress
ω	radius ratio

1 INTRODUCTION

1.1 Overview

Throughout the world there is a large number of existing structures, which need to be replaced or retrofitted. This may be due to a change of social needs, upgrading of design standards, increased safety requirements or deterioration (Dunker et al. 1993 and Hamilton et al. 1995). Even for newer structures, which are not part of the architectural heritage, rehabilitation is, in many cases, the only viable option as it is often a superior use of resources, when compared to the replacement of the structure. The problems are particularly severe in the case of reinforced concrete bridges where chloride induced deterioration is responsible for the need of rehabilitation methods (Clarke 1993). Strengthening requirements for existing structures may demand either, or both, an increase in flexural or shear resistance.

An overview of the current technology and future applications of advanced strengthening methods is given by Meier and Betti (1997). The application of externally bonded steel plates for flexural strengthening purposes as described by Bresson (1971) has been used for more than 25 years in Western Europe. Ruhnau and Kupfer (1985) summarise a number of applications where external post-tensioned steel stirrups have been used for shear strengthening purposes. The major drawback of both strengthening methods is the lack of stress corrosion resistance of the externally applied material being exposed to the environment (Herbsleb and Theiler 1989). Carbon Fibre

Reinforced Plastic, (CFRP) would be an ideal replacement for externally applied steel reinforcement. The use of CFRP's would offer the essential environmental resistance in combination with high specific strength, high stiffness and superior fatigue properties (Hull 1981).

CFRP for externally bonded flexural strengthening purposes, as described by Meier (1987), has been used successfully in recent years. The strengthening method is experiencing an economical breakthrough in Switzerland with about 12 tons of CFRP used for retrofitting purposes in 1996. Meier (1997) is predicting a world-wide usage of 850 tons per annum for such applications in about twenty years.

Similar systems based on externally bonded fabrics or sheets for post shear strengthening purposes have been developed in the US by Chajes et al. (1995) and in Canada by Hutchinson et al. (1997), Drimoussis and Cheng (1994).

A different and more effective approach is the use of an active strengthening method. By post tensioning a structure, the occurrence of cracks can be delayed and the width of existing cracks can be reduced, which results in a superior performance. This has been shown by Deuring (1993) for the flexural strengthening method using pretensioned externally bonded CFRP sheets.

The above mentioned infrastructural applications of polymeric composite materials are exclusively based on thermosetting matrix systems. A thermoplastic matrix would be most desirable for future applications for a number of reasons, such as environmental issues and the potential of cost reduction (Vodermayer 1992).

The aim of this research project is the development of a CFRP tendon with an efficient load transfer and a high flexibility in terms of length for active shear-strengthening purposes of existing reinforced concrete structures. The challenge is the development of an appropriate end anchorage to account for the orthotropic mechanical properties of the CFRP. An overview of different types of anchorage systems used for CFRP tendons is given by Winistoerfer (1998). An additional requirement is the use of a thermoplastic matrix material.

1.2 Post shear strengthening

The behaviour of steel reinforced concrete beams under shear loading does not seem to be well understood. Collins et al. (1996) state that the shear design provisions of the current American Concrete Institute design code consist of about 43 empirical equations for different types of members and loading situations. The shear resistance of a reinforced concrete beam is thought to be comprised of a combination of aggregate interlock, dowel action of the flexural reinforcement, the concrete compressive zone and the shear reinforcement. However, it is unclear which of these contributions is the most important in determining the ultimate shear capacity of a reinforced concrete beam.

This lack of understanding is one reason why practising engineers prefer the use of active shear strengthening methods (Guckenberger et al. 1985). These active methods are based on post tensioning the structure in through-thickness direction using an external stirrup. The post tensioning enhances all the possible effects which contribute to the shear capacity of a reinforced concrete beam by providing confinement and reducing crack widths.

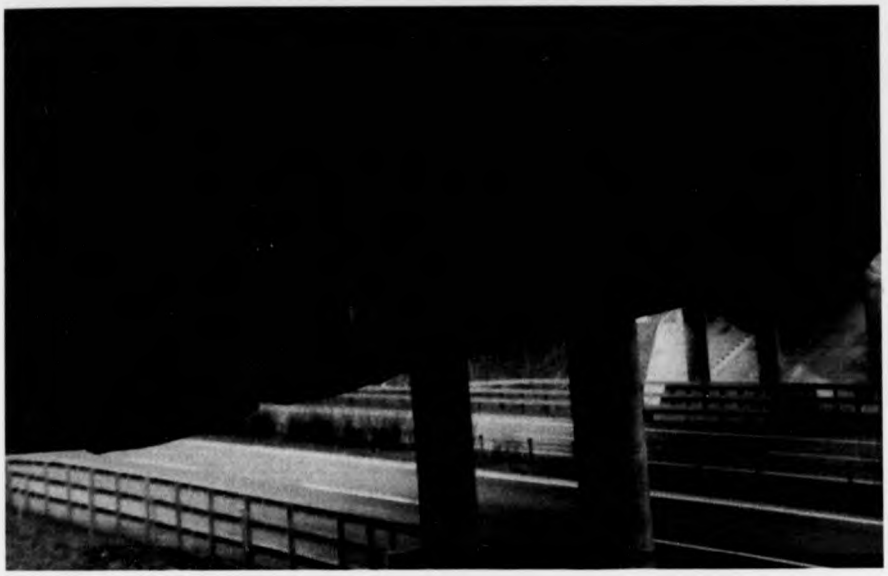

Figure 1.1: Reinforced concrete bridge which has been shear strengthened in 1997.

The Derendingen-Deitingen bridge in Switzerland shown in Figure 1.1 is an example which has been shear strengthened using external steel tendons which were post tensioned. This method is very expensive because of the necessity of custom-made fittings and excessive corrosion protection means. The long-term performance is questionable since stress corrosion may take place if the corrosion protection fails. It is for these reasons that a corrosion resistant alternative tendon is sought.

1.3 Pin-loaded strap elements

1.3.1 Laminated pin-loaded strap elements

A non-metallic pin-loaded strap element, as shown in Figure 1.2, may provide a practical means of joining different parts. These elements consist of a unidirectional fibre reinforced plastic wound around two circular steel pins in a racetrack like manner. No machining of holes is required. The pins transfer the load into the laminated and fully consolidated strap.

These straps have many desirable characteristics, including; high tensile strength, low weight, low thermal conductivity and low thermal expansion. As a result, laminated pin-loaded straps have been used in many different structural applications. The US-Army has investigated such components for temporary bridges (see Bauersfeld 1984), due to the structural efficiency and ease of application. Rotor-blades for wind turbines and helicopters are connected to the rotating shafts in a pin-loaded strap configuration as described by Knaust (1988). Pin-loaded straps made from glass fibres reinforced plastics are used as support structures for cryogenic applications (see Niemann et al. 1978 and Weintz et al. 1994). The reason for this particular design solution is the combination of structural efficiency and low thermal and electric conductivity.

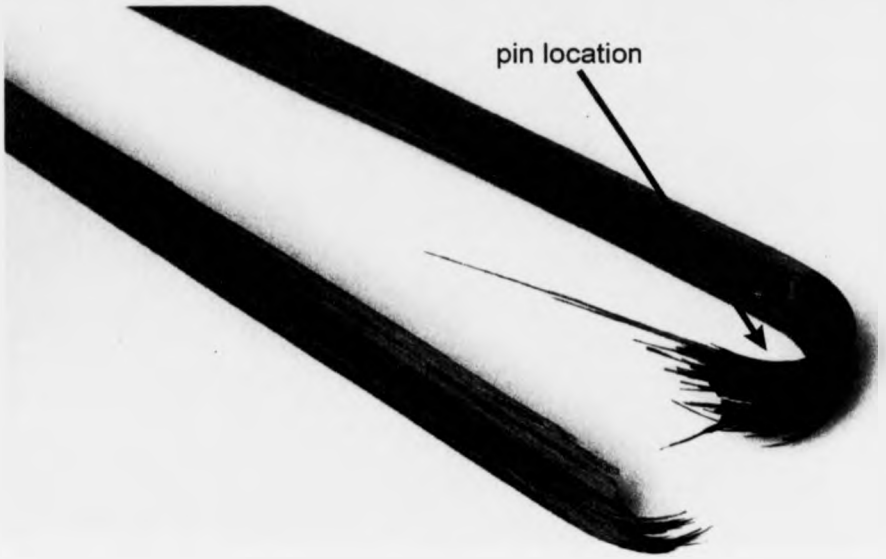

Figure 1.2: Premature failure due to stress concentrations in the load transfer zone of laminated pin-loaded straps made out of CFRP

A laminated, pin-loaded strap could be used as an external stirrup for the shear strengthening of existing bridges. Both experimental and numerical investigations (see Section 4.4.1 and 5.5, respectively) have revealed that adjacent to where the strap leaves the pin, there are 'high' stress concentrations resulting in premature failure as indicated in Figure 1.2. The effect of these concentrations is to reduce the failure load to about 60% of that of the same laminate, as determined by a standard coupon test.

In addition, the production process described in Section 3.4.1, for such a component is not trivial despite the simplicity of the shape. The manufacturing process may result in local misalignment of the fibres in the same location as the above mentioned stress concentrations occur.

Cost of the material is crucial when deciding whether or not to apply a system and so it is necessary to use the material to its full potential. Furthermore, the manufacturing process has to be optimised to reduce the cost of the tendon.

1.3.2 Conceptual design of non-laminated pin-loaded strap elements

One means of reducing the undesirable stress concentrations and to overcome the manufacturing difficulties is outlined by Meier and Winistoerfer (1998). The consolidated laminate shown in Figure 1.3(a) is replaced by an equivalent non-laminated system shown in Figure 1.3(b), where the strap is comprised of a number of non-laminated layers formed from a single, continuous, thin, thermoplastic matrix tape.

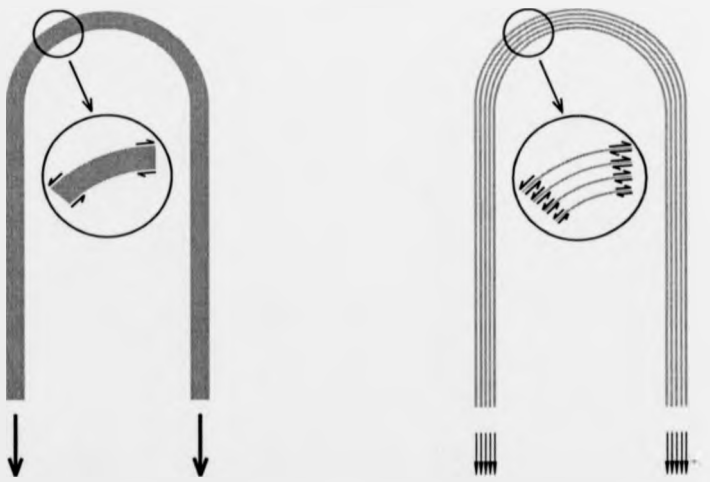

(a) (b)

Figure 1.3: Load transfer area of a laminated (a) versus a non-laminated (b) pin-loaded strap

In the non-laminated system the tape is wound around the pins and only the end of the outside, final layer is anchored. It can either be anchored to the previous layer or to the surrounding concrete using an end fixture. However, the reliability of the anchorage of the final layer is crucial for a successful strap concept.

Such a strap system enables the individual layers to move relative to each other. The undesirable stress concentrations are reduced since this structural form is more compliant. Careful control of the initial tensioning process allows interlaminar shear stress concentrations to be reduced such that a more uniform strain distribution in all layers is achieved. In addition, the system allows for a great flexibility in terms of the length of the tendon since the winding can be performed on site, for example to account for dimensional tolerances of the structure to be strengthened. Moreover the cost effectiveness compared to a laminated pin-loaded strap is superior due to the absence of a consolidation process which is required in the production of a laminated pin-loaded strap.

1.4 Objectives of Research

The primary objective of this research is to investigate the feasibility of the concept of non-laminated pin loaded strap elements as the basis for the development of a CFRP strap for post shear strengthening purposes. This proposed application imposes certain constraints on the system such as temperature range, environmental conditions and methods of application. With these constraints specific objectives are outlined as follows:

- A thermoplastic matrix material should be employed to explore possible cost reductions.
- A suitable joining method has to be developed to facilitate the anchorage of the final layer.
- To provide fundamental information as a basis to establish the technique of non-laminated pin-loaded straps of CFRP.

1.5 Outline of Thesis

The thesis is organised into seven chapters. Some of the work outlined is not as rigorous as one could expect since the experiments were fact finding to prove the concept and to provide appropriate testing procedures. The methods presented will enable a more rigorous investigation when the concept will be commercialised.

Chapter 2 is devoted to the materials used and in particular to the manufacturing process of the thermoplastic prepreg tape. The quality of the thermoplastic prepreg tape used is crucial to the success of the novel concept. A number of different commercial products were evaluated, and the performance of these products was found to be unsatisfactory. Favourable results were eventually achieved as a result of certain modifications made by the author to a new manufacturing process for thermoplastic prepreg tape at Sulzer Innotec Ltd, in Winterthur, Switzerland.

The initial development work which was necessary to demonstrate the feasibility of the concept is outlined in Chapter 3. The methods of manufacturing laminated pin-loaded straps which were used for reference purposes are described in detail. The process used

for the manufacturing of the characterisation specimens is also presented. Particular attention is given to the joining method employed to anchor the last layer of a non-laminated pin-loaded strap. The methods for static and long term creep tests on various strap elements are also given.

The performance of non-laminated pin-loaded straps, made from different commercially available materials, is presented in Chapter 4. The measured characteristics of the modified material supplied by Sulzer Innotec Ltd. are described. Furthermore, a comparison of laminated- and non-laminated pin-loaded strap elements is made.

Chapter 5 is concerned about the stress analysis on pin-loaded strap elements. Particular attention is given to the difficulties associated with the modelling of contact and friction problems using MARC K6.2, a commercial finite element software package. In addition, simple analytical models describing the stress distributions in strap elements are presented.

The main findings of the research into the feasibility of non-laminated pin-loaded straps is summarised in Chapter 6. Suggestions for further investigations needed to commercialise the concept, and future applications are presented.

Conclusions regarding the feasibility of pin loaded straps and recommendations for further investigations needed to make the concept exploitable are given in Chapter 7.

2 THERMOPLASTIC PREPREG

2.1 Introduction

In this chapter, the constituent properties of the different thermoplastic prepregs used within this research are considered. Furthermore, a list of important requirements for prepreg tape for non-laminated pin-loaded straps is presented. In addition, a brief outline of the problems associated with different production processes of unidirectional thermoplastic prepreg is given. The aqueous powder impregnation technique described by Taylor (1981) and O'Connor et al. (1988) is reviewed and certain specific modifications to this process are introduced to improve quality of the material.

2.2 Polymeric composites

The major problem in the application of polymers in engineering is their poor mechanical properties compared to structural materials such as metals. One method to offset this deficiency is the addition of reinforcing fibres to the polymer to form a composite material. The characteristic of such a composite reflects the properties of its constituents.

Common types of reinforcing fibres are glass, aramid, carbon, boron and high strength polyethylene. The ideal selection of the fibre type ought to be based on technical as well

as economical decisions, depending on the application. Carbon fibres were found by Meier and Winistoerfer (1991) to be the most appropriate for infrastructural applications due to their excellent mechanical properties in combination with the corrosion resistance.

CFRP's based on thermosetting matrix materials and continuous fibres are well established in a large number of industrial applications. However, this is not yet the case for CFRP with a thermoplastic matrix material. According to Anon. (1998a), the turnover of carbon fibre prepreg with thermosetting matrix in the US and Europe is about US$ 700 million per annum, compared to US$ 30 million for thermoplastic prepreg. Despite the superior properties of thermoplastics such as, a higher fracture toughness, a higher strain to failure, an excellent environmental resistance and no requirements for special storage conditions, applications have been limited to selected components in the aerospace-, automotive- and the sport industry (Anon. 1998b). One reason for the reduced number of applications is the difference in the order of magnitude of the melt viscosity of thermoplastic polymers compared to the generally low viscosity thermosets prior to the cross-linking process. A thorough impregnation of the fibres is crucial for the usage of CFRP's for load bearing structures, and this is difficult to achieve with thermoplastic melts because of their relatively high viscosity.

The thermoplastic matrix systems available can be divided into two main groups. The first group represents the high performance plastics such as PEEK (polyetheretherketone), PAI (polyamideimide), PEI (polyetherimide), PES (polyethersulphone) and PPS (polyphenylenesulphide). The second group contains the so-called engineering- and commodity plastics such as PET (polyethyleneterephthalate),

PMMA (polymethylmethacrylate), PC (polycarbonate), PA (polyamide), PS (polystyrene), PE (polyethylene) and PP (polypropylene). The high performance thermoplastics function well in high temperature (> 100° C) and chemically hazardous environments. Whereas the engineering and commodity thermoplastics are less expensive and offer lower processing temperatures (< 300° C).

The choice of the different matrix systems used in this research is purely based upon availability of prepreg tape. An ideal matrix for a shear strengthening application would be PP or PA 12. Both polymers fulfil the requirements imposed by the working environment at the lowest cost.

2.2.1 Carbon fibre

Carbon fibres are produced from PAN (polyacrylonitrile) fibres, rayon (cellulose based fibre), or fibres gained from a melt spinning process of pitch. These precursors are converted into graphite through a sequence of heat treatment operations under tension. The aim of this process is to preserve the high degree of orientation of the initial precursor, ensuring that the final graphite structure has a similar high degree of crystal orientation (McCrum et al. 1988).

A schematic representation of the sheet like structure of a carbon fibre is shown in Figure 2.1 (from Hull 1981). Carbon atoms with strong covalent bonding are hexagonally arranged within the sheets or layer planes. However, the layers are held together by weak Van der Waals forces. The result is a highly anisotropic fibre with a theoretical longitudinal modulus of 910 GPa compared to 30 GPa in transverse

direction. These moduli assume a perfect, flawless, crystalline structure (Hull 1981). In reality, the structure of a commercial carbon fibre is always somewhat disordered and micro-voided as shown in Figure 2.1. This is reflected in a large number of commercially available fibres with a longitudinal modulus ranging from 230 to 650 GPa (Toray 1997). In addition, the density of a single crystal of graphite is, according to McCrum (1988), about 2200 kg/m^3, whereas the lower value quoted in Table 2.1 for commercial products indicate an imperfect crystalline structure with many voids.

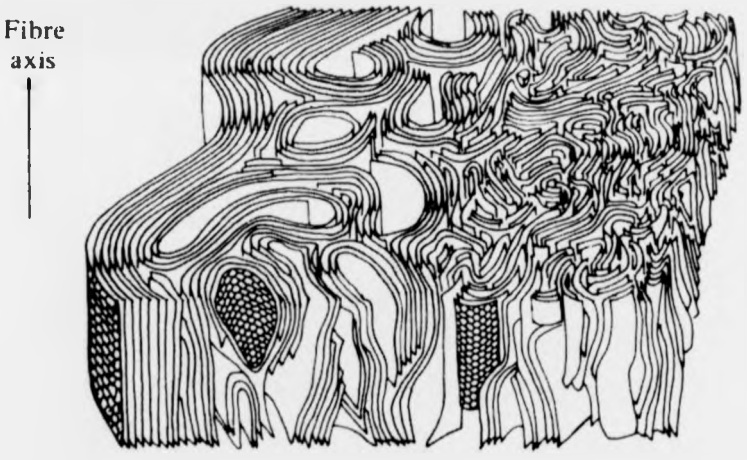

Figure 2.1: Schematic representation of the graphitic structure of a carbon fibre filament (From Hull 1981).

The degree of perfection of the alignment of the crystalline structure influences the mechanical properties of the fibre. It can be influenced by optimising the heat treatment parameters. The result of different parameters is a diverse range of commercially available fibres with different mechanical properties. In Appendix A, the fibre products of a single supplier are compared with the fibres used in this research project.

The different carbon fibres used in this investigation are AS4, by Hercules Inc., 34-700 by Grafil Inc., and T700S made by Toray Inc. The mechanical properties stated in Hercules (1989), Grafil (1996) and Toray (1997) are given in Table 2.1.

Table 2.1: Properties of the carbon fibres used in this research.

Fibre	Tensile strength X_f [MPa]	Tensile strain ε_{fU} [%]	Modulus E_f [GPa]	Filament diameter d_f [µm]	Density ρ_f [kg/m^3]
Hercules AS4	4100	1.65	248	7	1800
Grafil 34-700	4500	1.9	234	6.9	1800
Toray T700S	4900	2.1	230	7	1800

2.2.2 Matrix

The objectives of the matrix in fibre reinforced plastics is described by Michaeli and Wegener (1989) as follows:

- To maintain the chosen orientation of the fibres according to the design.
- To transfer the load into the fibres.
- To provide lateral support to prevent buckling under compressive loading.
- To protect the fibres from the chemicals in the environment.

Thermosets, the more frequently used matrix materials are characterised by a highly cross-linked structure restricting chain motion (Young and Lovell 1991). After the forming and curing, or cross-linking, the macromolecular chains are intractable and degrade rather than melt upon the application of heat.

However, thermoplastics can be moulded and remoulded into virtually any shape upon the application of heat and pressure. They consist of large macromolecules which are highly coiled and entangled. Thermoplastics are separated into crystalline or amorphous types, based on their molecular structure (Frank and Biederbick 1984). In most cases the crystalline types are semi-crystalline with both crystalline and amorphous regions. The crystalline phases of a thermoplastic material can be characterised by T_m, their melting temperature. The amorphous phases are characterised by T_g, their glass transition temperature. At T_g, the amorphous regions transform from a glassy to a rubbery solid due to increased motion of the macromolecular chains.

The crystalline structure, the size and number of the spherulites and the degree of crystallinity of a thermoplastic matrix is influenced by processing conditions such as cooling-rate, mass and geometry. The strength and stiffness of a thermoplastic material increase with increasing crystallinity, whereas the fracture toughness decreases (Young and Lovell 1991).

The molecular structures of the three different matrix materials used in this investigation are shown in Figure 2.2. They are like many other high-performance polymers prepared by polycondensation. The benzene ring, shown in Figure 2.2 as a common feature of PEEK and PPS, is a typical constituent of many thermoplastics with high softening temperature (> 150° C).

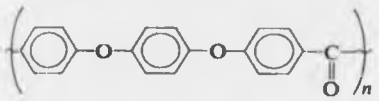

Polyetheretherketone PEEK

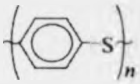

Polyphenylenesulphide PPS

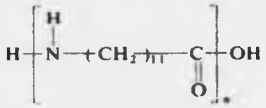

Polyamide PA12

Figure 2.2: Molecular structure of the different matrix materials used.

The mechanical properties and suppliers of the matrix materials are given in Table 2.2. The data are taken from Victrex (1998), Kohan (1995), Hoechst (1996) and Hüls (1996) for Matrix 1, 2, 3 and 4, respectively.

Table 2.2: Properties of the different matrix materials used.

	Matrix 1	Matrix 2	Matrix 3	Matrix 4
Material	PEEK	PA 12	PPS	PA 12
Glass trans. temp. T_g [°C]	143	50	85-100	48
Melting temp T_m [°C]	334	172-178	280-285	178
Modulus E_m [MPa]	3650	1450	3700	1400
Tensile strain ε_{mU} [%]	50	250-300	4	300
Tensile strength X_m [MPa]	92	65	75	40
Water absorption c_m [%]		1.6	0.01	1.5
Density ρ_m [kg / m^3]	1320	1010	1350	1020
Brand-name	APC-2	unknown	Fortron 0205 B4	Vestosint 2159
Supplier	ICI	unknown	Hoechst AG Frankfurt Germany	Hüls AG Marl Germany

2.3 Prepreg tape

The fibre and matrix materials outlined above resulted in four different prepreg tapes which have been investigated in this research project to show the feasibility of the concept of non-laminated pin-loaded straps. The prepreg properties supplied by the manufacturer are given in Table 2.3. The manufacturing characteristic 'slit-tape' refers to prepreg tape which is produced at a standard width, typically 305 mm, and then cut longitudinally to the required width according to the customer requirement. A 'tow' is produced from a single roving, without any longitudinal cutting at the free edges, ensuring a minimum of damaged filaments.

The Tape IV prepreg is a combined development of Sulzer Innotec Ltd and the author. Details of this development are outlined in Section 2.6. Continuous improvement of the new processing at the Sulzer plant resulted in three different qualities of the Tape IV prepreg supplied. The different qualities are characterised by different fibre volume fraction as indicated in Table 2.3. To account for the different qualities, the materials will be referred to as Tape IV-1 (V_f = 41 %), IV-2 (V_f = 49 %) and IV-3 (V_f = 56 %), respectively.

The longitudinal stiffness, E_1, and the longitudinal tensile strength, X_1, were not specified for the products supplied by the University of Berlin and Sulzer Innotec Ltd. Therefore, these values are not given in Table 2.3.

Table 2.3: Overview of the prepreg tape used.

(Information is based on written quotes from the supplier).

	Tape I	Tape II	Tape III	Tape IV
Fibre	AS 4	34-700	T700S	T700S
Yield T_f [g/1000m]	---	804	800	800
Matrix material	PEEK	PA 12	PPS	PA 12
Matrix type	1	2	3	4
Manufacturing	slit tape	tow	tow	tow
Dimensions w x t [mm]	6.1-1520 x 0.125	6.35 x 0.178	---	6 x 0.19, 0.16, 0.14
Fibre content V_f [%]	60	38	61	41, 49, 56
Modulus E_l [GPa]	138	83	---	---
Tensile strength X_l [MPa]	2068	1246	---	---
Product name	APC-2 AS 4	C / PA 12	C / PPS	CF / PA 12
Supplier	ICI Fiberite Europe Germany	Baycomp Burlington Canada	TU Berlin Germany	Sulzer Innotec Winterthur Switzerland

2.4 Product requirements

The prepreg tape used for non-laminated pin-loaded straps has to fulfil the following requirements:

- A high strength which can only be achieved if the continuous fibres are thoroughly impregnated and minimal fibre damage occurs during the processing.
- A low flexural stiffness of the lamina is necessary in order to reduce the bending stresses. Therefore, a minimal tape thickness is desirable which implies a high fibre volume fraction. Furthermore, the combination of high fibre content and low thickness provides superior creep properties in the through-thickness direction, which is important in the load transfer region of pin loaded straps.

- Accurate edge contours and small width tolerances are necessary to ensure an even support to all the layers.
- Depending on the application, a suitable matrix material has to be selected to withstand the environmental conditions.
- Sufficient matrix material has to be present to ensure an even surface texture for a constant coefficient of friction. In addition, the matrix rich surface will facilitate the end anchorage of a single layer. This is particularly useful when two layers of tape have to be joined in a welding process.
- A high processing speed during impregnation is required to reduce cost and, therefore, to make the material more attractive to applications in the construction industry.

The properties of the prepreg will, to a certain extent, be a result of the chosen manufacturing process, some of which are introduced next.

2.5 Melt impregnation

The impregnation of unidirectional fibres with a thermoplastic matrix is principally carried out using a melt impregnation process. Rovings are pulled through an impregnation tool which is filled with polymer melt. The tool contains features such as a number of steel pins which change the direction of the fibres and thereby force the matrix into the roving. This process is very similar to the pultrusion process applied with thermosetting matrix materials where a production speed of 0.1 – 3 m/min can be reached according to Kempe (1997).

Augustin (1989) developed an impregnation tool which was capable of impregnating unidirectional glass fibres at a maximum line speed of 5 m/min, having a fibre volume content of 60 %. However, glass fibres typically have a diameter of 17 µm, whereas carbon fibres have a typical diameter of 7 µm. The smaller carbon fibres cause a higher flow resistance to the molten polymer and are therefore more difficult to impregnate. In addition, the orthotropic carbon fibres have poor transverse strength properties and are susceptible to damage during processing. As a result, line speeds of only one fifth (see Vodermayer, Kaerger and Hinrichsen 1993) of the maximum obtained in the melt impregnation of glass fibre rovings were found with carbon fibres.

An overview of alternatives to melt impregnation is given by Neitzel and Breuer (1997). Those include solvent impregnation for amorphous thermoplastics (Zepf 1997), the use of commingled materials (Singkofer and Mehn 1996) and a number of powder based processes. One established method described by Werner (1997) is to use an electrostatic fluidised bed to deposit powder particles on the fibres. Powder based processes, in particular the aqueous powder impregnation technique, reduce fibre damage and facilitate the fast impregnation of carbon fibre rovings (see Hartness 1988).

2.6 Aqueous powder impregnation

The aqueous powder impregnation of rovings has been used for several years. The most cited literature is the US patents by Chabrier et al. (1986) and O'Connor (1987). The process is characterised by the following advantageous features:

- A short flow length can be achieved due to the small powder particles used (see Section 2.6.4). This offers the possibility of high production velocities.

- A large number of different types of polymers (i. e. different viscosity) can be used.
- Minimal fibre damage occurs since very simple guiding mechanisms are used in the impregnation bath.
- There is little thermal degradation of the polymer due to the short time in the molten stage.
- A controlled fibre volume content in the range of 30-70% can be achieved.
- Operators are not exposed to health hazards.

The major drawback of the technique is that the cost of the polymer in powder form is higher compared to that of granular form. In addition, availability of appropriate particle sizes is often a problem (see Section 2.6.4).

2.6.1 Set-up and principle of the process

The prepreg manufacturing process employed by Sulzer Innotec Ltd. is based on aqueous powder impregnation. Many of the parameters in the process cannot be quantified due to commercial reasons. The impregnation facility is shown schematically in Figure 2.3. A roving is pulled off the spool with a constant force, which is controlled by the belt drive at the end of the line. The tension in the roving is measured just before it enters the impregnation bath. The actual impregnation takes place in the bath where the roving is pulled through an aqueous polymer powder dispersion. Details of the impregnation mechanisms involved are given in Section 2.6.2. As the wet roving leaves the bath, it contains evenly distributed powder particles. In the next stage, the water on the surface of the filaments is evaporated in the drying chamber. Industrial air guns are installed in the chamber to increase the airflow within the chamber. The drying process

is very important and determines the production rate of unidirectional fibre reinforced tapes. All the water has to be removed prior to the melting stage to ensure a low porosity in the final composite. A damping unit (as described in Section 2.6.6) is situated at the exit of the drying chamber to prevent extensive vibration of the roving.

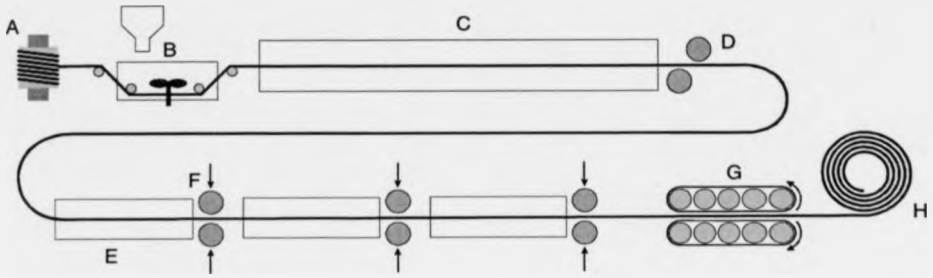

A	roving spool	E	heating oven
B	impregnation bath	F	profile rollers
C	drying chamber	G	belt drive
D	damping unit	H	prepreg tape

Figure 2.3: Powder impregnation process (Sulzer Innotec Ltd.)

The evenly distributed polymer particles are subsequently melted in three consecutive heating ovens. Profile rollers (as described in Section 2.6.6) are located at the exit of each oven. These rollers are free to roll but provide consolidation pressure responsible for the final impregnation and for controlling the geometrical properties of the tape. The consolidation pressure between the profile rollers can be varied by putting weights on the top roller fixture. To produce high quality tape, the option of a single oven-roller combination was found to be unsatisfactory.

The process described above enables fast production at a rate of up to 60 m/min of unidirectional carbon fibre reinforced thermoplastic prepreg, fulfilling all the requirements listed in Section 2.4.

2.6.2 Summary of important parameters

A number of critical parameters are mentioned, but their influence on the properties of the prepreg is very complex since many of these parameters are interrelated. The parameters influencing the quality of the impregnation can be divided in three different groups:

1. Bath parameters (see Section 2.6.3 and Figure 2.4):

- The total contact angle between the impregnation pins and the roving in the bath.
- The number and the diameter of impregnation pins.
- The distance between the impregnation pins.

2. Processing parameters:

- The roving velocity.
- The tension in the roving.
- Temperatures in the drying chamber and the heating ovens.

3. Material parameters:

- The particle size (see Section 2.6.4).
- The concentration of powder in the dispersion (see Section 2.6.4).
- The filament diameter of the fibres.
- The viscosity of the dispersion.

2.6.3 Impregnation bath

The aqueous dispersion is agitated in the impregnation bath using five magnetic stirrers to prevent the segregation of the particles in the dispersion. As shown in Figure 2.4, the roving is guided through the bath by five fixed steel impregnation pins of 10 mm diameter, which are submerged in the dispersion.

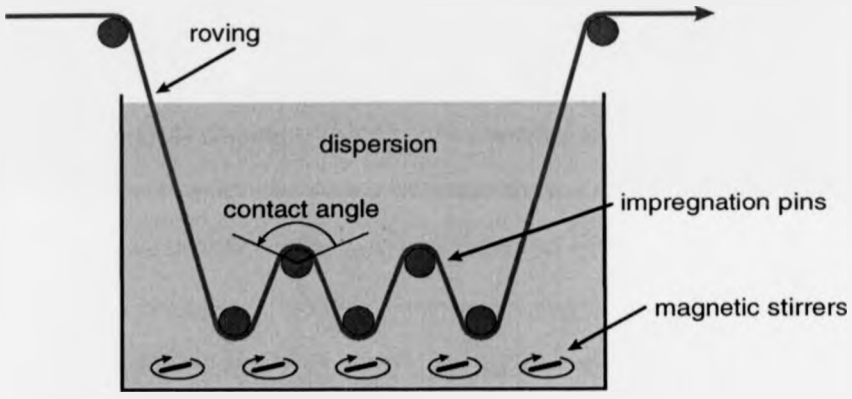

Figure 2.4: Impregnation bath.

Four different mechanisms are involved in the impregnation process. However, the pressure impregnation mechanism is considered to be the most important. The four mechanisms are:

- **Pressure impregnation:** The contact forces between the pins and the roving force the powder particles into the fibre bundle. Ideally, the overall contact angle between pin and roving should therefore be the same on the top and the bottom of the roving. This is not the case in practice. In addition, the particles act as spacers and cause the roving to spread to about twice its original width. The water acts as a lubricant and very little fibre damage is introduced.

- **Diffusion:** Only a minimal number of particles are acquired by the roving as a result of diffusion. The increased surface area due to the pins will increase the amount of diffusion that occurs.
- **Capillary impregnation:** The capillary effect at the entrance and exit of the bath is negligible since it mainly results in the movement of the water and not the polymer particles.
- **Surface tension:** The roving collects a small number of particles on the surface due to the surface tension of the water. The surfactant present in the dispersion to improve the wetting behaviour will enhance this effect.

2.6.4 Particle size

The ideal particle size is found by minimising the distance between two adjacent particles (in the fibre direction) with a given fibre diameter and fibre volume fraction. The aim is to reduce flow length of the polymer melt. It can be determined using the geometrical model by Vodermayer (1992). The model is based on the following simplifying assumptions:

- Idealised shapes for the constituents are utilised. Spherical particles with identical diameters and cylindrical fibres with a diameter of 7 µm, which is a typical value for carbon fibre filaments.
- The particles and the fibres are arranged in a hexagonal array as shown schematically in Figure 2.5.
- Closest packing conditions are assumed with a certain fibre spacing corresponding to the particle diameter.

- Rheological influences such as viscosity and wetting behaviour in the melting and consolidation processes are neglected.

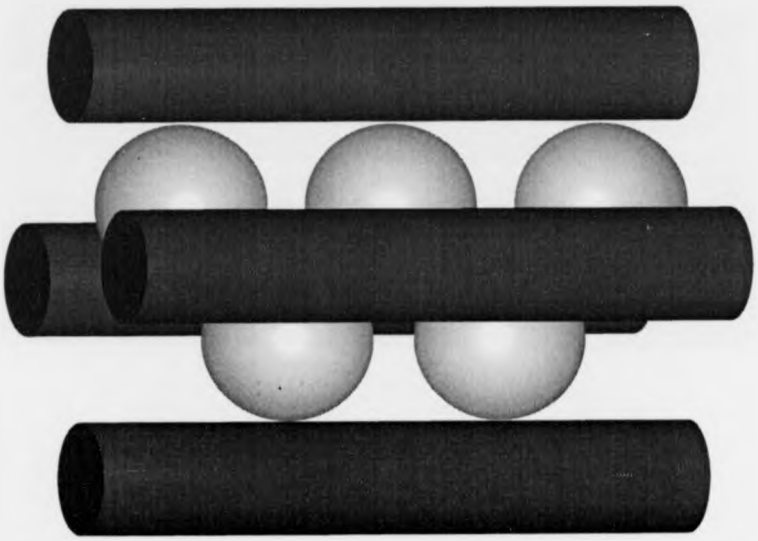

Figure 2.5: Hexagonal array of fibres and polymer particles.

The resulting fibre volume content, V_f, as a function of the particle radius, r_p, assuming perfect consolidation and no porosity, is shown in Figure 2.6. In practice, the matrix flows not only in the longitudinal direction but also in the perpendicular direction. Since this model neglects the flow in the perpendicular direction, it will tend to underestimate the ideal particle size.

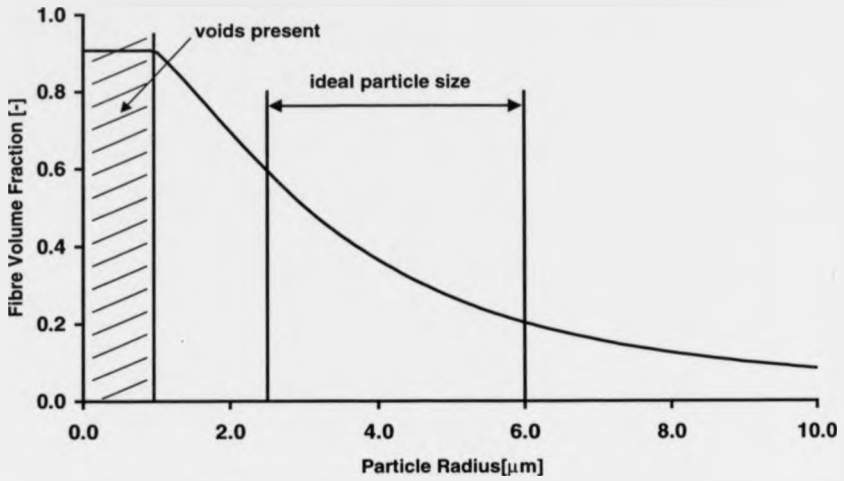

Figure 2.6: Fibre volume fraction, V_f, vs. particle radius, r_p, after consolidation of the impregnated fibres.

The longitudinal spacing, L_p, of the particles is the minimum distance the polymer melt has to flow (see Figure 2.7) for a complete impregnation in the molten stage of the polymer matrix. The free volume in the elementary cell, V_E, (which has to be filled with matrix material during the melting and consolidation processes) vs. the particle radius, r_p, is shown in Figure 2.8. Figures 2.6 to 2.8 show the 'mathematically' ideal particle size ranging from a radius of 2.5 to 6 µm maintaining a reasonably small flow length and free volume. The exponentially increasing longitudinal spacing and free volume, as a function of the particle diameter, demonstrates that the particle radius should not exceed 10 µm in order to exploit the advantages of the aqueous powder impregnation. Practical considerations such as the non-availability of small particles and the wetting of a large number of these small particles in the aqueous solution may force the use of larger particles. This compromise with the ideal situation not being achieved may result in an increased porosity of the composite.

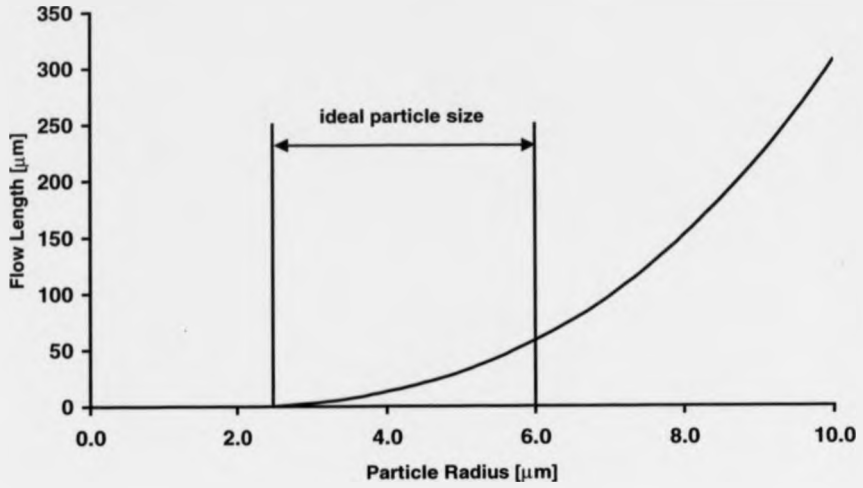

Figure 2.7: Flow length, L_p , vs. particle radius r_p ($V_f = 60$ %).

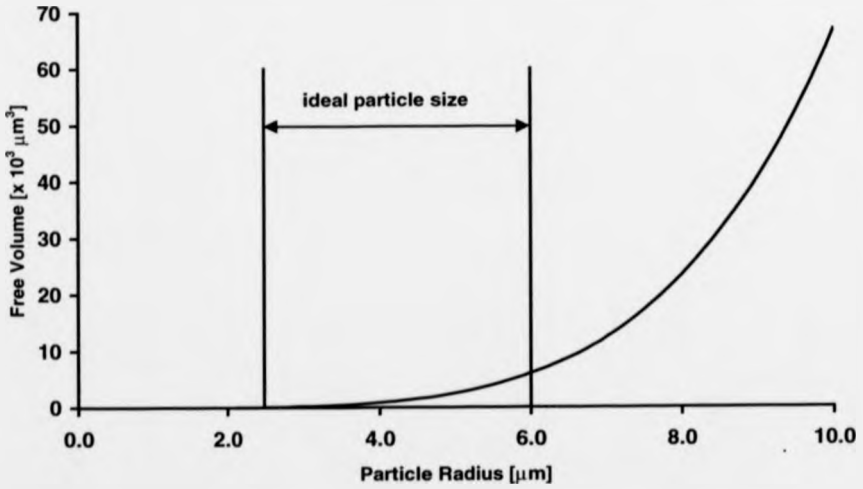

Figure 2.8: Free volume, V_E , vs. particle radius r_p before consolidation ($V_f = 60$ %).

2.6.5 Particle concentration

A critical aspect of the impregnation process is the concentration of the polymer powder in the aqueous solution. Ideally, the concentration of the particles in the bath should be equal to the concentration in the roving leaving the bath. This is to ensure a constant fibre volume fraction during the impregnation process.

The ideal concentration of particles, c_{opt}, (in grams per litre) in the aqueous solution for a certain fibre volume fraction can be calculated using Equation (2.1), assuming that the free volume (see Figure 2.8) in the unit cell is filled with water.

$$c_{opt} = \frac{\frac{4}{3}\pi r_p^{\,3} \times \rho_m \times 1000}{V_E} \qquad (2.1)$$

In Equation (2.1), r_p, is the polymer particle radius, ρ_m, the density of the polymer and V_E, the free volume in the unit cell.

A small amount of surfactant, typically <1%, has to be added to the water to attain an even distribution of particles in the dispersion with the required concentration. This is achieved by improving the particle's wetting behaviour by reducing the surface tension of the water.

2.6.6 Modifications of the process

Commercially available thermoplastic prepreg tape manufactured by the methods described in Sections 2.5 and 2.6 are fabricated as raw materials for further processing. Dimensional accuracy and edge contours are not important features for such a raw

material since the processing generally involves heating and reforming of the polymer composite.

This is not the case for an application such as non-laminated pin loaded straps. Accurate edge contours and small width tolerances are necessary to ensure an even support to all the layers in the strap. These dimensional properties are determined by the consolidation rollers in the impregnation process. The standard roller sets used by Sulzer Innotec Ltd. are machined with a width, w, of 5 mm from a single piece of stainless steel. The radii, r_{con}, of the female corners in the bottom rollers (see Figure 2.9) are typically in the range of 0.15 mm which is about the thickness of an impregnated roving. A polished cross-section of a tape section produced using these rollers is shown in Figure 2.10. The variable shape of the cross-section of the tape and the irregular surface texture may be responsible for some of the difficulties encountered at the beginning of this project.

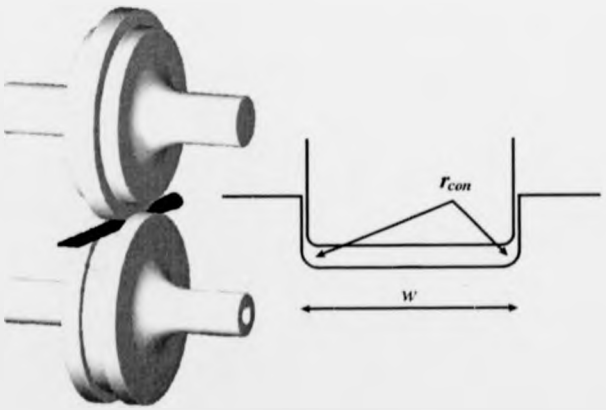

Figure 2.9: Set of consolidation rollers.

An alternative method had to be found to produce consolidation rollers with high accuracy in the width dimension of the slot, reduced surface roughness and sharp edges in contact with the thermoplastic prepreg. This improvement to the existing Sulzer process was developed by the author.

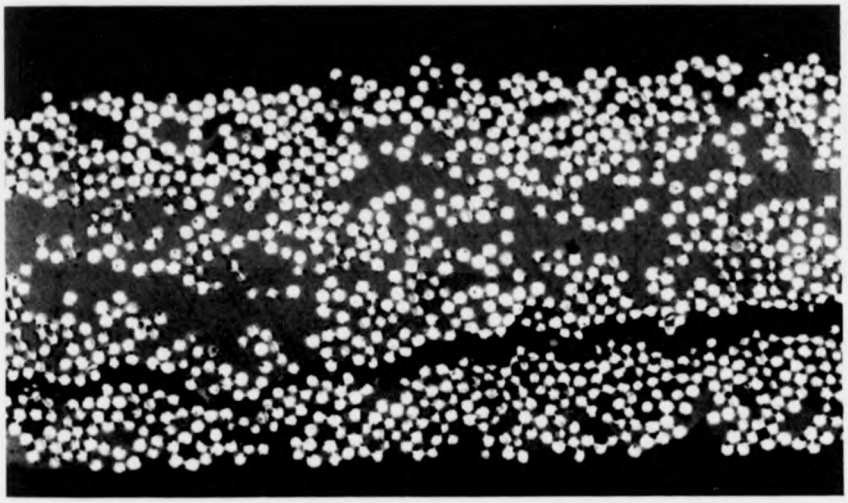

Figure 2.10: Polished cross-section of a prepreg tape produced using the unmodified impregnation process.

The bottom roller in Figure 2.9 was machined from three different pieces of stainless steel. The central piece was shaped like the top roller with polished (surface roughness < 0.5 μm) outer diameter and contact faces for the two circular disks. A 'perfect' perpendicular fillet at the junction of base and sides was thereby obtained. Two circular disks with polished (surface roughness < 0.5 μm) contact faces were then bolted to the two sides of the central piece. The top roller was produced in the same manner as the bottom central piece. This resulted in two precisely matching tools with separate

machined and polished faces and an exact rectangular gap ($w = 6$ mm) between top and bottom rollers. The improvement of the quality in terms of fibre distribution and surface texture of the tape can be seen by comparing the materials in Figures 2.10 and 2.11. Both materials exhibit many cracks which may have been introduced in the processing.

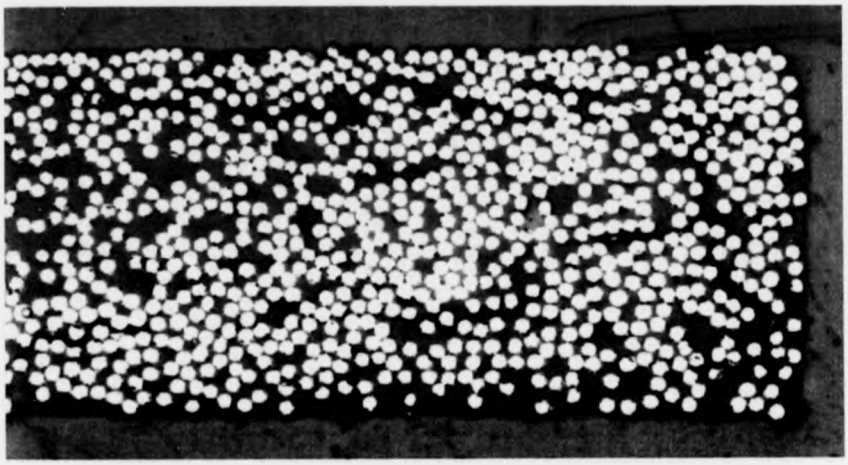

Figure 2.11: Polished cross-section of a prepreg tape after modifications of the impregnation process.

A second source of problems was a damping unit located at the exit of the drying chamber. The large airflow inside the drying chamber caused the tape to vibrate to such an extent that the tape came into contact with the chamber wall. Hence, the author chose glass for two restraining pins, since the glass surface was expected to minimise adhesion of the molten polymer. They were placed horizontally about 1 mm above the moving tape to prevent excessive vibrations. It was found that residues of molten polymer and damaged fibres were collected at these pins. The residue has to be removed

periodically by an operator to maintain high quality tape. Otherwise large deposits were to be found along the length of the tape.

The tapes used by the author in the project were manufactured when the drying chamber had glass pins at the exit. Further improvement has been achieved since then using the damping roller system shown in Figure 2.12. The working surface of the steel rollers was coated with Teflon to reduce the amount of collected residues. The time period between each cleaning operation has now increased significantly.

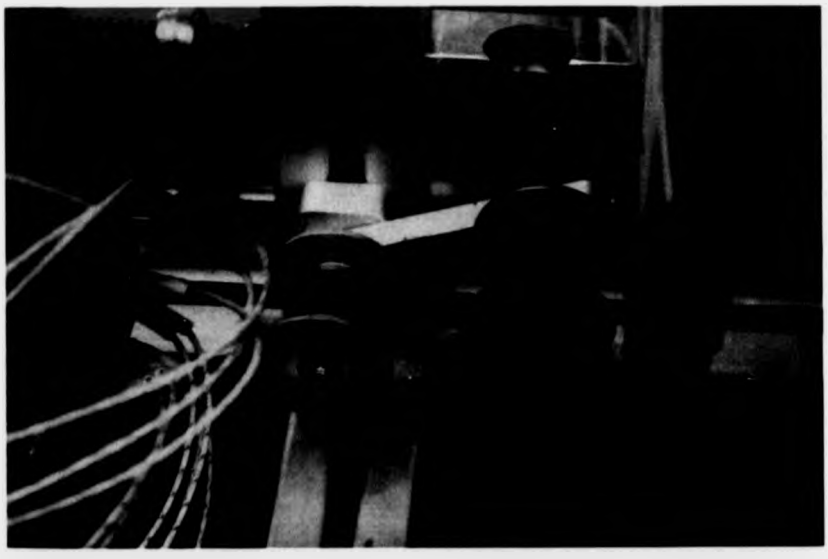

Figure 2.12: Damping rollers to prevent vibration of the tape due to the airflow in the drying chamber.

3 EXPERIMENTAL METHODS

3.1 Introduction

This chapter presents the experimental work used to show that the pin-loaded strap has a future. The work detailed is of a preliminary nature for the reasons given in Chapters 1 and 2. It includes characterisation of the tape material's mechanical properties, the successful development of a fusion bonding process for end anchorage, and the development of a practical manufacturing process for laminated pin-loaded straps.

3.2 Characterisation of the material

3.2.1 Longitudinal properties

The sensitivity of unidirectional CFRP's in the directions other than the fibre direction leads to the problem of load transfer between a composite specimen and the grips of a testing machine. An inappropriate load transfer can cause premature failure of the specimen and leads therefore to inaccurate material properties. Standards, such as EN 2561, are available to determine the longitudinal properties of laminates with a specified geometry. This standard considers specimens cut from a prefabricated sheet of 1 mm thickness. The properties of Tape I material were determined following EN 2561. A single ply of the prepreg was used instead of a prefabricated sheet, which would

comprise of eight layers of prepreg. Cutting the Tape I material with a scalpel made it difficult to accurately control the width of the strip. A crack tip progressed into the material several millimetres ahead of the scalpel resulting in a unacceptable variation of several millimetres in the tape's width. Hence, the following method was developed to overcome the preparation problem.

About 10 m of the 305 mm wide Tape I material was wrapped tightly around a plastic pipe of 200 mm external diameter. The outer end was fixed to the layer below with adhesive tape. A diamond coated grinding wheel was used to cut slices from the pipe at 11 mm widths. The grinding process did cause some damage to the tape edges and the heat generated allowed a number of layers to be fusion bonded together, such that these layers could not be unwrapped. To remove the damaged zone, the slices were machined on either side using wet abrasive paper to a final constant width of 10 mm. This process resulted in tape of controlled width, but there were still fibres damaged and exposed at the edges.

Aluminium end tabs were adhesively bonded to the 160 mm long specimens in the gripping area to distribute the clamping force more uniformly. A toughened epoxy adhesive (Scotchweld® 9323) was used to bond the 2 mm thick end tabs with squared edges to the specimens. Degreasing using Acetone was the only pre-treatment method employed.

A more effective system to transfer load into a specimen was found by modifying the clamping device used by Gerritse (1990) for anchorage purposes of Arapree tendons (i.e. tendons of aramid fibres). The clamping device is shown in Figure 3.1. It consists

of a base plate having 26 threaded holes, two rubber pads and a 1 mm thick steel cover sheet with the same hole pattern as the base plate. The 500 mm long specimen was clamped between the rubber pads by using steel bolts which were tightened to different torque values. The torque on the pair of bolts at the front of the anchorage was 0.6 N·m, and it increases linearly to a torque of 2 N·m at the back. The thin steel cover sheet deformed non-uniformly under the bolt loading. This resulted in a gradient in the through-thickness compression forces which restrained the specimen at the back while maintaining adequate shear flexibility towards the front. This fixture reduced the peak shear stresses, τ_{13}, at the front end and therefore prevents premature failure due to interlaminar shearing. A trial and error procedure was used to establish the optimum torque values ensuring no slip at the back of the anchorage.

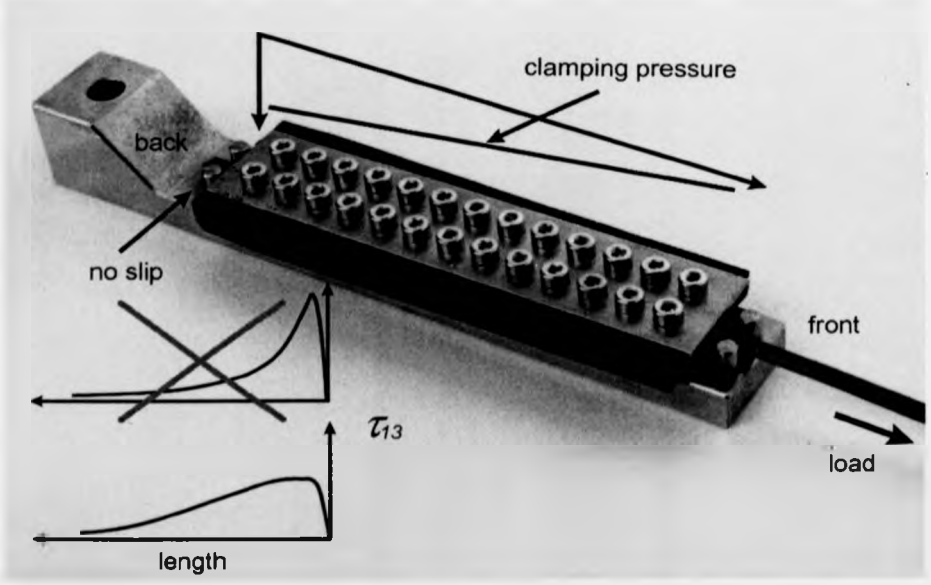

Figure 3.1: Rubber padded clamping device for anchorage purposes.

The measured strength properties (see Chapter 4.2.1) suggest that the clamping fixture was not performing satisfactorily. An alternative anchorage system, based on the principles described by Meier et al. (1998), was therefore also used in conjunction with the final Tape IV-3 material. The cast anchorage system using a conical shaped socket, as shown schematically in Figure 3.2, has been used successfully in a cable stayed road bridge in Winterthur, Switzerland. One pair, out of the total of 12 pairs, of stay-cables are made of CFRP material. The cables have a load carrying capacity of 12 MN.

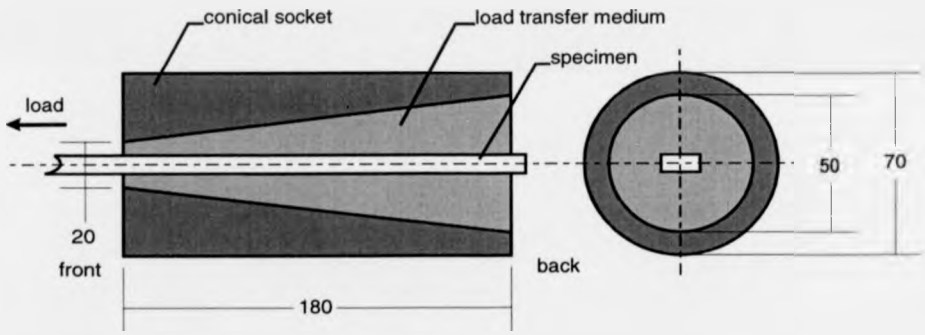

Figure 3.2: Conical cast anchor.

The tape specimens were anchored in steel sockets using Araldite® 5052 as the load transfer medium. This is a commercially available, room temperature curing epoxy resin. The back ends of the sockets were closed with a cover plate containing a clamping mechanism to position the specimen centrally. Specimens of 500 mm length were clamped at both ends and the two sockets pushed apart to tension the tape and to ensure specimen alignment. Acetone was used in the region of the anchorage to degrease the specimen. The sockets were kept in a vertical position in the oven at 40° C while the epoxy resin was poured into the first socket from the open front end. The

elevated temperature reduced the viscosity of the resin and therefore facilitated the casting process. The system was left in the oven at 40° C for twelve hours to cure. The casting process was repeated for the second socket. The resulting specimen gauge length was 140 mm.

The same anchorage system was used with a specimen made from twenty layers of Tape IV-3 material. To consolidate the laminate, a simple steel tool was made from rectangular sections which are commercially available with polished faces (surface roughness < 10 μm). The ends of the tool were left open as shown in Figure 3.3. The lower die was made from three standard sections whereas the dimensions of the central piece defined the 6 mm wide slot. The same section was used for the lower part of the upper die. The steel tool was prepared by the application of Release-All® 70, a releasing agent, before the twenty layers of prepreg were placed between the two dies. The upper die was clamped to the lower using steel springs to maintain the consolidation pressure throughout the whole production cycle in the oven. The system was placed in the oven at 190°C for 2 hours to allow the polymer to melt and therefore to consolidate the layers to a thickness of 3 mm. The system was left in the oven to cool down before it was demoulded by disassembling the steel tool.

The matrix on the surface of the specimen was removed with abrasive paper to bond to the fibres. The specimen was anchored in the conical steel socket using the process outlined above.

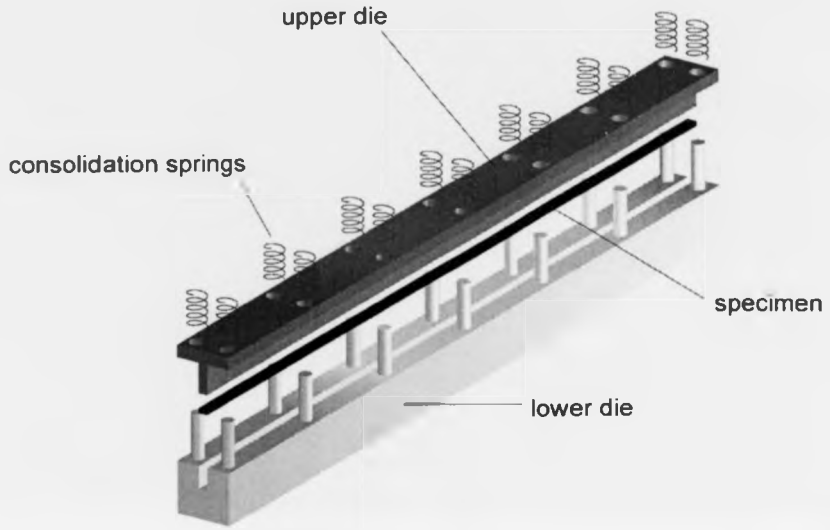

Figure 3.3: Steel tool to consolidate layers of prepreg tape.

The anchorage method using the rubber padded clamping device was found to give the highest strength values although the measurements given in Section 4.2.1 suggest that there is scope for further improvement of the anchorage system.

The strain measurements were performed using an optical extensometer which is built into a Zwick 1474 standard testing machine. The loading rate of 2 mm/min was selected to reach the failure load within about 1 minute.

3.2.2 Transverse and shear properties

The properties of the tape material in other than the fibre direction are required for the stress analysis in the load transfer region of a pin-loaded strap. The geometry of the prepreg tape does not allow the use of standard coupon testing to determine transverse and shear properties. Puck and Schürmann (1982) proposed a very suitable, but expensive method based on tubular specimens. This method allows material characterisation under multiaxial loading conditions by combining axial, torsional and internal pressure loading on the tubular specimens.

To determine transverse properties a tubular specimen is loaded in axial tension. The tube would have continuous fibres aligned in the hoop direction. The load is transferred into the tube by way of metal end fixtures that are adhesively bonded to the composite tube.

The tubular specimens were produced by wrapping prepreg rings of 6 mm width onto a cylindrical aluminium mandrel of 40 mm diameter, as shown in Figure 3.4. The mandrel was first prepared by the application of the releasing agent Release-All® 70. A tapered laminate thickness was required to ensure that failure occurs in the centre of the specimen away from the end fixtures. The number of layers varied from twenty-two, at the ends of 60 mm length, to twelve in the central region of 90 mm length. Four intermediate steps were used to develop the gradual tapered region. The final layer was fixed temporarily using a temperature resistant adhesive tape. Each ring was pushed against the previous one using a stiff steel consolidation ring to ensure a well consolidated laminate in the longitudinal direction of the mandrel. A rubber shrinkage tube was placed over the prepreg rings. To achieve a more uniform pressure distribution

a polyester shrinkage film was wrapped around the rubber tube. The system was left in an oven at 190 °C for 2 hours. The prepreg rings were consolidated by the expanding aluminium mandrel and the contracting rubber tube and polyester film.

The aluminium mandrel was readily removed without damaging the specimen after the system was left in the oven to cool down. The central region of the specimens was machined on a lathe. This was necessary to achieve a defined cross-sectional shape and a central region of constant thickness for the application of strain gauges. The final specimen is shown schematically in Figure 3.5.

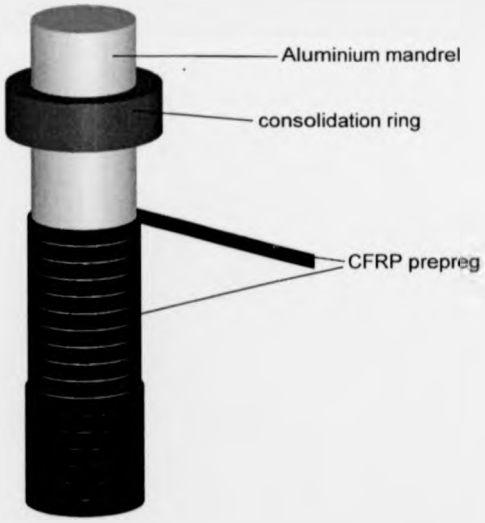

Figure 3.4: Schematic layout of the manufacturing process used for tubular specimens.

The steel end fixtures were bonded to the tubular specimen over a length of 40 mm using Scotchweld® 9323, a room temperature curing epoxy adhesive. The steel was pre-treated by grit blasting and the tubular CFRP specimen with abrasive paper to remove

the matrix on the surface to bond to the fibres. Acetone was used as a solvent for degreasing purposes. The specimen consisting of the CFRP tube and the two steel fixtures was clamped to a steel L-section until the adhesive was cured to ensure alignment of the two end fixtures. The base of the steel fixtures had features for either axial or torsional loading.

The experiments were performed on an Instron-1343 servo-hydraulic testing machine capable of tension, compression and torsion loading. The stroke controlled tensile test for the transverse properties of the CFRP was carried out at an actuator speed of 2 mm/min. Strain gauges with 10 mm gauge length were applied in the longitudinal direction of the tube at four different locations. These were equidistanced on the circumference and at the centre of the specimen.

To determine the shear properties of the CFRP a pure torsion test was performed at a rotational speed of 2 °/min. The control system of the machine ensured that no axial loading was applied as the specimen twisted. Two strain rosettes were applied equidistanced at the centre of the specimen. The torsional test is shown in Figure 3.5. Each rosette had three strain gauges of 10 mm length, positioned at 45°, -45° and 0° with respect to the tube's axis.

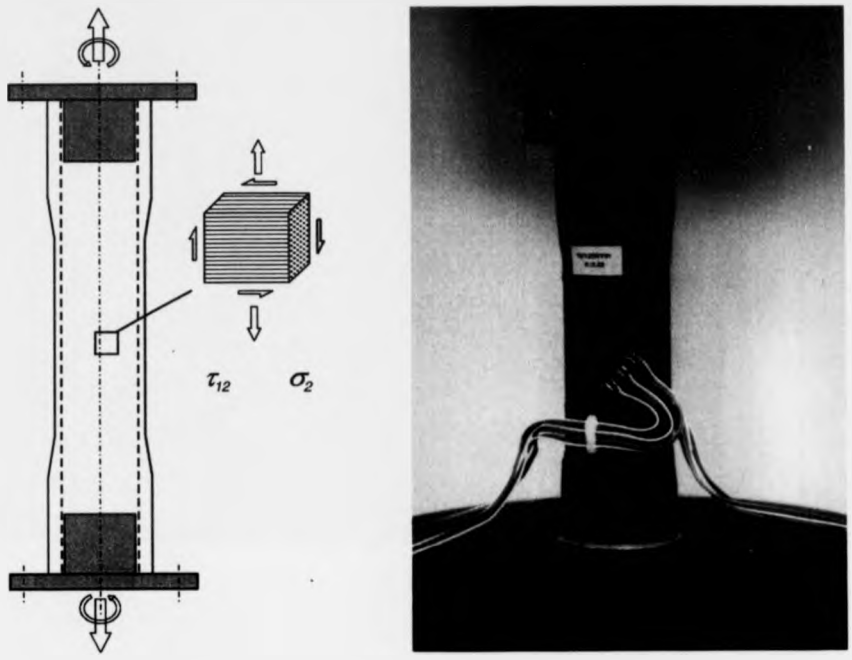

test specimen torsion test

Figure 3.5: Characterisation of the CFRP in transverse and shear direction.

3.2.3 Frictional properties

The load transfer into individual layers of a non-laminated pin-loaded strap is based on friction. Therefore, the friction properties of different material combinations (see Section 4.2.3), which could occur in a non-laminated strap, were determined according to standard DIN 53375. The standard is used to characterise polymeric film materials. The layout of the experiment is shown in Figure 3.6. Specimens I and II, or friction partners, were respectively fixed to the base plate using a clamping device, and to the weight using double sided adhesive tape. This procedure ensured that the movement

took place between the friction partners. The contact pressure between the partners was varied by adding weight on top of specimen II. The maximum weight was limited due to the tensile strength of the nylon string used to transfer the horizontal friction force to a vertical one, so an Instron 1122 testing machine could be used. The maximum weight resulted in a normal stress, σ_n, of 0.17 MPa. The length of the two strips for specimen I was 200 mm, whereas it was 140 mm for the specimen II strips. A constant contact pressure could be maintained over a travel distance of 60 mm. The cross-head speed of 100 mm/min was defined by the standard.

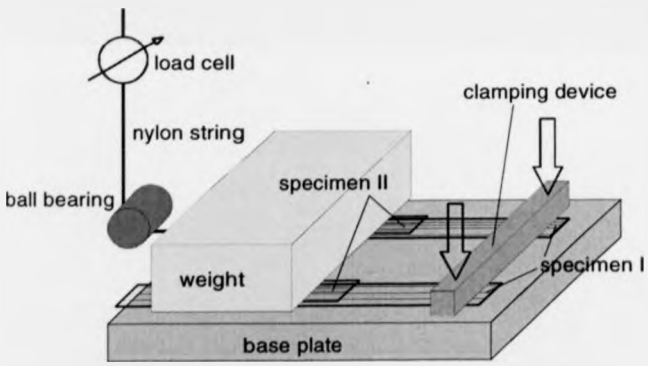

Figure 3.6: Schematic layout of the friction measurements.

3.3 Anchorage methods

A critical issue for the feasibility of non-laminated pin-loaded straps was the development of a suitable end anchorage for the final layer. General concepts of anchorage systems which could be used, are described by Winistoerfer (1998). Failure modes associated with the anchorage of CFRP laminae are presented in Section 4.3.

3.3.1 Clamping

The clamped end anchorage system used by the author is equivalent to the system described in Section 3.2.1. The rubber padded clamping device is attached to the fixture containing the steel pin, as shown in Figure 3.7. One drawback of this system is the lack of control over the required length of the non-laminated strap specimen. The frictional forces in the load transfer region of a non-laminated pin-loaded strap build up as the pins are moved apart under tension. Hence, the load displacement behaviour of a specimen critically depends on the quality of the wrapping process.

Figure 3.7: Clamped end anchorage system of a non-laminated pin-loaded strap.

3.3.2 Fusion bonding

The fusion bonding methods described by Arias (1998) and Wise (1992) involve CFRP materials with thermoplastic matrix to be joined by the application of heat and pressure. In the process the surfaces of the two parts to be bonded have to be heated such that the matrix can fuse. Possible heat sources are hot plates (which are removed before the surfaces are brought together), resistive implants, induced eddy currents, ultrasound, microwaves or vibrations.

The particular geometry encountered in the end anchorage of the final layer of a non-laminated pin-loaded strap, particularly when anchored to the previous layer, allows the application of heat from the outside of the joint. The process developed by the author to fabricate a single lap-joint which anchors the final layer in the non-laminated pin-loaded strap is shown schematically in Figure 3.8. The two layers of prepreg tape to be joined are clamped between two electric heating elements. The option of having the polymer film between the two mating surfaces does result in a higher joint capacity when the material is Tape IV-3 material (see Section 4.3). The heat was applied until one of the thermocouples placed on the outside of the heating elements reached a predetermined value. The temperatures were varied, as described in Section 4.3, to optimise the joint capacity. The maximum use temperature of the heating elements was 250°C and this was sufficient for fusion bonding of Tapes II and IV material. The developed welding rig was, however, not suitable to fusion bond of Tapes I and III material. The resulting lap-joint length was about 90 mm. This length cannot be reduced using the apparatus shown in Figure 3.9, but it could be increased by placing two consecutive joints next to each other with a partial overlap. The joint length was not varied for this research. The fan contained in the control unit shown in Figure 3.9 allowed a reduced cycle time

through forced convection cooling. The applied pressure was kept constant during the fusion bonding process by placing a steel block (not shown in Figure 3.9) of 1.5 kg mass on top of the welding rig.

Single lap-shear specimens of 250 mm total length were produced to determine the load carrying capacity of the fusion bonded joint. The lap shear tests were carried out using the rubber padded clamping device described in Section 3.2.1. The test was performed under stroke control at a rate of 2 mm/min. The maximum load was recorded.

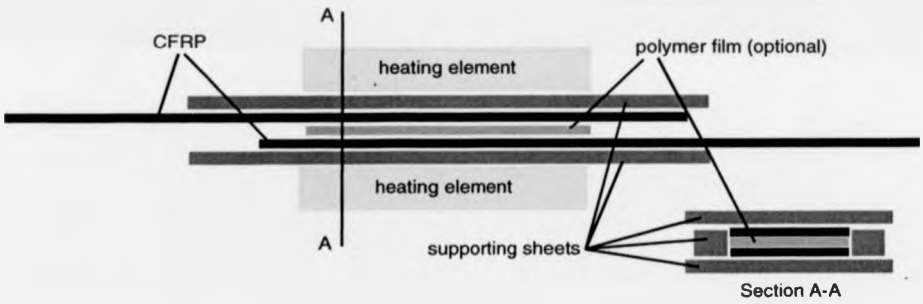

Figure 3.8: Schematic layout of the fusion bonding process.

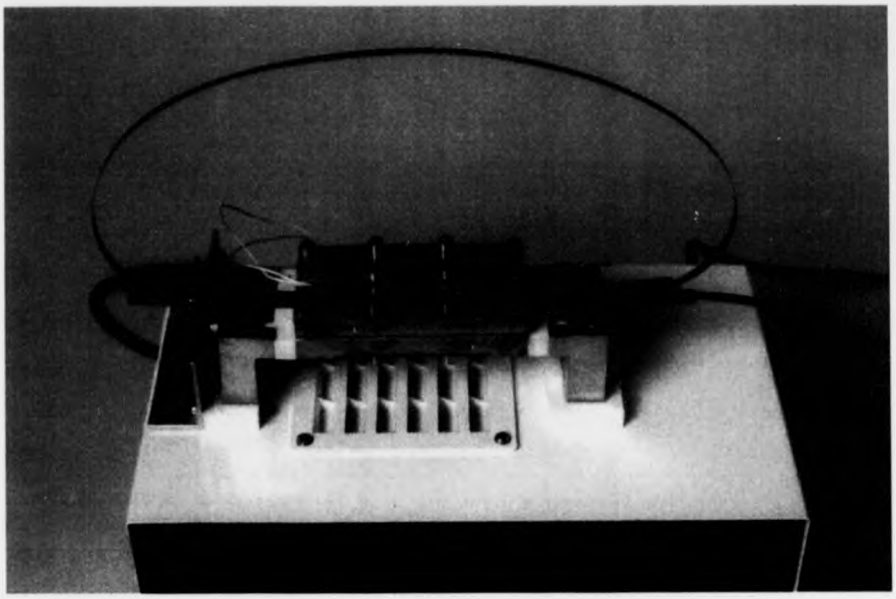

Figure 3.9: Welding rig for thermoplastic prepreg tape.

During the early stages of the development of the process, difficulties were encountered with misalignment of the fibres. The nature of this problem is shown schematically in Figure 3.10. Of particular importance is the misalignment out-of-the-plane of the tape since the resulting comparatively small radii of curvature reduce the joint strength dramatically. In severe cases the lap-joint could be pulled apart by human effort. The influence of the transverse in-plane deformations of the tape was not investigated.

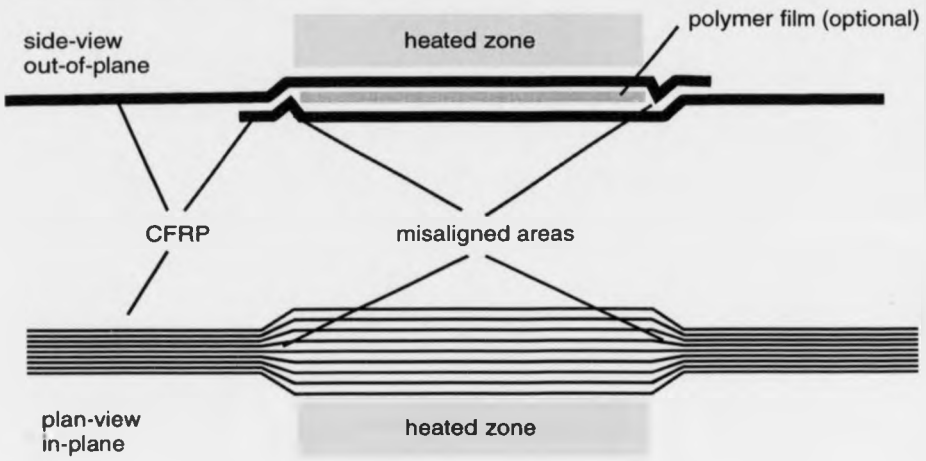

Figure 3.10: Difficulties encountered in a fusion bonded joint.

These difficulties were overcome by stainless steel sheets supporting the joint in both directions where the misalignment occurred. The supporting sheets shown in Figure 3.8 extend beyond the length of the heating elements to ensure alignment just outside the heated zone where the flow of heat energy is sufficient to cause the matrix to melt. The sheets on top and bottom of the joint are 0.6 mm thick to minimise the mass. The supporting sheets at the sides had to be matched to the exact thickness of the joint. Strips of 10 mm width are commercially available in thicknesses every 50 µm. The next smaller size compared to the overall joint thickness was selected. All the sheets in contact with the prepreg tape were treated using the release agent Release-All® 70.

3.4 Pin-loaded straps

The experimental investigation on pin-loaded straps, where dynamic loading was required, were performed on an Instron 1152 servo hydraulic testing machine. The static

tests were performed on a spindle operated universal testing machine made by Zwick. The cross-head, or actuator speed was 2 mm/min throughout the whole investigation. If not otherwise stated, the specimen length was kept constant at 200 mm separation between the centres of the two steel pins, independent of the pin diameter.

The loading pins had a slot machined to match exactly the width of the strap. These slots restrained the strap in the transverse direction and ensured the centred position of the specimen relative to the end fixtures.

3.4.1 Laminated

The most appropriate method to produce laminated pin-loaded straps from thermoplastic prepreg tape would be the use of a fibre placement machine. In this continuous process (Kempe 1997), the prepreg tape is placed on a mandrel which represents the inner contour of the component to be made. The thermoplastic matrix is heated locally to the molten stage just before contacting the mandrel. A consolidation roller is placed in front of the placement head to press the tape onto the mandrel. The roller cools the tape sufficiently to keep the tape in place.

For the manufacture of the author's specimen such a machine was made available by the ABB corporate research centre in Daettwil, Switzerland. Unfortunately, the control unit of the robot allowed only rotational symmetric components to be made. An unsuccessful attempt was made to use the so called 'teaching option' to programme the robot manually.

Instead of using the ABB fibre placement machine the method shown schematically in Figure 3.11 was developed by the author. The prepreg tape was wrapped around a steel centre mould which represented the inner contour of a strap. A silicon rubber pad containing a slot representing the outer contour of the strap was placed over the steel mould. The slot in the rubber pad was made using a numerically controlled water jet cutting machine. The size of the slot was varied according to the number of tape layers wrapped around the steel mould. A ring made from 2 mm thick aluminium sheet material was placed around the perimeter of the silicon rubber pad (see Figure 3.11). Two steel sheets of 2 mm thickness were placed above and below the specimen and the whole system placed in a heatable press. The silicon rubber pad tries to expand with increasing temperature. However, the expansion of the rubber pad was restrained by the outer aluminium ring and therefore a consolidation pressure was exerted on the specimen. Once the temperature in the plates of the press reached 190°C the heating was switched off and the system left to cool down.

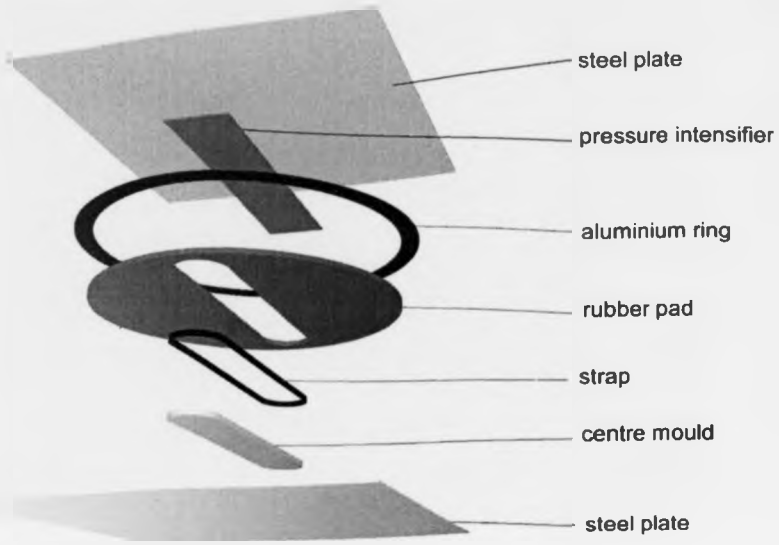

Figure 3.11: Schematic layout of the manufacturing process used for laminated pin-loaded straps.

Figure 3.12 shows a laminated strap produced when there was a problem in controlling the thickness in the mould. One reason for such thickness changes was the inherent variation in dimensions in the off-the-shelf silicon rubber sheet. Another reason for thickness changes was the mismatch in thermal expansion between the rubber pad and steel mould parts. The gaps which occurred at 190° C became filled with the composite material and the resulting poor quality strap is shown in Figure 3.12. To produce straps which had the right shape a steel plate acting as a pressure intensifier was introduced during the development of the process. This pressure intensifier shown in Figure 3.11 overlapped the perimeter dimensions of the strap by about 10 mm.

The applied pressure of the heatable press had to be optimised for each rubber pad used. The range of the oil pressures and the resulting press clamping force are given in Table 3.1 for the three different inner contours.

Table 3.1: Processing parameters for laminated pin-loaded straps.

Inside radius r_i [mm]	Oil pressure [bar]	Force [kN]
15	20 - 45	10.1 – 22.6
25	35 - 60	17.6 – 30.2
75	50 - 140	25.1 – 70.4

Figure 3.12: Laminated pin-loaded strap produced with an imperfect rubber pad.

The developed process is limited in terms of the maximum number of layers that can be consolidated with this method. Straps consisting of fifteen layers of Tape IV-1 material were produced successfully whereas twenty layers of Tape IV-1 material could not be consolidated to a strap of satisfying quality. The mismatch of the thermal expansion coefficient between the steel centre mould and the CFRP strap resulted in a high contact pressure in the curved region of the strap where the pin is located. Hence, at the maximum operating temperature of 190°C, the fibres were believed to be orientated parallel to the inner contour of the strap. As the system cooled down, the centre mould contracted more that the strap. The consequence of the mismatch in thermal expansion was local fibre misalignment, particularly at the transition from the curved to the straight section of the strap. This misalignment is shown in Figure 3.13. Furthermore, the wrapping process prevented that the tape matched exactly the contour of the mould at the centre since the straight section did not provide any contact pressure to the tape. Both effects supported the development of the poor quality fibre architecture shown in Figure 3.13. As the number of layers was increased the poor quality of the straps became more severe.

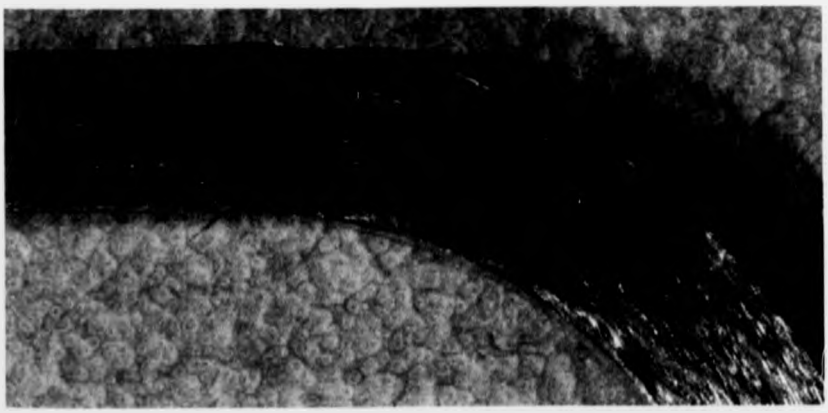

Figure 3.13: Discontinuity in the fibre orientation in laminated pin-loaded straps.

3.4.2 Non-laminated

The processes employed to produce non-laminated pin-loaded straps evolved in conjunction with the development of the materials (see Chapter 2). The initial screening tests on Tape I material were performed with an adhesively bonded end anchorage using Scotchweld® 9323, a room temperature curing epoxy adhesive. The length of the single lap-joint was about 60 mm. The lap-joint strength achieved was not sufficient and specimens consisting of five layers failed in the joint region by way of interfacial failure. Additional mechanical clamping was introduced along the joint region to increase the low adhesive bond strength.

Specimens consisting of five layers of Tape I material were wrapped around an aluminium tool representing the inner contour of the strap. The final layer was anchored to the previous one by adhesive bonding. The inner layers were separated from the joint with a layer of release film ensuring no contamination of any other layers with adhesive. The release film and excessive adhesive was removed after curing. Two longitudinal strain gauges were applied to the innermost and outermost layer as shown in Figure 3.14. All the specimens were loaded dynamically (between 1 kN and 10 kN) with 30 cycles (at 6 Hz) prior to testing to failure. These dynamic loading cycles where introduced to promote the relative displacement necessary to attain an even strain distribution throughout all the layers in the strap (see Section 4.4.2 for further details). The strain was measured continuously at an acquisition rate of 5 Hz.

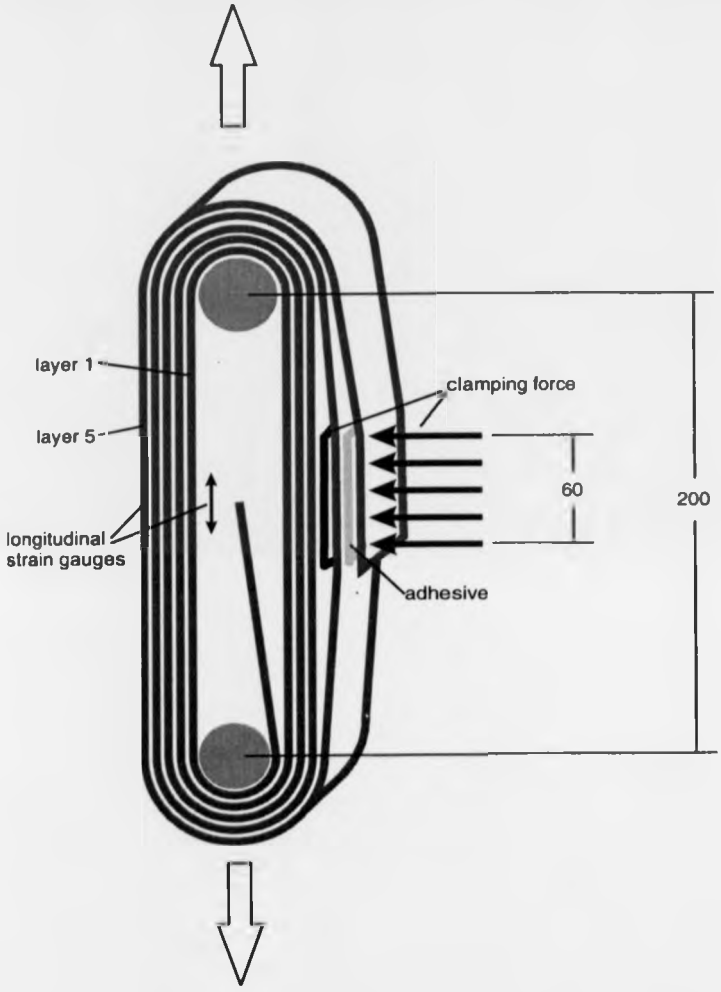

Figure 3.14: Configuration of screening tests for non-laminated straps with Tape I material.

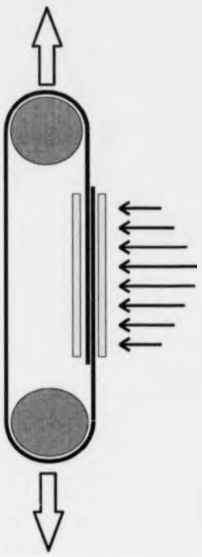

The influence of the pin diameter on the performance of the load transfer was investigated using pin-loaded strap elements consisting of a single layer of Tape II or Tape IV-2 material. Different steel pins of 25, 30, 35, 40, 50 and 150 mm diameter were used. The prepreg tape was wrapped around two identical pins and anchored as shown schematically in Figure 3.15. The concept of the anchorage was identical to the system described in Section 3.2.1. The gradient in the clamping force was symmetrical about the centre of the lap-joint.

Figure 3.15: Test set-up.

The next generation of non-laminated pin-loaded straps consisted of Tape III material with a clamped end anchorage for the final layer. Seven layers of Tape III material were wrapped around two steel pins with the final layer clamped between a rubber padded steel fixture, as shown in Figure 3.16. The steel fixture was equivalent to the clamping device described in Section 3.2.1. It was attached to the fixture containing the bottom pin. The top and bottom pin were fixed to the testing machine by two universal joints ensuring only axial loading in tension. The top universal joint was equipped with a battery operated laser pointing to a pre-set mark on the bottom fixture to ensure no twist of the two pins. The tape edges were marked with white paint to visualise the relative displacements between individual layers. A steel ruler was placed next to the marked specimen for coarse displacement measurements. A digital camera was placed in front of the marks. It provided the author with a picture of the instantaneous response of the

strap so that the stroke could be continuously updated. The author could visually inspect the specimen and operate the controls of the machine at the same time.

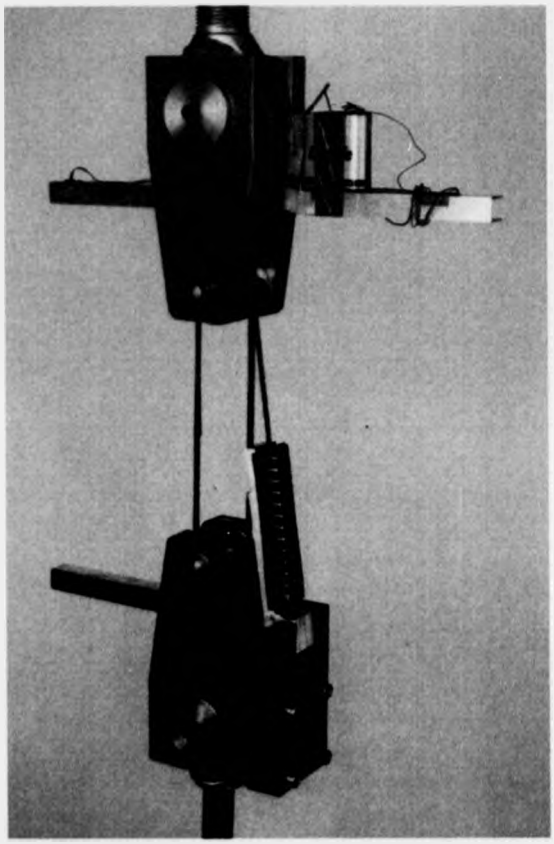

Figure 3.16: Test layout with a clamped end anchorage for the final layer.

The internal signal generator of the Instron testing machine was modified to superimpose a signal of a second, external generator. This allowed an independent control of the ramp rate at 2 mm/min with an additional high frequency ripple of 30 Hz having an amplitude of 5 % of the anticipated failure load. The resulting load-time history is shown schematically in Figure 3.17.

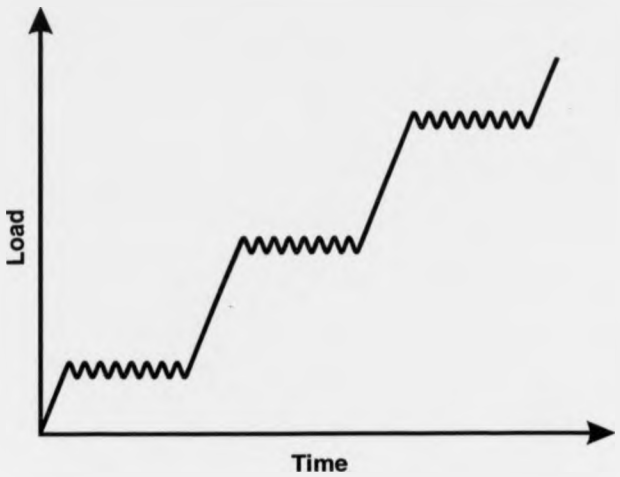

Figure 3.17: Schematic load-time history

The last generation of non-laminated pin-loaded straps were of the Tape IV-3 material. The manufacturing process for those strap specimens was changed because the fusion bonding process was available. The length for the bonding of the outermost layer was calculated and the end position marked on the tape coming directly off the roll. The joint was made according to the procedure described in Section 3.3.2. After removing it from the welding rig (see Figure 3.9), the strap consisting of a single layer was turned inside out and the number of layers wrapped towards the inside of the strap. This method enabled the length of the final strap to match the predetermined length accurately.

Strain gauges were applied to different layers in two specimens consisting of 5 and 10 layers, respectively. The strain gauges were applied on the side of the strap opposite the fusion bonded joint spaced longitudinally. The spacing was determined such that there

was no interference between the different strain gauges due to the increased thickness. The experimental set-up is shown in Figure 3.18. Measurements were made at discrete loading steps. The results are presented in Section 4.4.2.

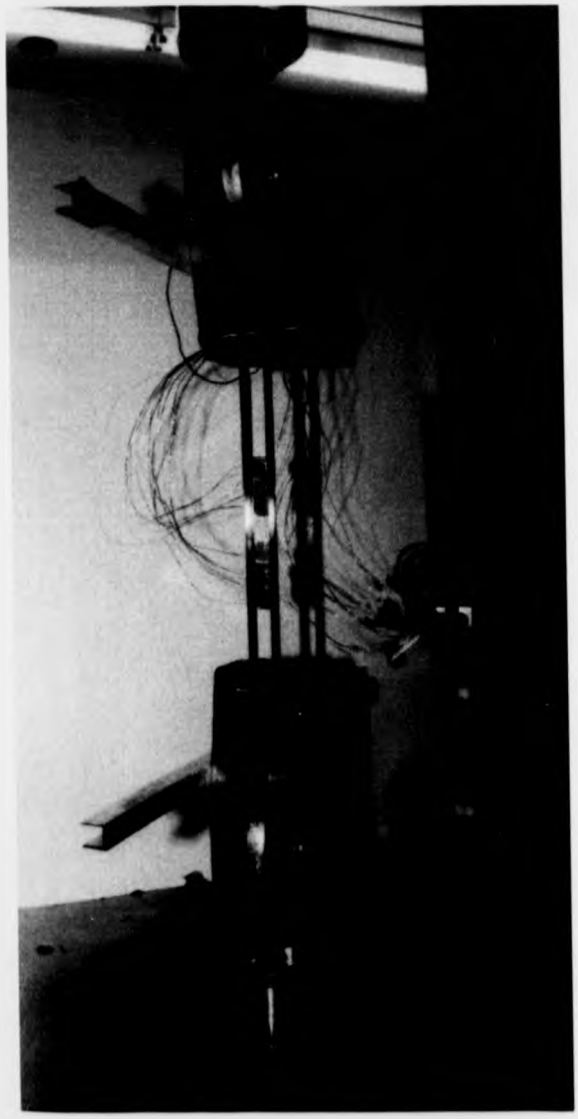

Figure 3.18: Non-laminated pin-loaded strap equipped with strain gauges.

The influence of the two different anchorage systems developed for the final layer of non-laminated pin-loaded straps by the author was investigated. Hence, the load carrying capacity of non-laminated straps with clamped and the fusion bonded end anchorage systems were compared. The two different types of non-laminated pin-loaded strap elements are shown schematically in Figure 3.19. The specimens were identical in every respect except for the method used to anchor the final layer.

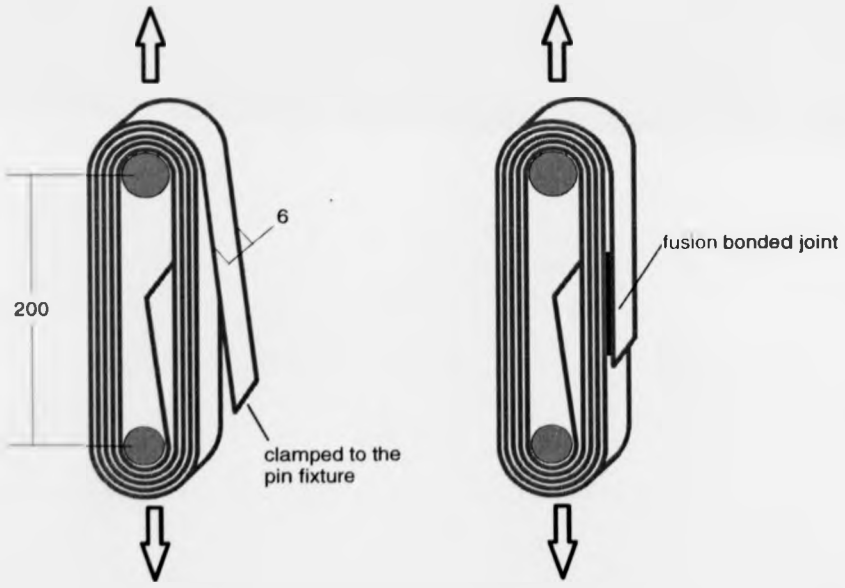

Figure 3.19: Last generation of non-laminated pin-loaded straps.

The fusion bonded specimens were produced as described earlier but without the strain gauges. The specimens with the clamped end anchorage were wrapped using the winding rig shown in Figure 3.20. The two pins were held against the retractable fixture by the tape which was tensioned by hand during the strap wrapping process. The retractable fixture with the specimen was placed into the testing machine and the final

layer anchored using the fixture shown in Figure 3.16. Finally, the retractable fixture was removed and the specimen tested in tension to failure. This procedure developed by the author ensured a reproducible specimen length of 200 mm.

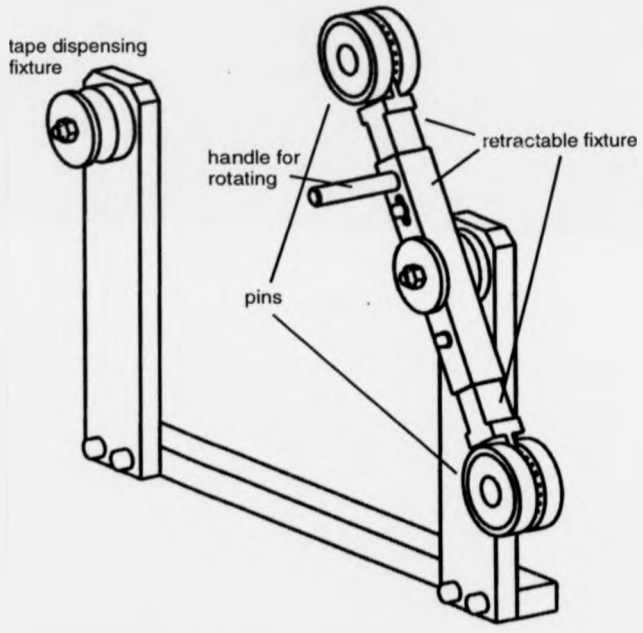

Figure 3.20: Schematic layout of the winding rig used to produce non-laminated pin-loaded straps.

An important aspect was the normalisation procedure used to compare the performance of laminated and non-laminated pin-loaded straps with clamped and fusion bonded end anchorage systems. The number of load carrying layers in a non-laminated pin-loaded strap was reduced because the first layer does not carry load until it has passed over a

pin. Equation 3.1 was used to determine the number of load carrying layers, n_{Load}, from the number of layers wrapped, N_L.

$$n_{Load} = N_L \times 2 - 1 \tag{3.1}$$

3.5 Long term creep performance

The creep properties of non-laminated pin-loaded straps were determined using three purpose made test rigs. The rig shown in Figure 3.21 was built 20 years ago for earlier creep measurements on glass fibre composites. The design allows a constant load up to 20 kN to be applied to the specimen. The use of a circular segment for the load support of the dead weight in combination with a thin spring steel sheet, supported on a circular disk, for the specimen support ensures constant loading and zero moments even at large creep strains. The three test rigs were located in an air conditioned laboratory. The constant environment had a temperature of 23°C and a relative humidity of 50%. The test rigs were calibrated prior to the experimental investigation by replacing the specimen with a calibrated load cell.

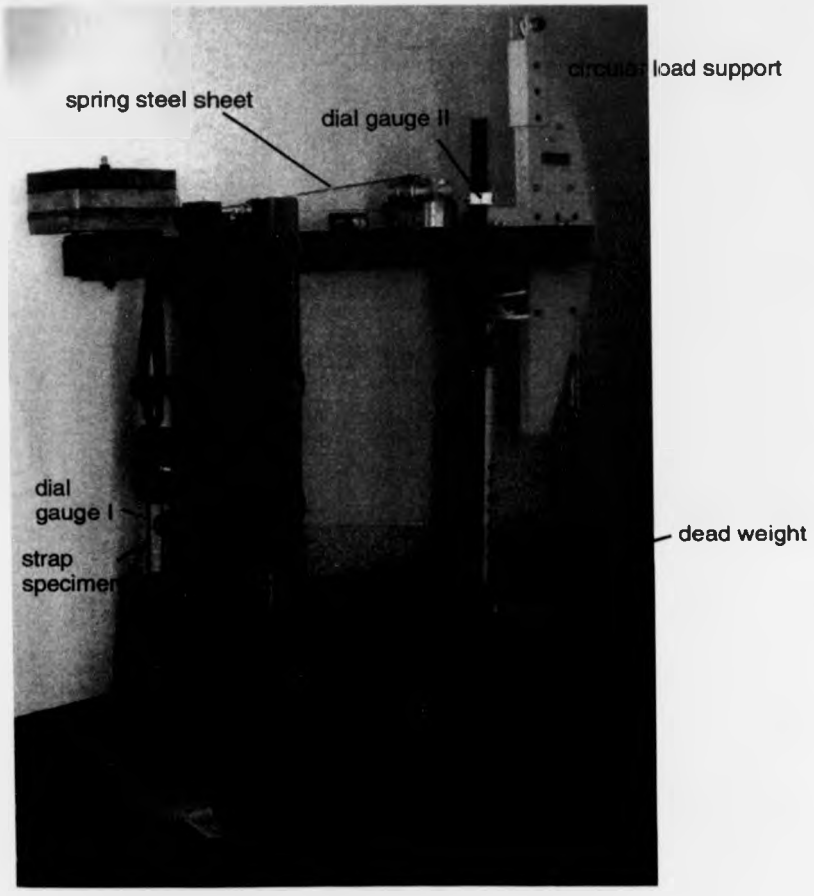

Figure 3.21: Creep test rig.

The rigs were originally not equipped for deformation measurements. The author fitted two dial gauges with a resolution of 0.01 mm to each rig to determine the creep strain at two different locations. The gauges are labelled in Figure 3.21. Gauge I measured the extension of the strap at the upper pin. Gauge II is located at the back of the cantilever beam. This resulted in an amplification of the strap displacement of 8.4. However, the displacement recorded by gauge II did also include deformation from within the test rig.

The three different pin diameters of, 30, 50 and 150 mm were used in the test rigs to isolate the different contributions to the total creep strain of a specimen. Further details are given in Section 4.5 where the results are presented and discussed. Lead blocks of variable weight were placed at the rear end of the cantilever beam to ensure a constant load of 9.6 kN load applied to each specimen.

The three specimens consisted of five layers of Tape IV-3 material. The lengths of the specimens were 209, 202 and 245 mm for the 30, 50 and 150 mm pin diameter specimen, respectively.

3.6 Verification of numerical model

An experimental investigation was performed using a single layer of Tape IV-3 material to provide data that could be used to verify the numerical and analytical models presented in Chapter 5. The single layer of prepreg tape with a fusion bonded joint was instrumented with five strain gauges as shown in Figure 3.22. A steel pin of 50 mm diameter was chosen since it was large enough for the four gauges to be placed on its circumference. The strains were measured continuously at an acquisition rate of 20 Hz. There were errors in the strain measurements because of variations of the bond-line thickness of the strain gauges. These errors were compensated as described in Section 5.4.3.

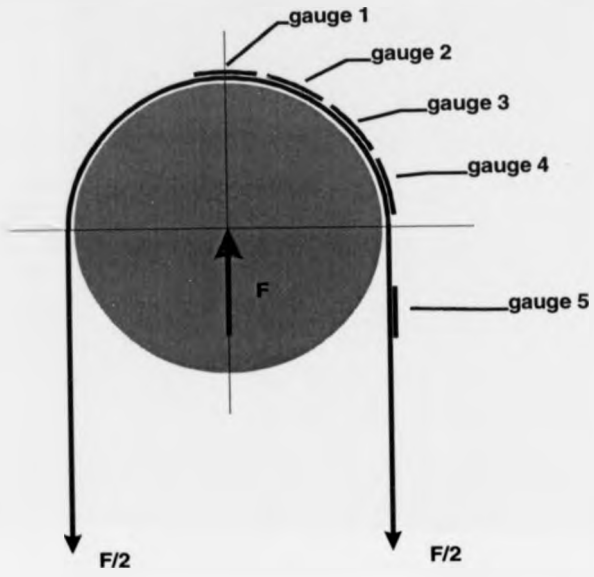

Figure 3.22: Experimental verification of the strain distribution around a steel pin.

4 EXPERIMENTAL RESULTS

4.1 Introduction

This chapter presents and discusses the experimental results obtained from the test programme detailed in Chapter 3. The characteristics of the different tape materials are described. The performance of the fusion bonding process as a joining technique using one of the tape materials is presented. The load carrying capacities of laminated and non-laminated pin-loaded strap elements are compared. Creep data on non-laminated pin-loaded strap elements are given. The raw data of the measurements are given in Appendix B.

The order in which the test results are presented in each section corresponds to the availability of the tape materials. Load carrying capacities are quoted instead of stresses since the surface texture of the earlier materials did not allow accurate measurement of cross-section dimensions.

Rheological influences on the polymer's properties (as described in Section 2.2.2) have been neglected since all the processes used to prepare specimens did not allow controlled cooling rates. Matrix dominant properties may have been affected slightly by this lack of process control. It is realised that these properties are important since they can affect the performance of a pin-loaded strap.

4.2 Characterisation of the material

4.2.1 Reference data

The mean values of the load carrying capacities, F_U, the standard deviation, s, the number of specimens, N, and the coefficient of variation, $C.O.V$, of the different tape materials introduced in Chapter 2, are given in Table 4.1. These values are the basis for various performance comparisons in this thesis. The measured properties of the Tape I material in Table 4.1 were determined according to the test method given in Section 3.2.1. Tape I material was supplied in the form of 305 mm wide, thin sheets. It was cut into 10 mm wide tape strips using the method described in Section 3.2.1. The Tape I material, therefore, had its tensile strength determined following the standard EN 2561. Aluminium end tabs were bonded to 10 mm wide specimens in the gripping area, where the failure initiated in most of the specimens. The measured load carrying capacity of 1840 N was significantly below the tensile capacity of 2540 N, as quoted by the material's supplier (Section 2.3). This suggests that the standard tensile test method used is not appropriate to characterise such tape material. As a result, a different gripping method was developed using rubber padded clamps. The method is described in Section 3.2.1. This improved testing method was used to measure the tensile properties of the remaining five materials in Table 4.1. Because Tape I material was not suitable for pin-loaded strap elements, its tensile strength was not determined after the preferred testing method was developed.

A theoretical value for a lower bound of the load carrying capacity, F_{U1}, can be determined using Equation (4.1) and fibre properties supplied by the fibre manufacturer (see Tables 2.1 and 2.3). The upper bound of the load carrying capacity, F_{U2}, can be

calculated for a 12K roving using Equation (4.2). It assumes a perfectly circular cross-section for each filament. In both cases the contribution of the matrix is neglected. This assumption is deemed acceptable.

$$F_{U1} = X_f \times \frac{T_f}{\rho_f} \tag{4.1}$$

$$F_{U2} = X_f \times \frac{d_f^{\,2} \times \pi}{4} \times 12000 \tag{4.2}$$

X_f is the tensile strength of the fibre, T_f is the yield, the weight per unit length, ρ_f is the density of the fibre and d_f is the diameter of a single filament. The fibre properties are given in Table 2.1.

Table 4.1: Load carrying capacities of different tape materials

Material	N [-]	F_U [N]	s [N]	$C.O.V$ [%]	F_{U1} [N]	F_{U2} [N]
Tape I	7	1840	110	5.98	---	---
Tape II	6	1780	74	4.19	2010	2020
Tape III	6	2060	55	2.67	2180	2260
Tape IV-1	10	1830	55	3.02	2180	2260
Tape IV-2	10	1790	111	6.21	2180	2260
Tape IV-3	10	1860	116	6.24	2180	2260

The discrepancy between the measured load carrying capacity and the expected lower bound value is attributed to the following possible effects:

- The particular fibre batch may not have the strength quoted by the manufacturer.
- The processing, mainly the impregnation process is responsible for a certain amount of residual stresses and damaged filaments.
- The interfacial properties between fibre and matrix (see Section 4.2.2) may not be sufficient to transfer the load into the high strength fibres.

- The sudden, brittle failure of the specimens caused considerable secondary damage due to the release of the elastic energy in the specimen. It was very difficult to determine the origin and nature of the failure in the tensile experiments described in Section 3.2.1. Hence, failure may have been initiated in the gripping area.

An attempt was made to have load-transferring fixtures, which would provide a more even stress distribution and therefore lead to a higher load carrying capacity. A conical shaped steel socket in combination with an epoxy based casting resin, as described in Section 3.2.1, was used to anchor single tape specimens of the Tape IV-3 material. A second specimen had a rectangular cross-section of 3 by 6 mm and was made from twenty layers of tape according to the procedure given in Section 3.2.1. Three single tapes failed without any longitudinal splitting at the end of the epoxy load transfer medium. The average tensile capacity was 58 % of its expected value. In the case of the thicker specimen it pulled out of the socket at 54 % of the expected load. There was no failure of the specimen to be seen.

4.2.2 Mechanical properties

The Tape IV-3 material (V_f = 56%) was characterised in detail. It is the author's recommendation that this material type will become the standard for future applications of non-laminated pin-loaded straps. The justification for this recommendation will be made using the results given in this Chapter.

A typical stress against strain curve for a Tape IV-3 specimen, measured according to the procedure given in Section 3.2.1, is shown in Figure 4.1. The non-linear nature of

the curve indicates a continual increase in the longitudinal stiffness with increasing load. This effect is believed to be attributed to non-aligned filaments which become more accurately aligned as the tensile load in the tape is increased. The presence of a slight fibre misalignment is inherent when the material is processed. It is also known that the carbon fibres experience a certain non-linearity in their stress-strain response. The microstructural graphite layers forming a single filament have been found to become more accurately aligned as the load increases (see Guigon, Oberlin and Desarmot 1984 and Bunsell and Somer 1992).

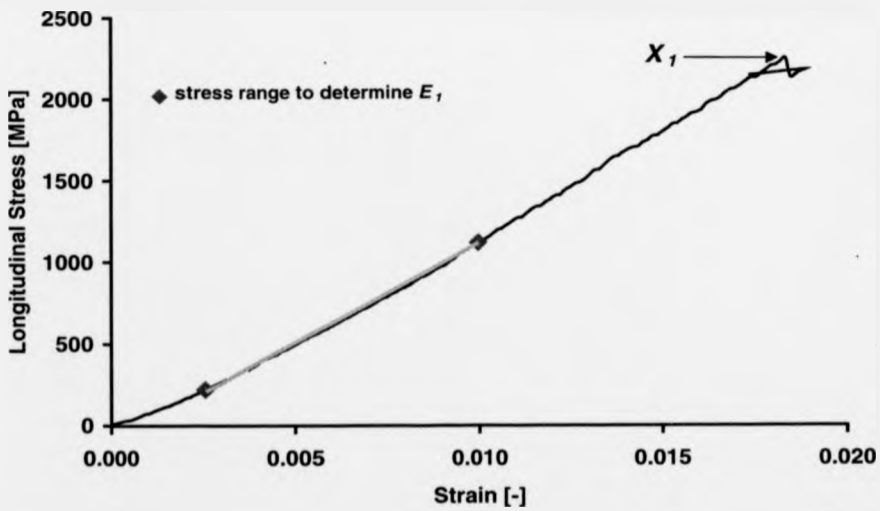

Figure 4.1: Stress-strain curve of Tape IV-3 material.

The longitudinal modulus, E_1, and the longitudinal strength, X_1, of a unidirectional composite can be calculated using the Rule of Mixtures equations

$$E_1 = E_f \times V_f + E_m \times (1 - V_f) \tag{4.3a}$$

$$X_1 = X_f \times V_f + \sigma_{mU} \times (1 - V_f)\,. \tag{4.3b}$$

Subscripts *f* and *m* are for the constituent fibre and matrix property, respectively, and V_f is the fibre volume fraction. Equation (4.3a) allows an accurate prediction of E_1 with, according to Hull (1981), an error of less than 2 %. E_1 was determined experimentally according to EN 2561 as described in Section 3.2.1 using the secant gradient between 10 and 50 % of the failure stress. This method to calculate E_1 is shown in Figure 4.1. The difference in Table 4.2 between the calculated and the measured E_1 suggests a certain amount of misaligned fibres in the tape. Equation (4.3b) is not particularly accurate, since strength not only depends on the average constituent properties but also on the fibre matrix interaction.

A number of micro-mechanical, semi-empirical models to predict the transverse modulus, E_2, and the shear modulus, G_{12}, of a unidirectional composite are described by Meier (1996). Equations (4.5) and (4.6) represent models for the particular case of a composite with orthotropic carbon fibres. Poisson's ratio, ν_m, for plastics is according to McCrum et al. (1988) about 0.4. The shear modulus of a carbon fibre, G_f, is quoted by Donnet and Bansal (1990) to be 21 GPa. The shear modulus, G_m, of the matrix is determined using equation (4.4), since it can be assumed that the polymer is an isotropic, homogeneous material. The remaining constituent properties used for the calculations reported in Table 4.2 are given in Section 2.3.

$$G_m = \frac{E_m}{2 \times (1 + \nu_m)} \tag{4.4}$$

$$E_2 = \frac{\frac{E_m}{1 - \nu_m^2} \times (1 + V_f^3)}{(1 - V_f)^{0.75} + 6 \times V_f \times \frac{E_m}{E_f \times (1 - \nu_m^2)}} \tag{4.5}$$

$$G_{12} = \frac{G_m \times (1 + 0.25 \times V_f^{0.5})}{(1 - V_f)^{1.25} + 1.25 \times V_f \times \frac{G_m}{G_f}} \qquad (4.6)$$

Table 4.2: Mechanical properties of the Tape IV-3 material.

Description		N [-]	Measured	s	$C.O.V.$	Calculated
E_1	[GPa]	10	121	3.60	2.98	129 (4.3a)
E_2	[MPa]	1	4830	n / a	n / a	3470 (4.5)
G_{12}	[MPa]	1	1550	n / a	n / a	1580 (4.6)
X_1	[MPa]	10	2250	141	6.29	2760 (4.3b)
X_2	[MPa]	1	27.7	n / a	n / a	---
S	[MPa]	1	40.9	n / a	n / a	---

Table 4.2 compares measured moduli and strengths with theoretical values using the micro-mechanical models outlined above. The transverse tensile strength, X_2, and the shear strength, S, quoted in Table 4.2 are given for completeness of the results. The measured values of the properties in transverse and shear direction are indicative, taken from one specimen only. The variation of the longitudinal properties is given with the standard deviation, s, and the coefficient of variation $C.O.V.$

The stress-strain curves in Figures 4.2 and 4.3 show the matrix dependent non-linearity of the Tape IV-3 material in the transverse direction and under in-plane shear loading. The measurements were performed using purpose made tube specimens and the method by Puck and Schürmann (1982). A description of this method is given in Section 3.3.2. The non-standard method of testing introduces errors in the measurements because the processing of the tube specimens alters the thermal history of the matrix material. It is therefore to be expected that the matrix-dominated properties have been altered. It is to

be noted that the geometry of the tape material does not allow the use of standard coupon testing, except in the longitudinal direction.

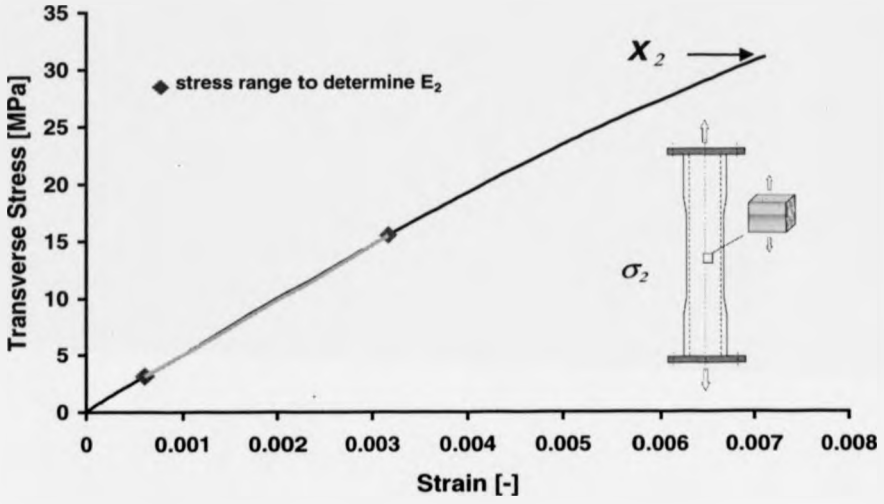

Figure 4.2: Non-linear stress-strain curve of Tape IV-3 material in transverse direction.

The transverse modulus E_2 and the shear modulus G_{12} were determined analogously to E_1, using a secant between 10 and 50 % of the stress at failure. This procedure is shown in Figures 4.2 and 4.3. The measurements given in Figures 4.2 and 4.3 represent the mean values of the four strain gauge locations (see Section 3.2.2) to account for bending effects due to possible misalignment. The shear stress, τ_{12}, is calculated for the outer surface of the specimen using Equation (4.7).

$$\tau_{12} = \frac{2 \times T \times r_o}{\pi \times (r_o^4 - r_i^4)} \qquad (4.7)$$

Where T is the twisting moment, r_o, the outside- and r_i, the inside radius of the specimen.

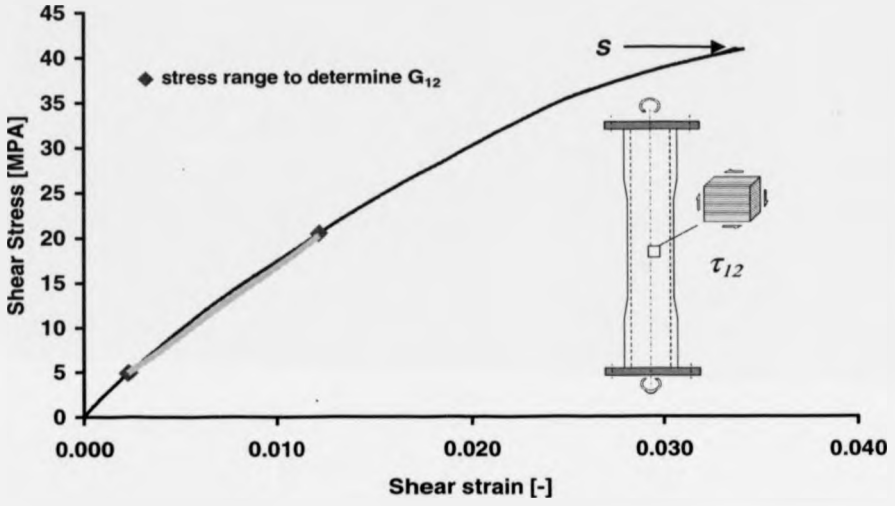

Figure 4.3: Non-linear shear stress-shear strain curve of Tape IV-3 material under in-plane shear loading.

4.2.3 Frictional properties

The frictional properties for Tape II material were determined in accordance with standard DIN 53375. The test method is described in Section 3.2.3. The DIN standard was originally developed to determine frictional properties of polymeric film materials. The applied dead weight was varied from 5.78 to 30.78 kg resulting in a normal stress, σ_n, from 0.03 to 0.17 MPa, which is considerably lower than the through-thickness stress in pin-loaded straps (see Sections 5.4 and 5.5). A typical load displacement curve is shown schematically in Figure 4.4. The horizontal force, F_h is the maximum and

represents the force at the transition from a stick to a slip behaviour. It is the static coefficient of friction which allows an even strain distribution in a non-laminated pin-loaded strap element. A high coefficient of friction prevents relative displacements between individual layers. Whereas a low coefficient of friction leads to an unwrapping process when a non-laminated strap is stretched to its working load (see Section 4.4.2). Therefore, the concept of non-laminated pin-loaded straps relies on controlled frictional properties between the individual layers. The friction coefficient, μ, is calculated from the normal force, F_n, and the horizontal force, F_h, for each specimen combination using

$$\mu = \frac{F_h}{F_n}. \tag{4.8}$$

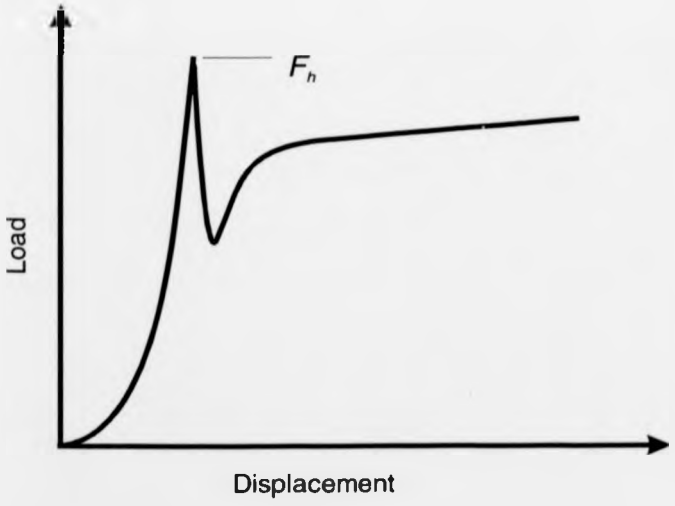

Figure 4.4: Schematic load displacement curve.

The measurements presented in Figure 4.5 indicate no influence of the normal stress within the investigated range. The error bars in Figure 4.5 represent the standard

deviation from three measurements for all the friction partners investigated except the Wrightlon®/CFRP combination where five measurements were performed.

In addition to the friction partners (Steel/CFRP and CFRP/CFRP) encountered in a pin loaded strap, two combinations with CFRP and polymeric films were also tested. A Teflon® film of 0.15 mm thickness between two layers of CFRP prepreg tape was found to reduce the coefficient of friction, μ, by 60 %. A Wrightlon® polymethylpentene film of 0.05 mm thickness increased the coefficient of friction by 90 %. This range of frictional properties may be used to optimise non-laminated pin loaded straps with a large number of layers.

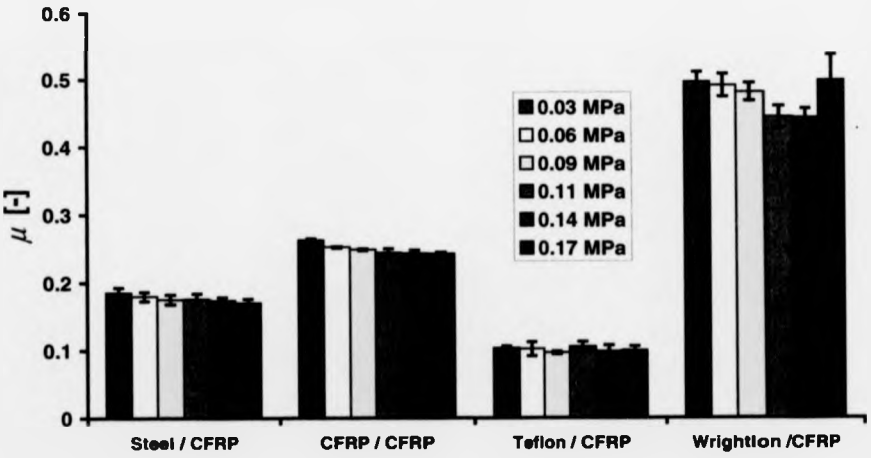

Figure 4.5: Frictional properties of Tape II material.

The frictional properties have not been determined on the other materials which replaced Tape II as the material development evolved. The experimental method used does not allow realistic testing conditions. The results in Figure 4.5 must therefore be

viewed with caution. In Section 6.1, the author proposes an improved test method to accurately determine the value of μ.

4.3 Anchorage methods

A critical aspect for a successful application of non-laminated pin-loaded straps was the development of a suitable end anchorage for the final external layer. There are two different options available. Both have their merits depending on the application. One option is for the end of the final layer to be anchored to the surrounding structure by means of clamping or bonding as shown in Figure 3.16. The alternative option is to anchor to the strap itself as shown in Figures 3.14 and 3.19.

The six distinct failure modes that may occur in the end anchorage, are shown schematically in Figure 4.6. Certain modes do not manifest themselves. The mode of failure found in the tests depends on material and strap design. The most effective anchorage is achieved when the tensile failure load of the parent material can be reached (mode A). Mode A occurs at a load level for the tape that is higher than the tape material will be subjected to in a non-laminated pin-loaded strap because of stress concentrations (see Sections 5.4 and 5.5) in the pin region. The desired mode A provides the highest margin of safety against strap failure due to an anchorage failure in the final layer.

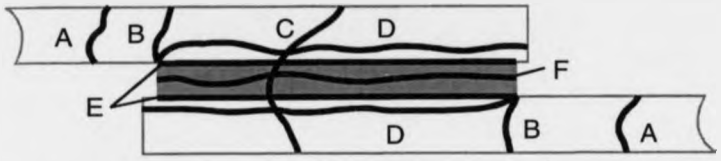

Labels

A Longitudinal tensile failure of the parent material

B Longitudinal tensile failure of the parent material at the joint edge

C Longitudinal tensile failure of the parent material within the joint location

D Transverse failure of the parent material

E Interfacial failure

F Cohesive failure

Figure 4.6: Possible failure modes of the end anchorage.

Adhesive bonding of thermoplastic composites requires extensive pre-treatment to prevent interfacial failures (mode E) by increasing the surface energy of the matrix. According to Rasche (1987), reasonable strength properties can be achieved using methods such as corona or gas plasma pre-treatment. Furthermore, these methods do not result in a permanent increase of the surface energy and should therefore be applied shortly before the bonding process (see Schindel 1988).

A more economic and environmentally friendly joining method is the fusion bonding method described by Arias (1998). This method is essentially a welding process using a thermoplastic matrix. Shear strength values of 50 MPa have been reported by Wise (1992) using a single lap-shear configuration and Tape I material. The supplier of Tape I material quotes an interlaminar shear strength of 97 MPa (Fiberite 1989) which results in a joint efficiency of about 52%.

The fusion bonding process described in Section 3.3.2 allows the production of very effective joints. The tensile load capacity of lap-shear specimens using Tape IV-1 material is shown in Figure 4.7. The bars represent the mean values taken from six specimens. The error bars show the standard deviation as a measure of the variation of the data. The reference is the parent material's tensile capacity taken from Section 4.2.1. The influence of the welding temperature is not significant within the investigated range with a maximum difference in the mean capacity of only 1.5%. Hence, the chosen welding temperature for all the following investigations was 185°C where 87% of the parent material's tensile capacity could be reached. The observed failure mode was a combination of modes B and D. The interlaminar failure of the parent material (mode D) is believed to be a secondary effect occurring immediately after the local tensile failure initiated (mode B).

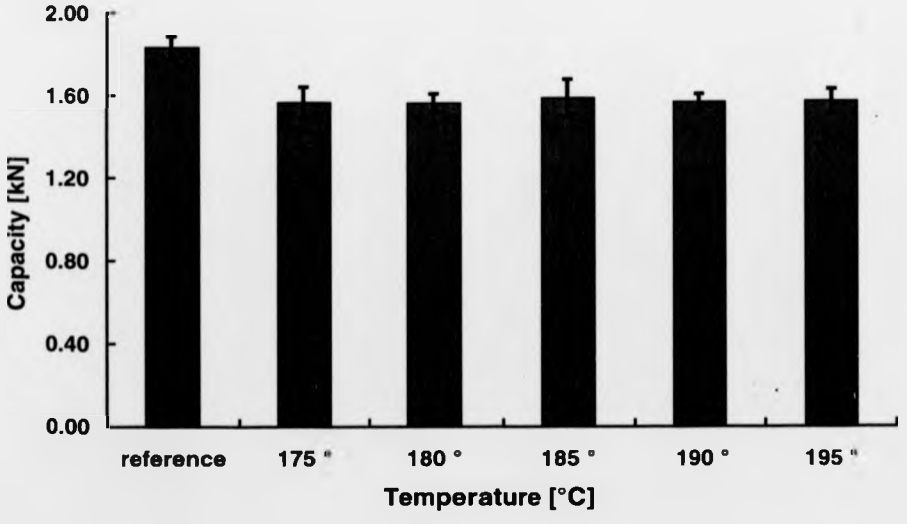

Figure 4.7: Lap shear properties of Tape IV-1 material at different welding temperatures.

The tensile capacity of lap shear specimens using Tape IV-3 material is shown in Figure 4.8. The error bars represent the standard deviation based on six specimens. The tensile capacity is clearly different to the one using Tape IV-1 material. Only 65 % of the load carrying capacity could be reached with the single lap-shear specimens described in Section 3.3.2. The Tape IV-1 material (V_f = 41%), having a considerably lower fibre volume fraction, allowed 87 % of the load carrying capacity to be transferred. The higher fibre volume fraction of the Tape IV-3 material (V_f = 56%) resulted in higher stress concentrations at the ends of the lap-joint. This may be due to the reduced bond-line thickness which has a considerable influence on the stress distribution (Bresson 1971).

The eccentricity in the load path is not considered to be important with a lap-length to joint thickness ratio of about 240 and a joint thickness of about 0.4 mm. Single lap-joints with such geometrical features are known to be relatively efficient (Mottram 1998).

The problem of a reduced joint strength with higher fibre volume fraction tape, such as Tape IV-3 can be solved by placing, before the fusion bond is made, a thin polymer film between the two mating surfaces. This approach to remedy the low joint strength is described in Section 3.3.2. The film used was of PA 12 material, the same polymer as the matrix of the tape. It has a thickness of 40 μm. Employing this approach to control the bond-line thickness resulted in a lap shear strength of 99 % of the strength of the parent material (see Figure 4.8). Hence, the failure of the single layer lap-joint was not governed by the presence of the joint. The mode of failure could not be established due to the damage associated with the failed specimens.

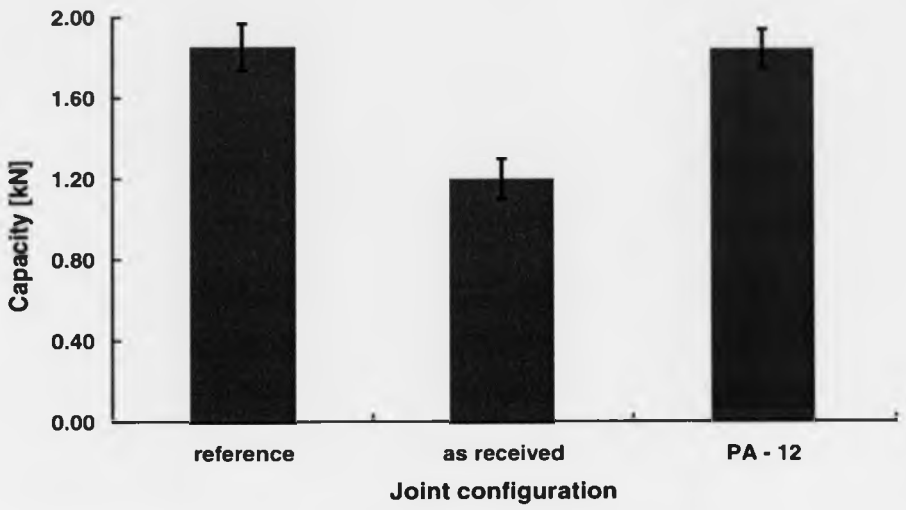

Figure 4.8: Lap-shear properties of Tape IV-3 material with different joint configurations.

4.4 Pin loaded straps

4.4.1 Laminated

Pin-loaded straps are generally described in the German literature (Michaeli and Wegener 1989) as a fibre conform design. A fibre conform design is defined as a preferred method for load transfer into composite materials. This statement may be valid for small radius ratios as indicated in Figure 4.9. The stress σ_{UStrap} in the gauge length at ultimate failure load of a strap is plotted versus the ratio of outside, r_o , to inside radius, r_i. The experimental values taken from the literature are based on different types of carbon fibre and have therefore been normalised with respect to the material's

virgin tensile strength X_1. The strength of the materials was determined by the author using the Rule of Mixtures Equation (4.3b) and information from the papers. This normalisation procedure provides a convenient way by which a measure for the efficiency of the load transfer can be achieved. Figure 4.9 shows a considerable variation of the experimental data. Although the general trend is a considerable reduction in the efficiency of the load transfer with increasing radius ratio. This is attributed to stress concentrations which reduce the load at failure compared to that of the virgin material, as determined by Equation (4.3b).

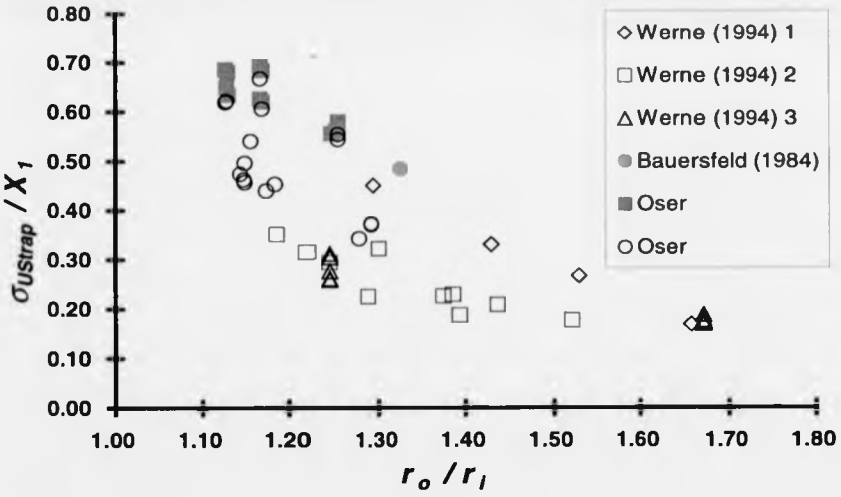

Figure 4.9: Efficiency of the load transfer versus radius ratio of laminated pin-loaded straps

The sources of the data plotted in Figure 4.9 are given in the legend. The number after the first author's name refers to a different manufacturing process. For the laminated strap specimens tested by Werne (1994) the processes are:

- 1: Filament wound; Oven cured.
- 2: Filament wound; Cured in a hydraulic press with integrated heating.
- 3: Filament wound; Cured in a hydraulic press with integrated heating using a multiple mandrel.

The different processes resulted in different fibre volume fractions, V_f, which may be a contributing factor for the variation in the load transfer efficiency.

The data in Figure 4.9 acquired by Oser have not been published previously and are taken from an unpublished internal report. His data given by the filled square symbols were from tests using an end fixture restricting transverse deformations. Oser's other data given by the unfilled symbols gave an inferior performance. These straps were tested without the restraining end fixture. Conen (1966) and Hütter (1966) have reported the same beneficial influence of having the transverse deformations limited (see Section 5.5) on pin-loaded straps made from glass fibres. Their work found an increase in the capacity of 35% when using a restraining end fixture.

Laminated pin-loaded straps were manufactured and tested by the author according to methods in Section 3.4.1. These straps of Tape IV-1 material were tested in order to provide performance indicators to compare with the non-laminated straps. Table 4.3 gives the mean measured, $F_{measure}$, and the predicted, $F_{predict}$, load carrying capacities based on the number of layers and the measured load carrying capacity of a single layer (see Table 4.1), assuming 100 % load transfer efficiency. The first number in the specimen identification represents the inside radius r_i, the second number refers to the number of consolidated layers of tape. The columns for the measured results contain the

mean load values, $F_{measure}$, the standard deviation, s, and the coefficient of variation, $C.O.V.$ from the number of specimens, N. The efficiency is the ratio of $F_{measure}$ to $F_{predict}$.

Table 4.3 Load carrying capacities of laminated pin-loaded straps made from Tape IV-1 material.

specimen	$F_{predict}$ [kN]	N [-]	$F_{measure}$ [kN]	s [kN]	$C.O.V.$ [%]	efficiency [%]
15-5	18.3	5	13.6	1.90	14.0	74
15-10	36.6	5	26.1	2.03	7.8	71
15-15	54.9	5	31.9	1.23	3.9	58
25-5	18.3	6	14.4	0.53	3.7	78
25-10	36.6	5	28.7	1.68	5.9	77
25-15	54.9	5	39.0	2.71	7.0	71
75-5	18.3	4	14.6	0.73	5.0	80
75-10	36.6	5	31.4	0.93	3.0	86
75-15	54.9	5	46.3	1.04	2.2	84

Larger radius ratios (> 1.2) could not be achieved using the manufacturing process described in Section 3.4.1. The data presented in Table 4.3 is also given in a different form in Figure 4.10. The measured load carrying capacity is plotted versus the ratio of outside, r_o, to inside, r_i, radius. The experimental data have been normalised with respect to the measured tensile capacity of the material and a theoretical load carrying capacity using Equation (4.1). The graphs show a substantial reduction of the load transfer efficiency, even at relatively small radius ratios (< 1.2), compared to what is seen in Figure 4.9. The high scatter of the results may have been caused by imperfections introduced in the manufacturing process of the specimens. The method used to manufacture the strap specimens is given in Section 3.4.1. The two graphs show

the discrepancy when measured and theoretical load carrying capacities are used for the normalisation procedure.

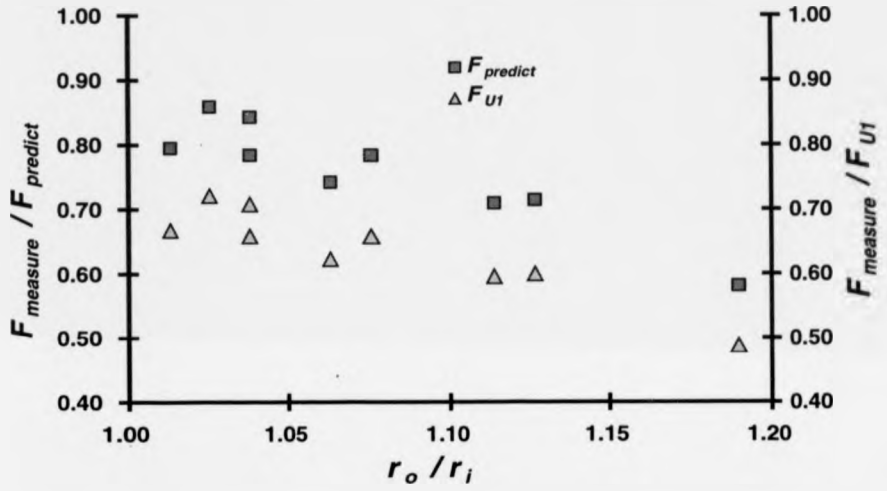

Figure 4.10: Efficiency of the load transfer versus radius ratio of laminated pin-loaded straps made from Tape IV-1 material.

An interesting observation was made during the experimental investigation. Premature fracture events could be detected acoustically at about 84 % of the ultimate failure load in 24 % of the tested specimens. These specimens experienced more delamination damage in the load transfer region, than others. This is shown in Figures 4.11 and 4.12, where a typical example of both types is presented. It is assumed that these pre-ultimate fracture events are interlaminar shear failures. They may even be beneficial to performance of the straps in alleviating the stress concentrations. The residual strength, after cyclic loading of similar laminated pin-loaded straps, was determined by Krüger

(1985). The fatigue loading increased the residual strength by about 15 %. This was attributed to relaxation effects in the epoxy matrix.

Figure 4.11: Failure mode of a laminated pin-loaded strap with extensive longitudinal splitting.

Figure 4.12: Typical failure behaviour of a laminated pin-loaded strap.

4.4.2 Non-laminated

To achieve the ideal situation of an optimum load transfer in a non-laminated pin-loaded strap all the layers should be strained equally (Winistoerfer and Mottram 1997). This can only be fulfilled if rigid body movement is superimposed on the elastic deformation of the tape. The rigid body movement has to be limited by controlled frictional properties in the load transfer region. An alternative method to uniform straining is a temporary reduction of the normal force caused by the contacting bodies.

Initial screening tests on non-laminated pin-loaded straps were performed using the Tape I material. Non-laminated pin-loaded straps of five layers with epoxy bonded end anchorages were produced for these screening tests. The clamped end anchorage described in Section 3.3.1 was not available at the time these tests were conducted. As outlined in Section 3.4.2, pressing plates were also applied to increase the strength of the adhesively bonded end anchorage. Static tests with monotonically increasing load where performed.

The relative displacements required to achieve a uniform load transfer throughout all the layers did not seem to take place. This poor results were due to the rough surface texture of the tape, it being similar to the texture shown in Figure 2.10. Therefore a number of dynamic loading cycles were introduced, prior to the final static loading, in order to overcome the 'stick-slip' transition by a temporary reduction of the normal force. The specimens were loaded with 30 cycles (between 1kN and 10 kN) at about 6 Hz before the load was increased up to failure. The measurements on Tape I material resulted in an average efficiency of the load transfer of 87 %, based on the measured load carrying capacity of the material given in Table 4.1.

One of the specimens was instrumented with two strain gauges, as described in Section 3.4.2, to determine the strain difference between the innermost and the outermost layers. In the perfect strap, when exact relative movement between individual layers is taking place, the two strain gauge measurements should be equal. The strain gauge measurements are given in Figure 4.13. Each loading cycle causes some movement between the individual layers to take place and the arrows in the figure show this development with the cyclic loading. Decreasing strain in the innermost layer (layer 1) and increasing strain in the outermost layer (layer 5) is evidence to support this observation. Even after thirty cycles there is still a considerable difference between the two strain measurements. This information suggests an uneven strain distribution throughout the cross-section of the strap, thus the non-laminated pin-loaded strap is not ideal.

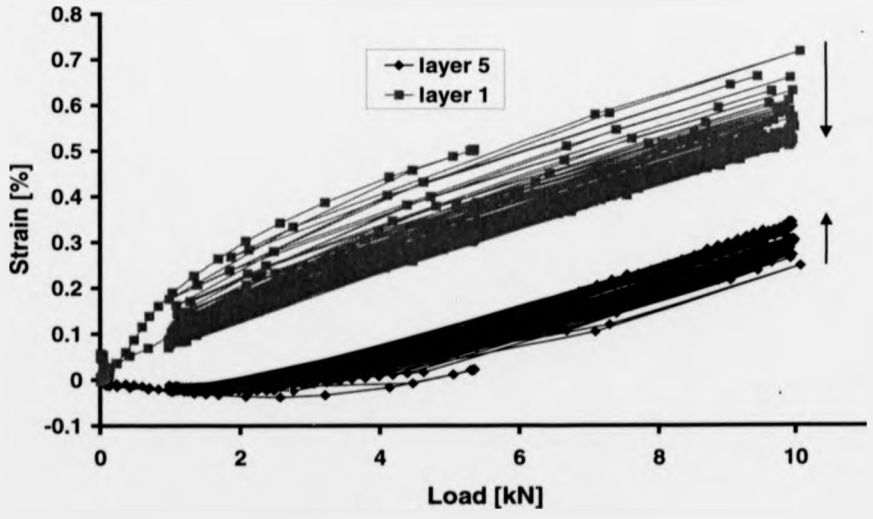

Figure 4.13: Strain gauge measurements of a non-laminated pin-loaded strap made of Tape I material subjected to cyclic loading.

To investigate the influence of the pin diameter on the performance of the load transfer, a parametric study was carried out varying the pin diameter. A single ply was wrapped around two identical steel pins and was anchored using pressure pads as described in Section 3.4.2. Each strap was loaded in tension to ultimate failure. The influence of the frictional properties was determined using a Teflon® film at the interface between the steel pin and the tape. The mean load carrying capacities of one leg of single layer straps are given in Figure 4.14. The error bar represents the standard deviation taken from ten specimens. A marginally higher mean load carrying capacity was found with the Tape II material and the reduced friction coefficient. The increase was more pronounced when the pin diameter was $\leq$ 35 mm. Within the investigated range of pin diameters, the load carrying capacity is not significantly influenced. This observation applies particularly to the Tape IV-2 material straps. Although a smaller pin diameter is expected to have considerable influence, the selected pin diameter for future investigations was 30 mm. This diameter is believed to represent the smallest and therefore the most critical that will be used in most practical applications.

The next development stage was achieved by a certain improvement in the tape quality. A strap specimen consisting of seven layers of Tape III material had the clamped end anchorage, as described in Section 3.4.2. It was placed into a purpose made test-rig in a servo-hydraulic Instron machine. Figure 4.15 shows that the tape edges were marked with white paint. A digital camera was placed in front of the marks to take pictures of the relative deformation as the load was increased. The digital camera is necessary to get immediate results of the relative displacements which allows instantaneous response on the controls of the machine.

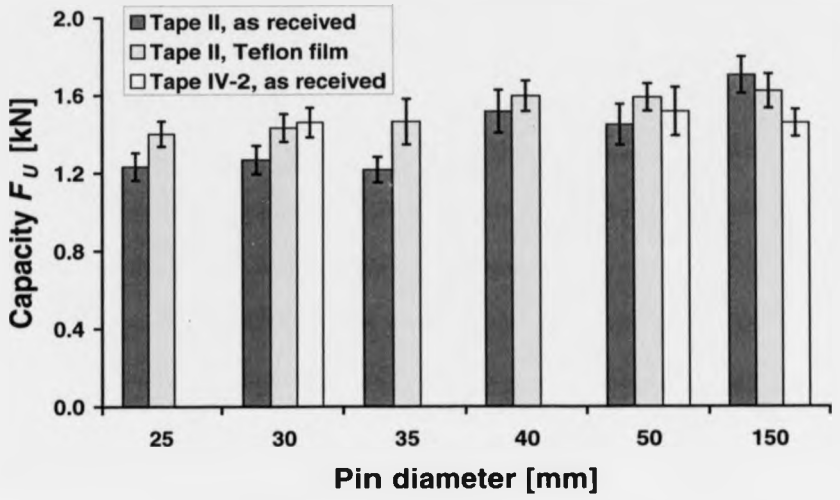

Figure 4.14: Load carrying capacities of one leg of a single layer of tape wrapped around steel pins of different diameters.

A small modification on the signal generator of the servo-hydraulic Instron machine allowed the use of a second external generator to superimpose a high frequency ripple to the applied load. The second generator was tuned to a frequency of 30 Hz and to an amplitude of 5 % of 20 kN (the anticipated failure load). These control conditions are beyond the limitations of the servo hydraulic testing machine and therefore it can be assumed that the specimen was subjected to a different loading condition.

The superimposed ripple is responsible for a temporary reduction of the normal forces acting in the through-the-thickness direction of the tape. It therefore reduces the frictional resistance and thereby promotes relative displacements between individual layers. A schematic load time history is shown in Figure 3.17.

The measurements displayed in Figure 4.15 show the relative displacements between individual layers with increasing load. The image on the far left is at the beginning of the experiment at 7% of the measured failure load. It indicates that there was no contact between different layers in the free length of the specimen. As the load was increased the layers move closer together and slide over each other as shown in the consecutive images at 27%, 67% and 94% of the measured failure load. This relative change in the positions of the layers is clearly seen in Figure 4.15.

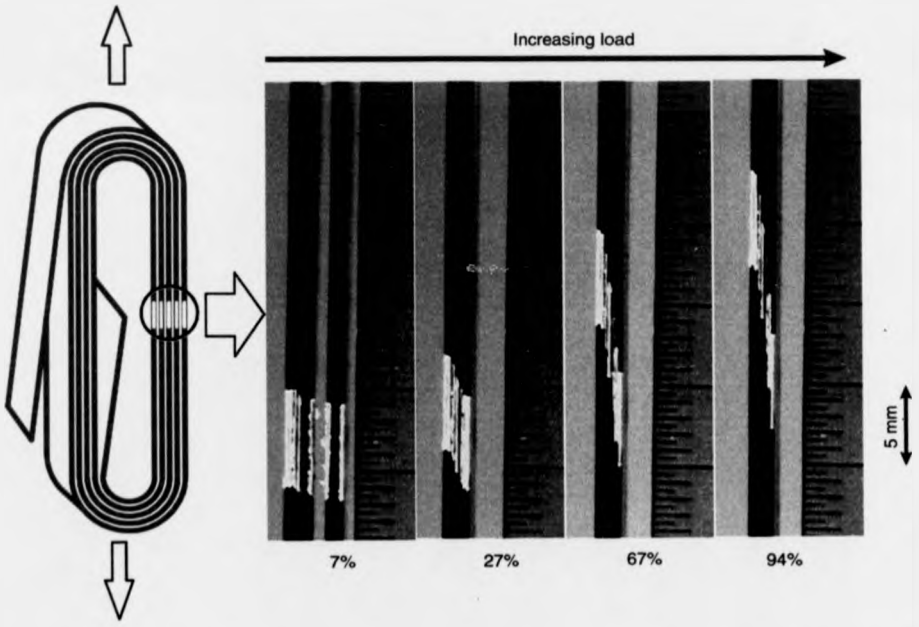

Figure 4.15: Relative displacements between individual layers at different load levels.

The drawback of this approach to produce an efficient non-laminated strap system is the lack of control over the amount of relative displacement. The final layer was clamped to the test fixture (see Figure 3.16), and so it did not provide any restraint to the maximum

length of the specimen. Under these test conditions it was found that the non-laminated pin-loaded strap gradually unwound as the load time history was applied. The amount of relative displacement between the innermost and the outermost layers was about 10 mm.

Simplification to the production of straps was achieved with the development of the Tape IV-3 material (see Chapter 2). The regular surface texture and the superior accuracy of the width and edge contours was found to improve the load carrying system substantially. Furthermore, the relative displacements needed for the uniform strain distribution to exist could be generated without the application of any sophisticated dynamic loading. This demonstrates that the correct material characteristics are essential if non-laminated pin-loaded straps are to find applications. The desired characteristics were achieved during the course of this project through the development of Tape IV-3 material.

A different approach to the one given above was used to show that the relative displacements had occurred. Strain gauges were applied to different layers in two straps made of Tape IV-3 material. The final layer was anchored to the previous one using the fusion bonding process described in Section 3.3.2.

The measured strains in specimens consisting of 5 and 10 layers are shown in Figures 4.16 and 4.17, respectively. In Figure 4.16 the discontinuities in the curves at loads above 10 kN were a result of three loading and unloading cycles being performed between 0 and 10 kN load, prior to increasing the load up to failure. This procedure was selected to determine any difference in the strain distribution after a number of loading

and unloading cycles. No significant difference could be found, hence only the last loading cycle is shown in the figures. The two figures show a very uniform distribution of the direct strain measurements throughout all the layers. The specimen consisting of five layers (Figure 4.16) shows hardly any difference, whereas the innermost layer (No 1) of the specimen consisting of ten layers (Figure 4.17) experiences an increase of 9 % compared to the outermost layer.

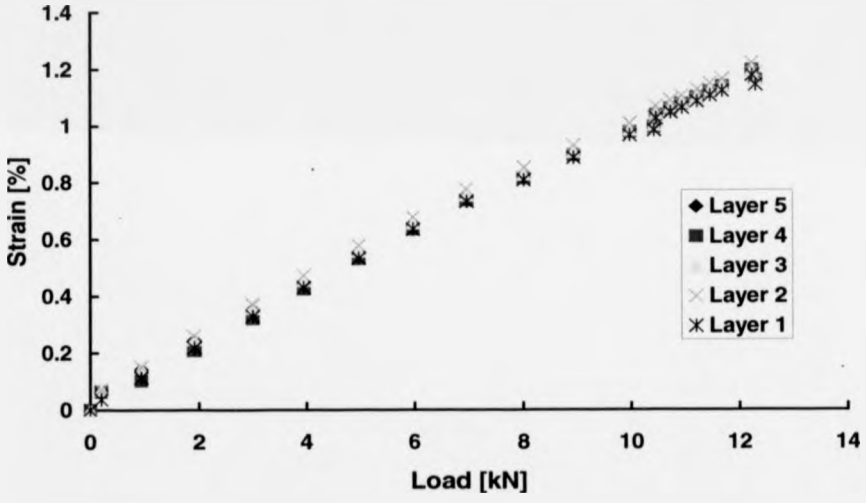

Figure 4.16: Strain in different layers of a five layer strap made of Tape IV-3 material.

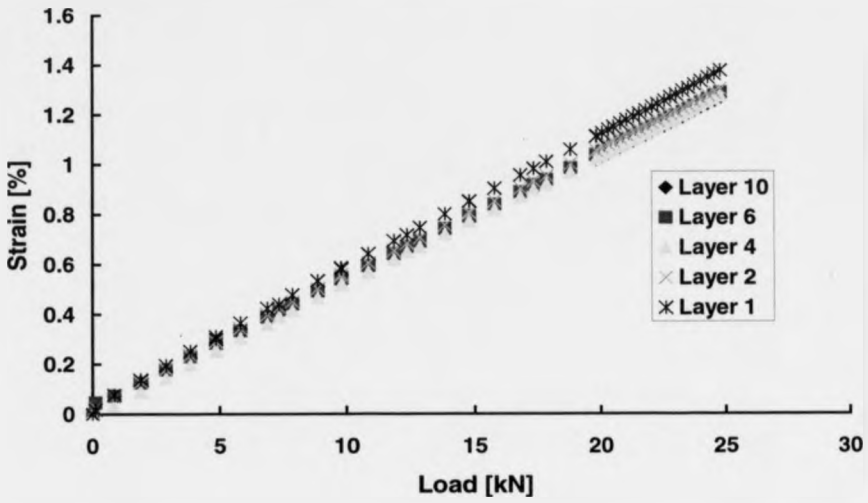

Figure 4.17: Strain in different layers of a ten layer strap made of Tape IV-3 material.

The mean capacities and the standard deviation, represented by the error bars, taken from three welded, non-laminated straps are shown in Figure 4.18. In addition, the capacities of equivalent straps with a clamped end anchorage, as described in Section 3.4.2, are given. There is almost a linear increase in the failure load with the number of layers. The clamped end anchorage configuration performed slightly superior compared to the fusion bonded technique.

Both fixing techniques, however, have their merits depending on the application of the strap. The results shown in Figure 4.19 represent the same experimental data with the mean failure load per layer normalised using the tensile capacity of the virgin tape material. The capacity of the tape was determined using the test method described in Section 3.2.1, and is given as the reference in Figure 4.19. For comparison, the tensile performance of laminated pin loaded straps is given for 5, 10 and 15 layers of tape. The

strength of the non-laminated strap is superior provided that the number of layers is larger than 10. A maximum increase of 29% is found with straps of 15 layers and clamped end anchorage. There appears to be a maximum in the failure load per layer at about 10 layers of tape. The load transfer mechanism relies on frictional effects between individual layers and the normal force acting on an individual layer is dependent on the number of layers. This may be a reason why there is an optimum number of layers. Future research is needed to establish the optimum number of layers.

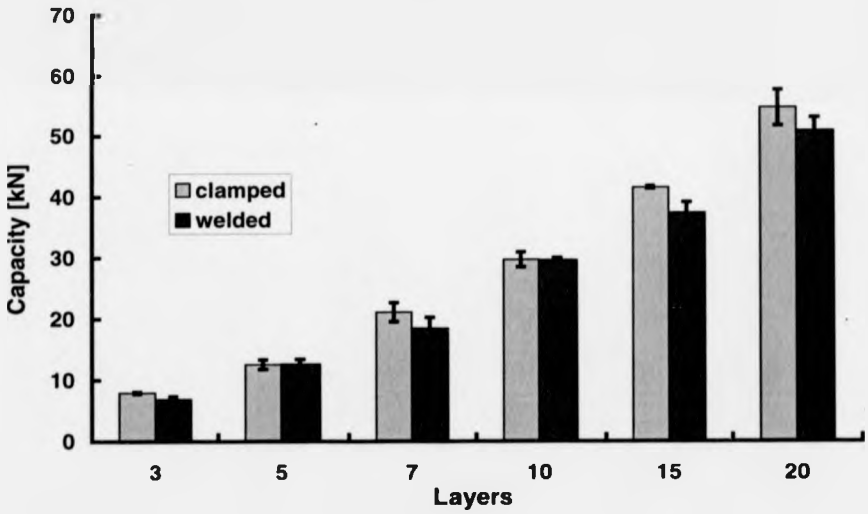

Figure 4.18: Tensile capacity of Tape IV-3 non-laminated pin-loaded straps

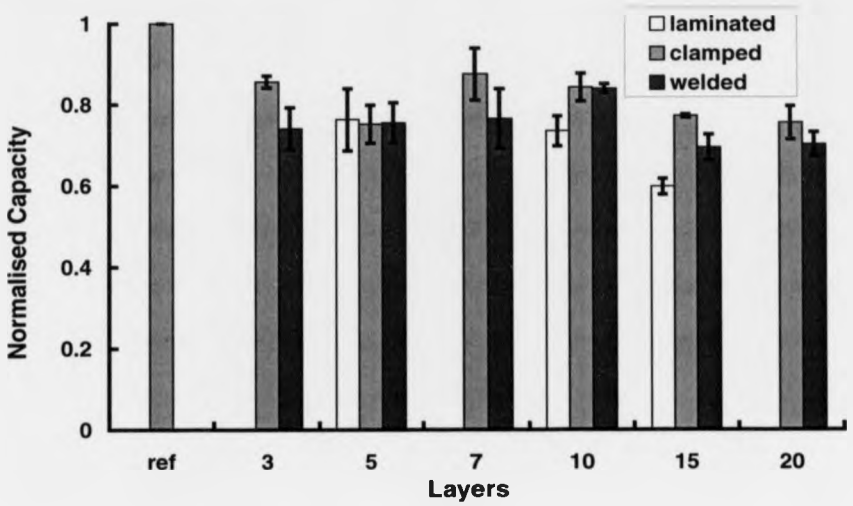

Figure 4.19: Normalised performance of non-laminated pin-loaded straps as a function of the number of layers

Observations during testing showed that the failure of a non-laminated pin-loaded strap was of a progressive type, starting within the innermost layer. Failure was initiated in the region adjacent to the pin-strap interface. This is supported by the failure seen of the specimen shown in Figure 4.20. It can be seen that the outside layers remained separate and intact, whereas the failed inner layers are severely fractured and joined together. The released elastic energy in a fracture event probably allowed sufficient relative displacement between damaged and intact layers to fusion bond these layers together.

The extensive failure in the pin region become more dominant as the number of layers increased. It would be expected, however, that if failure was governed only by the stress in the pin region then there would be no difference in capacity when the anchorage was either clamped or welded. It can be seen in Figure 4.19 that the straps with clamped

anchorage had a higher load carrying capacity, thereby indicating that failure was also dependent on the anchorage method. The reason for the contradictory results are unclear and this lack of understanding is one aspect for further work.

Figure 4.20: Load transfer area of a failed non-laminated pin-loaded strap

4.5 Long term creep performance

The creep properties of non-laminated pin-loaded straps made from Tape IV-3 material were determined on three specimens employing the method described in Section 3.5. Specimens consisting of five layers were tested with different pin diameters. The applied load was 9.6 kN which is 76 % of the average static load carrying capacity, as reported in section 4.4.2 for the strap with 30 mm diameter pins. The same load was applied to the other two specimens having pin diameters of 50 and 150 mm. The creep strain, ε_t, was determined using

$$\varepsilon_t = \frac{\Delta L_{creep}}{L_O} \times 100 . \qquad (4.9)$$

ΔL_{creep} is the creep contribution to the extension of the specimen, neglecting the elastic contribution and, L_O, the initial distance between the centres of the two steel pins.

Three different contributions to the total creep strain are anticipated and these are:

- Creep of the prepreg itself in the longitudinal fibre direction which is expected to be small since longitudinal mechanical properties are dominated by the continuous fibres (Bieling 1983).
- Creep of the prepreg in the through-the-thickness direction which is limited to the load transfer region around the pin where transverse stresses are caused by the contacting bodies.
- Creep in the end anchorage of the final layer, particularly in the fusion bonded anchorage.

Of these three contributions the first two can be neglected since they are small due to the material or geometric properties of the strap. However, the creep in the end anchorage is considered to be a problem which may be serious enough to cause failure of the strap due to creep rupture.

It was hoped that by using different pin diameters to change the through-the-thickness stresses in the load transfer region, the different creep effects could be isolated. Unfortunately the creep results are not conclusive in this respect.

The test rig, shown in Figure 3.21, was equipped with two dial gauges having a resolution of 0.01 mm to determine the creep strain. The results from dial gauge I are given in Figure 4.21, and give the direct length measurements at the specimen. The

length variations between two consecutive measurements was often within the resolution of the gauge. The calculated strain is based on the distance between the centres of the two pins. Specific conclusions cannot be drawn from the direct strain measurements. because of the measurement resolution problem.

Dial gauge II was placed at the rear end on top of the cantilever beam (see Figure 3.21). This resulted in a magnification with a factor of 8.4 compared to the direct measurement. The results from the second gauge are presented in Figure 4.22. These measurements appear to be more reliable because of the sufficient resolution of the measurements but the movements in the test rig are also included. The test with the 50 mm pin diameter had to be terminated after 8900 hours because the rig failed due to stress corrosion in the spring steel sheet carrying the specimen. The 50 mm specimen did not show any obvious damage from the severe creep loading.

The fusion bonded end anchorage of the 150 mm specimen failed due to creep after 9800 hours. The same specimen experienced damage of unknown origin at 8400 hours where a dramatic increase of the strain was observed. The further measurements show a larger strain rate after the event. The event itself is not shown in Figures 4.21 and 4.22 since the data are manipulated to reduce the plotted range. The real measured data are given in Figure 4.23.

The failure of the 150 mm strap may have been a typical creep rupture type (Callister 1997), which occurred after primary, secondary and tertiary creep took place. There is an urgent need for further investigations of the creep properties of non-laminated pin-loaded straps since failure occurred at a load level below the short-term static.

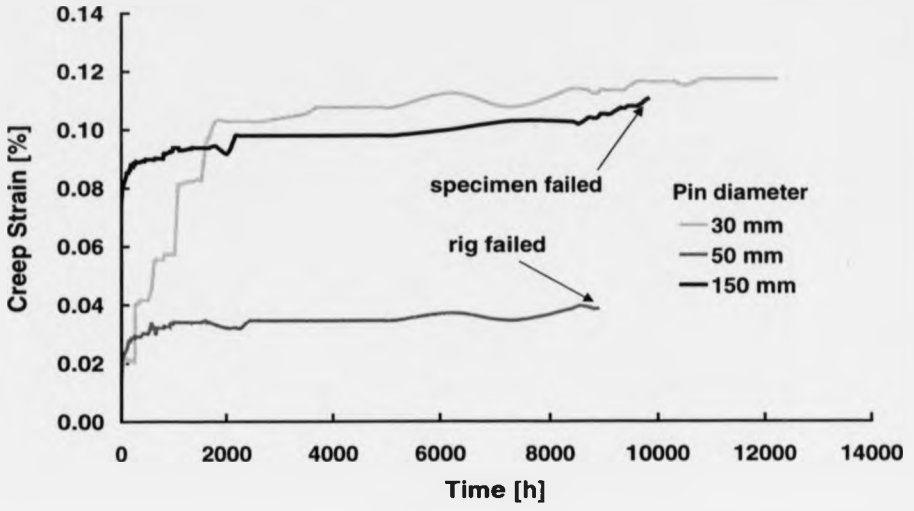

Figure 4.21: Direct measured creep data of Tape IV-3 straps with different pin diameters (150 mm data are manipulated).

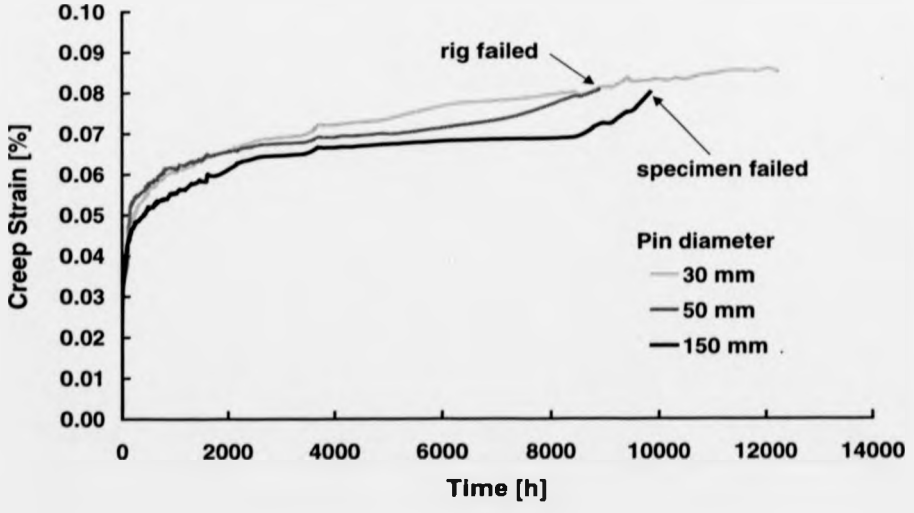

Figure 4.22: Indirect measured creep data of Tape IV-3 straps with different pin diameters (150 mm data are manipulated).

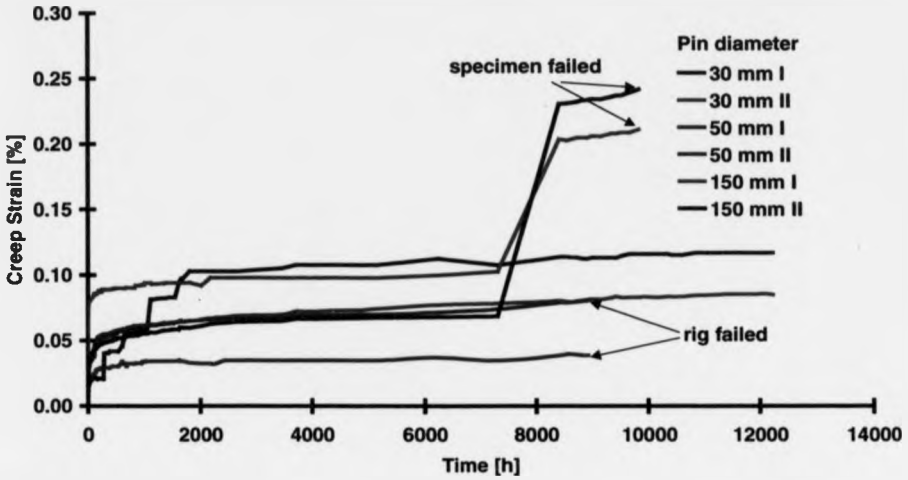

Figure 4.23 Measured creep data of Tape IV-3 straps with different pin diameters.

5 ANALYSIS

5.1 Introduction

This chapter gives the results of the analysis performed to determine stress distributions in pin-loaded straps. The modelling strategy employed is illustrated, and some of the difficulties encountered in finite element modelling, when the influence of contact and friction effects are considered. In addition, experimental results are compared with stresses from classical closed-form solutions and finite element models.

5.2 Modelling strategy

The ultimate goal of the numerical analysis was an acceptable model for a non-laminated pin-loaded strap consisting of a number of layers. MARC-Mentat, a general purpose finite element code was used for the finite element analysis (FEA). The software is, according to the vendor, very suitable to solve engineering problems involving contact and friction effects.

In reality, a pin-loaded strap is a three-dimensional contact problem which requires knowledge of the pin clearance, the frictional properties between pin and strap, the elasticity and support conditions of the pin, etc. As such the ultimate goal is outside the scope of this thesis. However, the essential features of a strap may be reproduced by

simplifying the problem to a two-dimensional one. This approximation is shown in Figure 5.1. The two-dimensional model will be generated in the x-y plane, cutting through the strap.

Since a non-laminated pin-loaded strap comprises a number of layers wrapped one on top of each other, the analysis commenced by studying a single layer of prepreg tape being wrapped 90° around a circular rigid body (representing the steel pin). Details and results are given in Section 5.4.2. The stress distributions resulting from this model were planned to be used as initial conditions for further analysis considering a multilayered non-laminated strap. Unfortunately, limitations in computational power and the sensitivity of the results, given in Section 5.4.2, to the numerical parameter described in Section 5.3 ensured that further analysis was not an option.

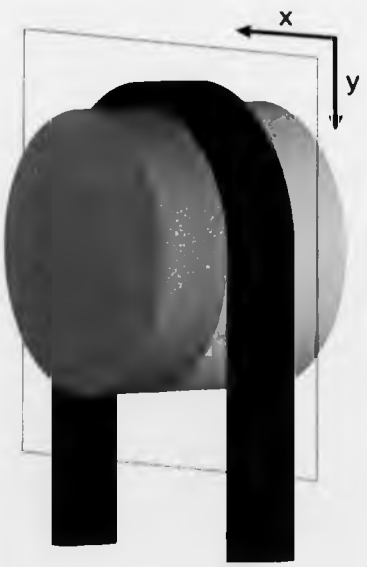

Figure 5.1: Schematic of a pin-loaded strap indicating the plane for the two-dimensional FE model.

5.3 Contact and friction modelling using MARC K6.2

Mechanical problems involving contact are inherently non-linear due to the unknown boundary conditions. A powerful way to deal with this non-linearity is to adopt a step-by-step incremental solution procedure. The time domain is thereby divided into a number of discrete steps, for which individual solutions are found, instead of finding a solution which satisfies all the required conditions at any time instant. Details of the incremental solution procedure can be found in Zienkiewicz and Taylor (1991). Contact problems always involve friction phenomena. In certain engineering problems where frictional forces are sufficiently small, they may be neglected to simplify the analysis. However, the frictional effects in non-laminated pin-loaded straps are vital to their successful performance and therefore cannot be neglected.

Unlike many other finite element software packages which require the use of designated contact elements, MARC K6.2 allows the user to define contact bodies within the standard set of elements. This enables the user to model complicated problems involving sliding contacts, whereby the location of contact does not have to be specified. The analysis of a metal blank in a sheet forming process is an example of an engineering problem where sliding contact exists.

In reality, such problems involve a transition from a state without relative motion between the two bodies to a state where the tangential force, F_t, reaches a critical value, and relative motion between the two bodies can occur. This effect will be referred to as the stick-slip transition. The numerical modelling of this effect requires a smooth transition instead of the step function which is typical in reality. The MARC K6.2 programmers invented a numerical parameter called relative sliding velocity, C, to

create a smooth stick-slip transition (MARC 1996). Equation (5.1) gives the expression for the tangential force in terms of C.

$$F_t = \mu \times F_n \times \frac{2}{\pi} \times tan^{-1}(\frac{v}{C}) \qquad (5.1)$$

Whereby, μ, and, F_n, denote the friction coefficient and the normal force, respectively. The user is required to provide this numerical parameter below which a sticking condition is simulated. The user manuals for MARC K6.2 does not give the analyst much guidance on how to determine the appropriate value for C. The author was also not able to find information on the contact algorithm in the open literature. The influence of C is shown in Figure 5.2 where the tangential force is plotted versus the tangential velocity, v. A small value for C (< 1mm/s in the example shown below) is a good representation of 'reality', but fails to provide a convergent solution. Whereas a large value for C (>10 mm/s) provides a convergent solution but represents the 'reality' inadequately. It is recommended by MARC (1997) that the value of C should be 1 to 10% of a typical tangential velocity, v. The influence of this parameter on the resulting stress distributions is investigated for a single layer strap in Section 5.4.2.

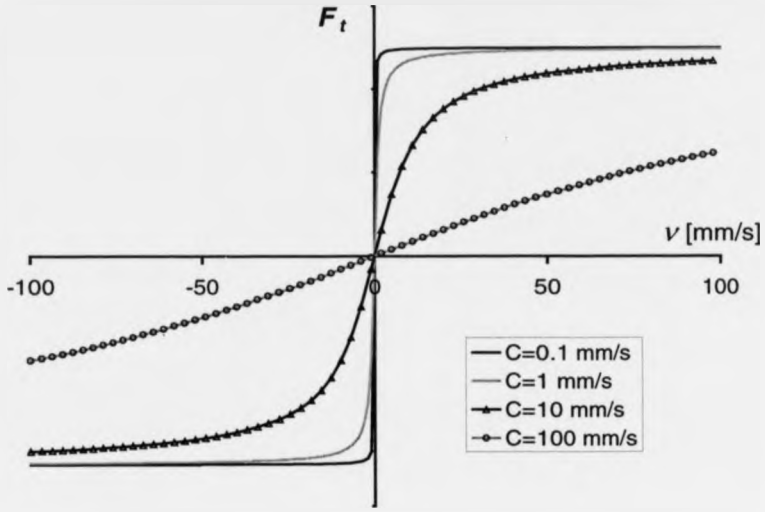

Figure 5.2: Stick-slip transition for various relative sliding velocities.

Details of the numerical methods used in the code to consider the influence of contact and friction causing non-linear boundary conditions are unknown to the user since the vendor does not reveal these for proprietary reasons. A common method to implement the contact constraint is the penalty method described by Zhong (1993) whereby the motion is constrained by applying a penalty to the amount of penetration that occurs. The contact constraint is based on nodal springs with a non-linear characteristic depending on the amount of penetration or the displacement ratio between the contacting bodies.

5.4 Investigations on a single ply

5.4.1 Classical modelling

Equation (5.2) describes, between B and C, the longitudinal stress at the surfaces of a single layer of prepreg tape wrapped around the circular rigid pin shown in Figure 5.3. The first term is also the constant stress in the free length of the tape (C to D). The second term in Equation (5.2) describes the bending stress due to a constant radius of curvature for the contact length between B and C. If frictional effects were to be considered Equation (5.3) is used, whereby the constant stress term is replaced by the Euler rope friction formula described by Dubbel (1995). The influence of the frictional effects are shown in Figure 5.4, where Equations (5.2) and (5.3) are plotted for a Tape IV–3 material wrapped around a 50 mm diameter pin, using the material and mechanical properties given in Tables 2.3 and 4.2 and Figure 4.4. The tape is assumed to be free of initial stresses or strains. The load, F_A, was defined such that a constant stress of 2000 MPa resulted in the free length of the strap.

The through-thickness direct stress and the shear stress distributions are given by Equations (5.4) to (5.7). The superscript * denotes the consideration of the frictional influence. Figures 5.4 to 5.6 show the stress distributions at the pin-tape interface from B to D, which is at the end of the strap. The graphs indicate a considerable influence of the frictional effects on the stress distribution. A comparison between these simple closed-form expressions, the FE modelling, and the experimental results will be given in Section 5.4.2.

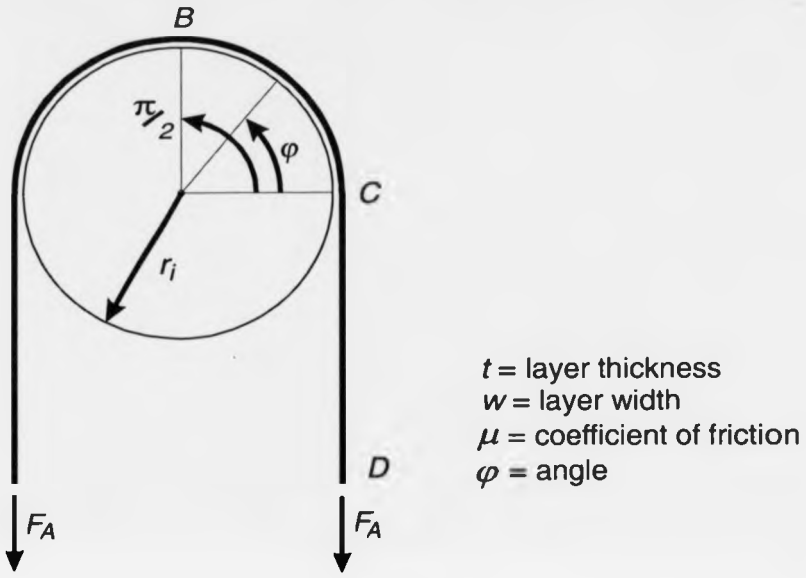

Figure 5.3: A single layer of tape wrapped around a circular pin.

$$\sigma_i = \frac{F_A}{t \times w} \pm \frac{t}{2} \times \frac{E_1}{r_i} \qquad \text{(no friction)} \qquad (5.2)$$

$$\sigma_i^* = \frac{F_A \times e^{-\mu \times \varphi}}{t \times w} \pm \frac{t}{2} \times \frac{E_1}{r_i} \qquad \text{(friction present)} \qquad (5.3)$$

$$\sigma_3 = \frac{F_A}{r_i \times w} \qquad \text{(no friction)} \qquad (5.4)$$

$$\sigma_3^* = \frac{F_A \times e^{-\mu \times \varphi}}{r_i \times w} \qquad \text{(friction present)} \qquad (5.5)$$

$$\tau_{13} = 0 \qquad \text{(no friction)} \qquad (5.6)$$

$$\tau_{13}^* = \mu \times \sigma_3^* \qquad \text{(friction present)} \qquad (5.7)$$

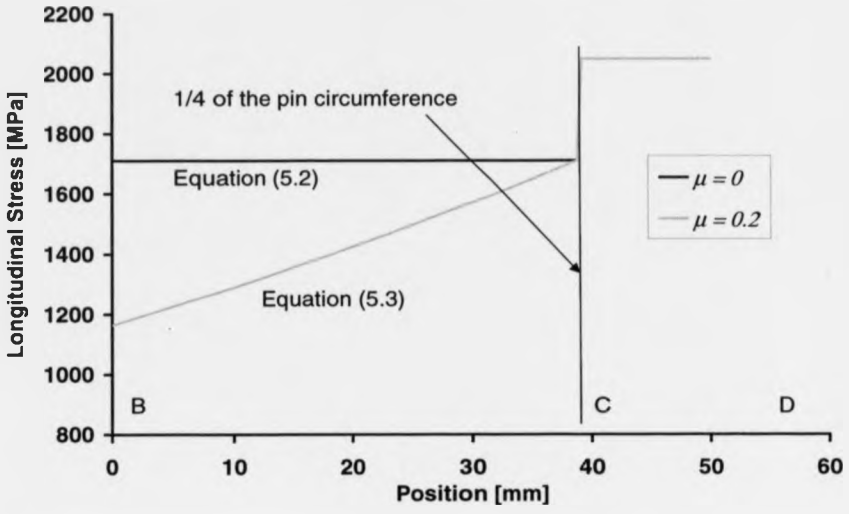

Figure 5.4: Longitudinal stress component at the pin-tape interface.

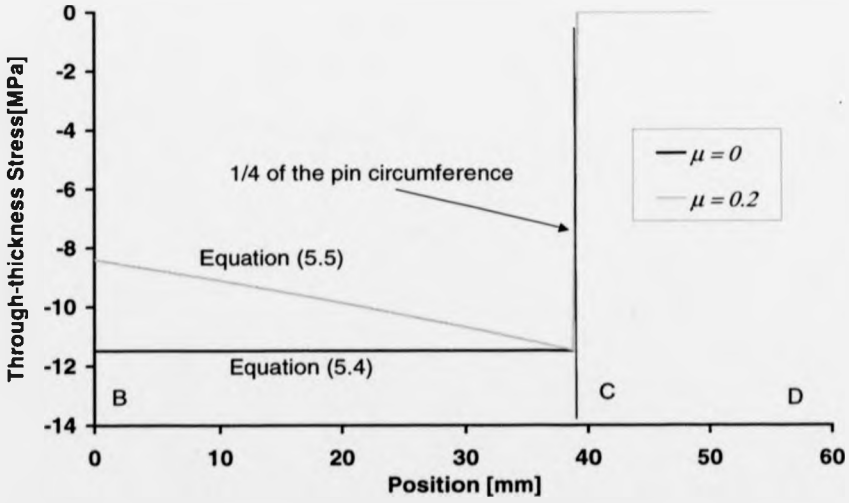

Figure 5.5: Through thickness stress component at the pin-tape interface.

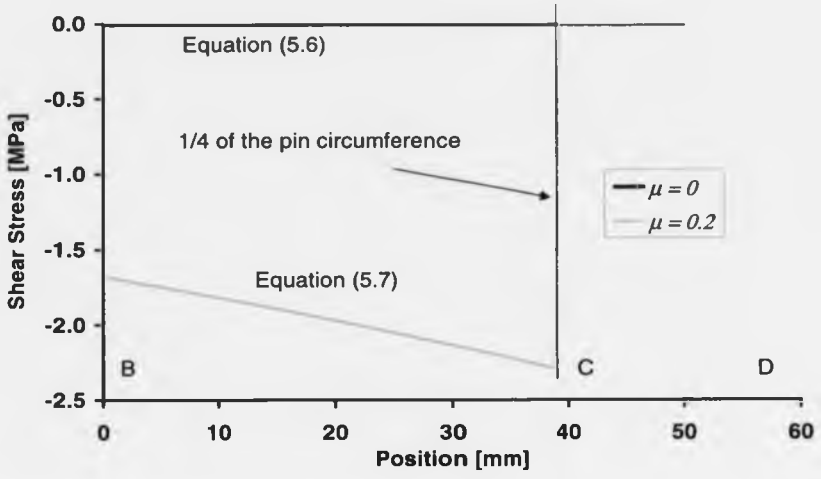

Figure 5.6: Shear stress component at the pin-tape interface.

5.4.2 Finite Element modelling

The initial condition was a straight section of prepreg tape fixed in a horizontal position at B (Figure 5.3). The tape was then wrapped around one quarter of the pin circumference and finally tensioned to a predetermined load. This problem is a highly non-linear one. In addition to the boundary non-linearity described in Section 5.3, it involves large displacements. Furthermore, the unidirectional orientation of the carbon fibres result in highly orthotropic material properties (see Table 5.1 for example).

Figure 5.7 shows the boundary conditions used to model the outlined problem. The nodes along the symmetry plane ($x = 0$) are free to move in the y-direction but not in the x-direction where symmetry forces the tape to be restrained. The bottom node on the plane of symmetry at B was also restrained in y-direction to prevent any rigid body

motion. The load was applied at the opposite end of the tape using a shear stress defined in the global coordinate system. This loading remains in the specified vertical direction and is gradually transformed to a direct stress as the tape end rotates around the pin.

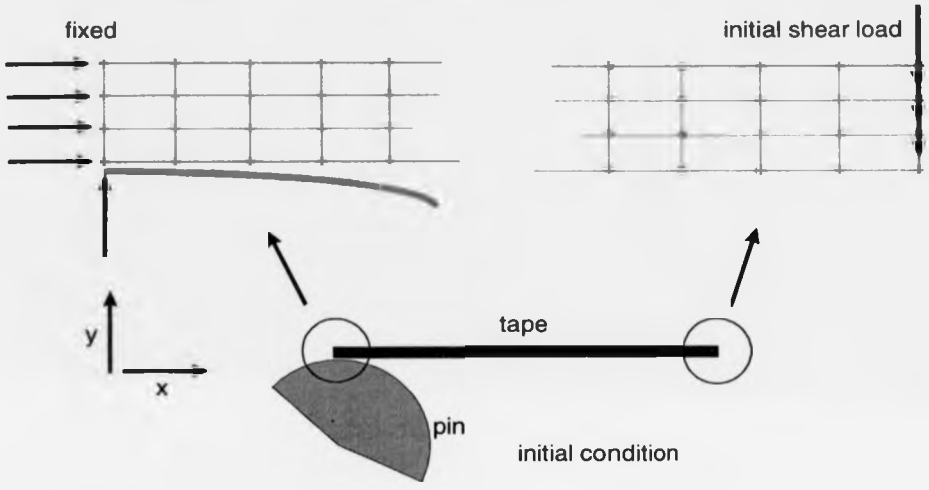

Figure 5.7: Boundary conditions.

The applied stress acting always in the negative *y*-direction was 2000 MPa. It was applied using the incremental loading sequence shown in Figure 5.8. The large number of increments in combination with the low stress level at the beginning (0.45 MPa) was necessary to prevent numerical instability because of the low flexural stiffness of the thin (ca. 0.15 mm) tape. The deformation of the tape at different stages in the analysis is shown in Figure 5.9. The magnitude of the vertical stress at the two intermediate stages of 150 and 200 increments was determined, from a trial and error approach, to be 0.45 and 100 MPa, respectively. The software contains an adaptive loading feature where an increment can be recycled a certain number of times creating sub-increments with even smaller load steps. This feature enabled the author to use the same loading conditions for all the geometries investigated.

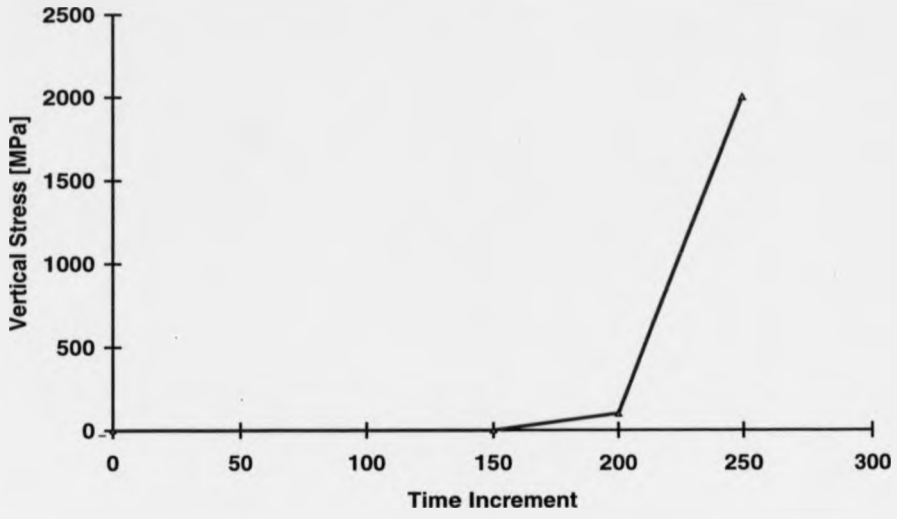

Figure 5.8: Incremental loading at the tape free-end.

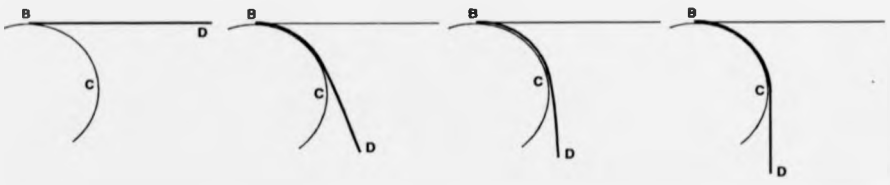

Increment 0 Increment 150 Increment 200 Increment 250

Figure 5.9: Tape deformation due to incremental loading.

The problem was assumed to be of plane stress type. The tape was modelled using isoparametric arbitrary, quadrilateral membrane elements with reduced integration capabilities. This element is preferred over higher-order elements due to the superior representation of the contact pressure (see MARC 1997). The element is suitable for contact analysis involving orthotropic materials. It was assumed that the stress-strain

relationships were linear. This assumption is considered acceptable despite experimental evidence given in Figures 4.1, 4.2 and 4.3 that the moduli are not constant.

The material properties used in the analysis in this Chapter are given in Table 5.1. The values used for the numerical models differ from the measured properties given in Chapter 4 because the finite element analysis was performed prior to some of the characterisation measurements.

Table 5.1: Mechanical properties used in the analysis.

	FEM	Classical
E_1	133 GPa	121 GPa
E_2	---	4.8 GPa
E_3	8.9 GPa	4.8 GPa
G_{13}	7.1 GPa	---
$\nu_{12} = \nu_{13}$	0.28	0.34
$\nu_{21} = \nu_{31}$	---	0.014
ν_{23}	---	0.4

One of the element edges was selected as a reference axis for the orthotropic material behaviour. The updated Lagrangian formulation option was used to account for the large rotations of the tape influencing the reference axis of the orthotropic material.

The measured, the classical and the FE stress distributions at the tape's outer surface are shown in Figure 5.10. The classical longitudinal stress is from Equation (5.3), although the term representing the superimposed bending stresses is added because the surface where bending generates tensile stresses is considered. The measured data points were

acquired, as described in Section 3.6, and scaled according to the measured distances, t_{gauge}, (see Figure 5.11) between the tape and the centre of the four strain gauges in the pin region where the tape was bent. The distances for the four gauges are given in Table 5.2. Only one measurement was taken at each strain gauge location.

Table 5.2: Measured distances between the tape surface and the strain gauge.

	t_{gauge}
Gauge 1	88 µm
Gauge 2	95 µm
Gauge 3	98 µm
Gauge 4	90 µm

The measured data points in Figure 5.10 contain error bars with a ±10% margin to indicate the error introduced by variations in the longitudinal modulus, E_l. Errors of such a magnitude are typical if the modulus is determined at different strain levels.

The outer fibre stress is higher at C than in the free length of the strap at D because of the bending deformation. The magnitude of the bending stress in C is found to be three times higher using the classical model than from the FE analysis. There is no experimental results to estimate the actual value for the bending stress at C. All three stress distributions show that the longitudinal stress increases from B to C such that there must be a shear stress at the tape-pin interface. The effect of the discontinuities at C are clearly seen and so the development of a failure criterion to determine load capacity of a strap will need to focus on the stress distribution here.

Both, the experimental and FE distribution from B to C give a non-linear increase in stress and comparing with the exponential relationship from Equation (5.3) it is observed that frictional effects are probably not constant.

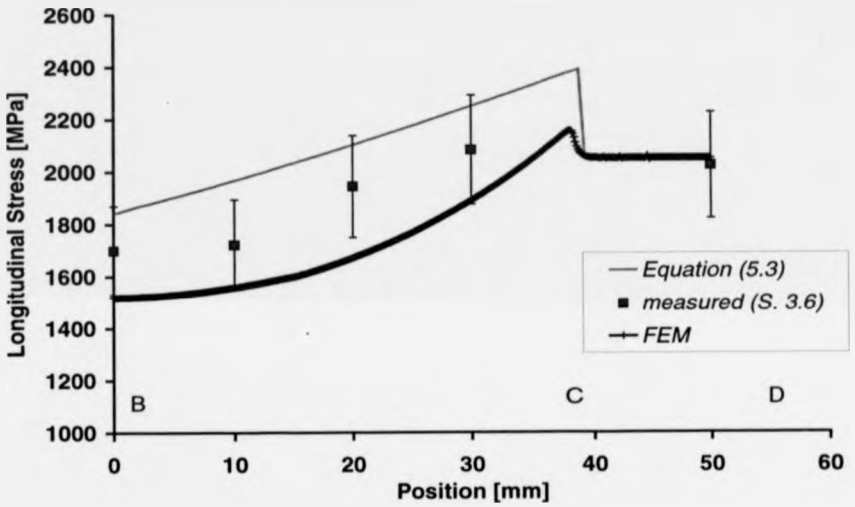

Figure 5.10: Longitudinal stress component at the tape's outer surface.

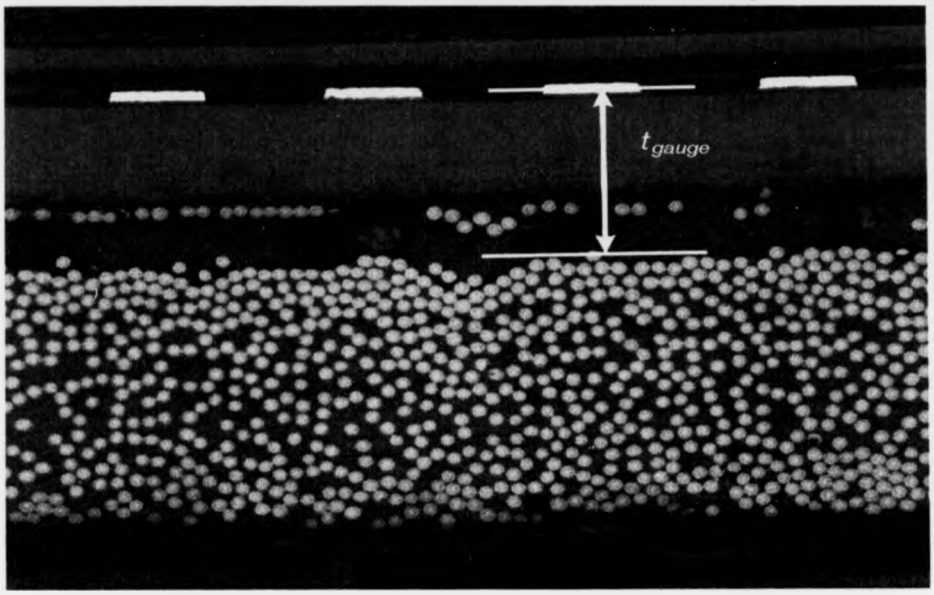

Figure 5.11: Cross-section through a strain gauge bonded to a prepreg tape.

The mesh density was one of the parameters investigated in this thesis since it is a critical factor influencing the computational time. Tape sections with length-to-thickness aspect ratios exceeding 300 were investigated. Elements of constant rectangular size were used in each model. The maximum element aspect ratio was selected to be 1.5 to minimise the distortional errors described by Cook et al. (1989). This resulted in models with about 12000 degrees of freedom. The majority of the runs were performed on a SUN server containing four UltraSPARC 50 MHz processors with 256 Mbytes RAM each. The larger models were submitted to a more powerful Cluster system at the Swiss Center for Scientific Computing CSCS in Manno. The computational time for each model was about 8 to 12 hours.

Figures 5.12 to 5.14 show the influence of the mesh density on the longitudinal, through thickness direct and shear stress distributions at the tape-pin interface. The number of elements in the legend refers to the number of equal sized elements across the tape thickness of 0.15 mm.

The numerical models used to investigate the mesh density were based on a pin with 20 mm diameter, a friction coefficient $\mu = 0.2$ and a relative sliding velocity of $C = 10^{-4}$ mm/s. In reality the relative sliding velocity varies along the tape length whereas the code allows only one specific value for each contact body.

The peak through-thickness direct and shear stresses at C (Figure 5.3) show the presence of a mathematical singularity. This is not a surprising result since there are both material and geometric discontinuities at this location. From Figure 5.12 to 5.14 it can be seen that the maximum stress at C increases as the number of elements increase. This lack of convergence at the location where failure is likely to initiate is one reason that prevented the author from considering a failure analysis.

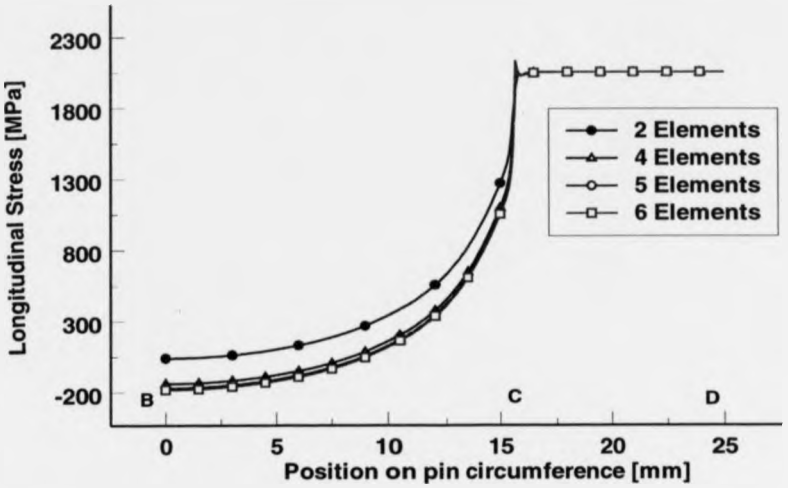

Figure 5.12: Longitudinal stress distribution at the pin-tape interface.

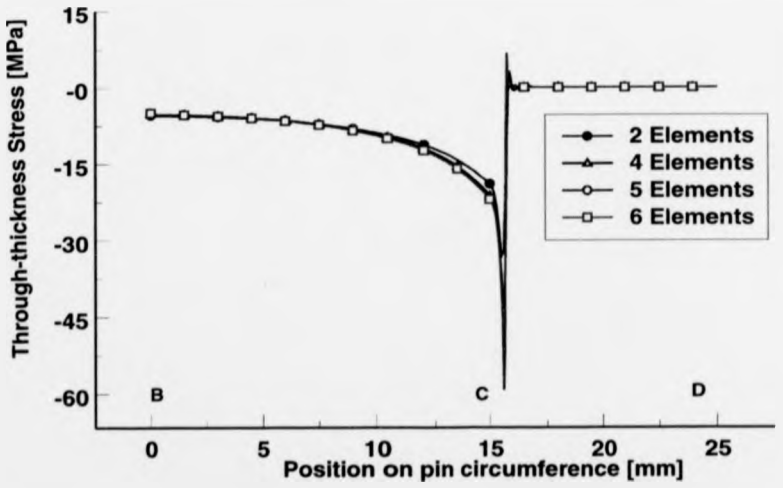

Figure 5.13: Through-thickness stress distribution at the pin-tape interface.

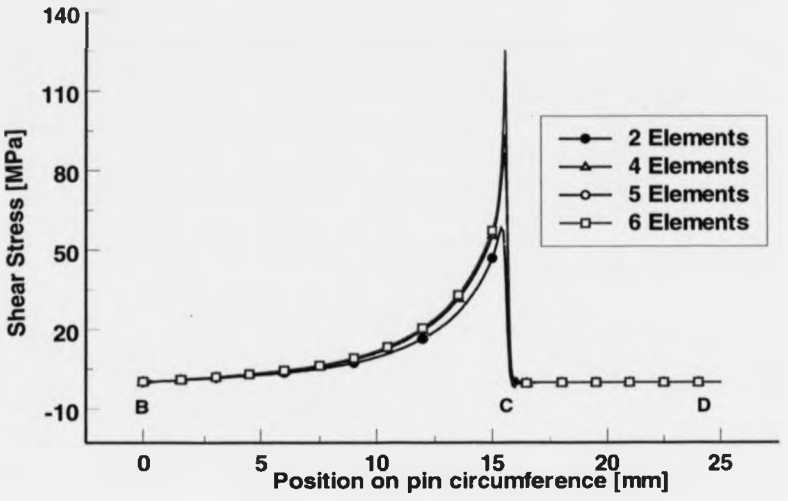

Figure 5.14: Shear stress distribution at the pin-tape interface.

The next model variable under consideration is the frictional influence which depends on the coefficients of friction, μ, and relative sliding velocities, C. The analysis is based on a pin with 20 mm diameter, a constant value for C of $5x10^{-3}$ mm/s and a varying μ, and a constant friction coefficient μ of 0.2 and a varying C. Figures 5.15 to 5.22 show the dominating influence of the relative sliding velocity on the stress distributions presented. The change in longitudinal stress range for the range of friction coefficients from 0.1 to 0.7 is about one third of the change which is found when the range of relative sliding velocities is increased from 10^{-5} to 10^{-1} mm/s. Hence the FE solution is far more sensitive to a numerical parameter, which has to be estimated by the analyst, than it is to the measurable frictional characteristic. The results in the figures show that for accurate modelling it will be necessary to know what C is in practice. The relative sliding velocity, C, may be determined experimentally but the resulting model may not

be very versatile since it is not a constant value as the wrapped tape has contact between B and C.

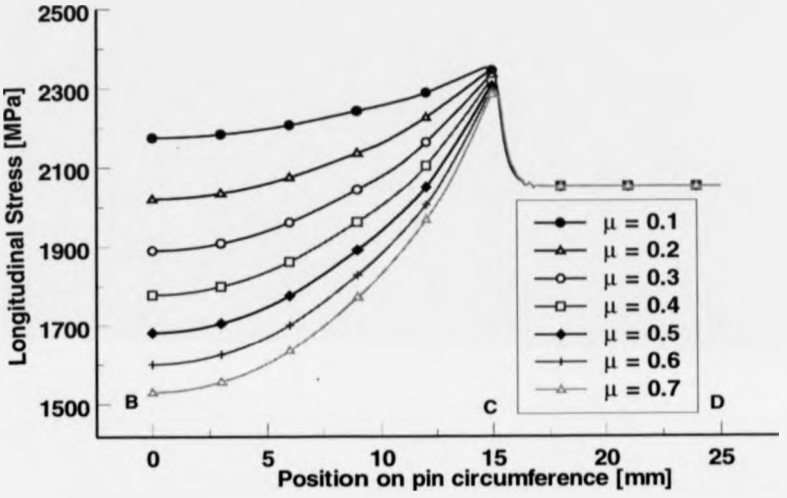

Figure 5.15: Longitudinal stress distribution at the tape's outer surface.

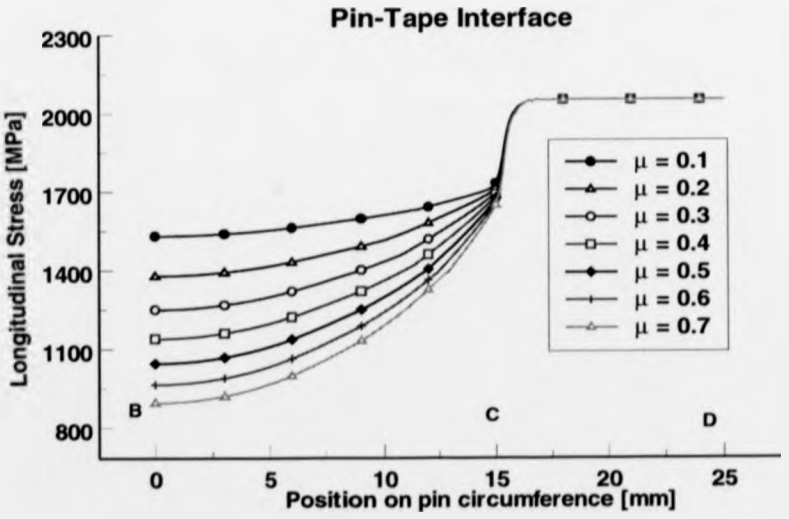

Figure 5.16: Longitudinal stress distribution at the pin-tape interface.

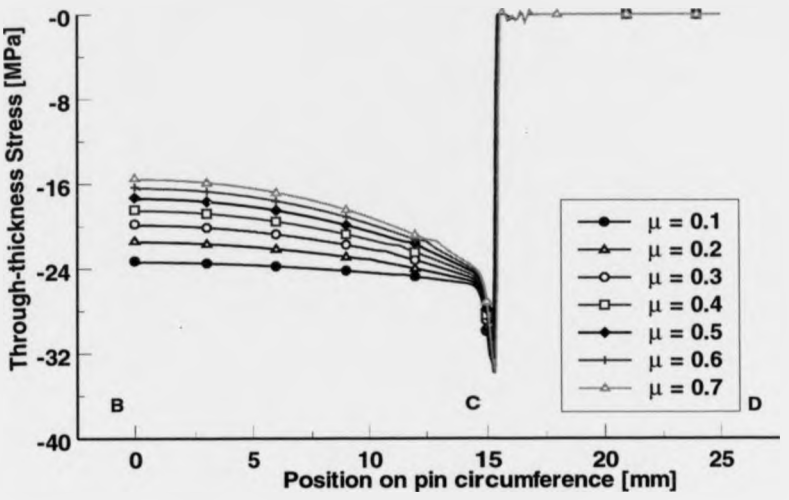

Figure 5.17: Through-thickness stress distribution at the pin-tape interface.

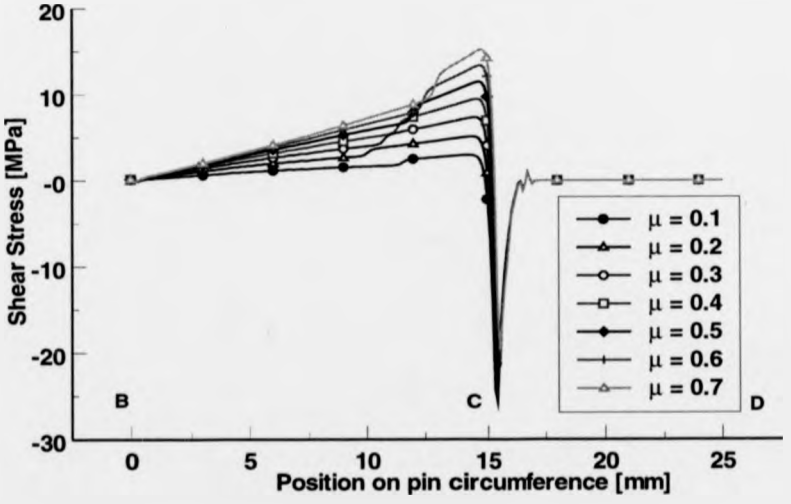

Figure 5.18: Shear stress distribution at the pin-tape interface.

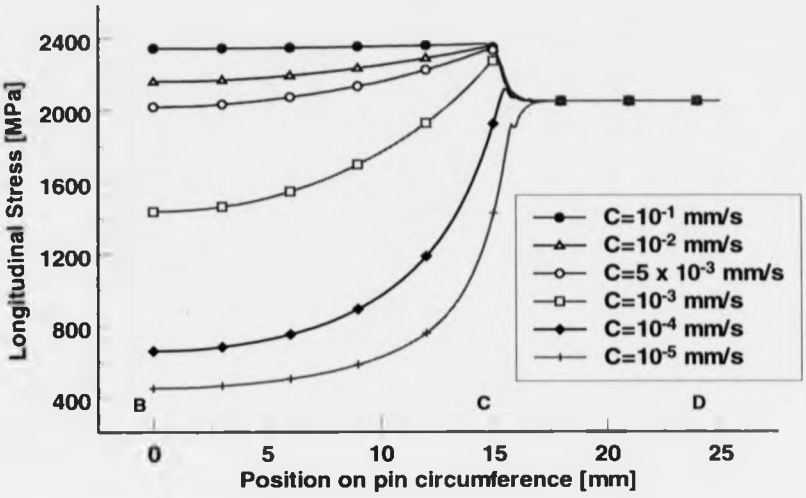

Figure 5.19: Longitudinal stress distribution at the tape's outer surface.

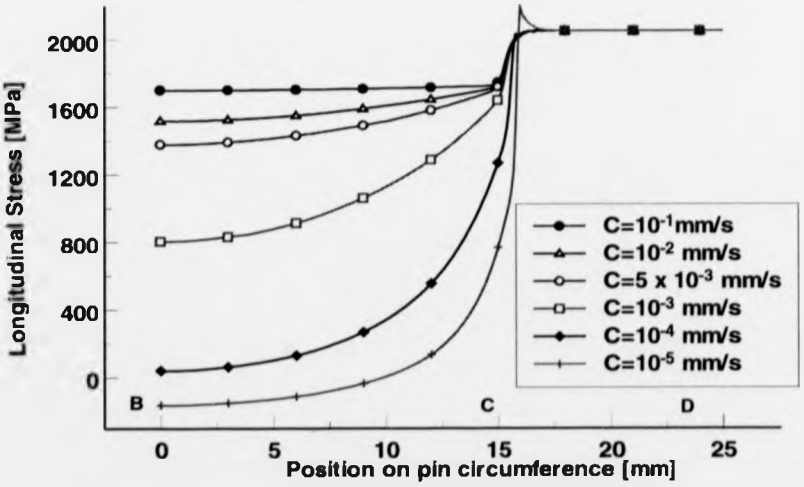

Figure 5.20: Longitudinal stress distribution at the pin-tape interface.

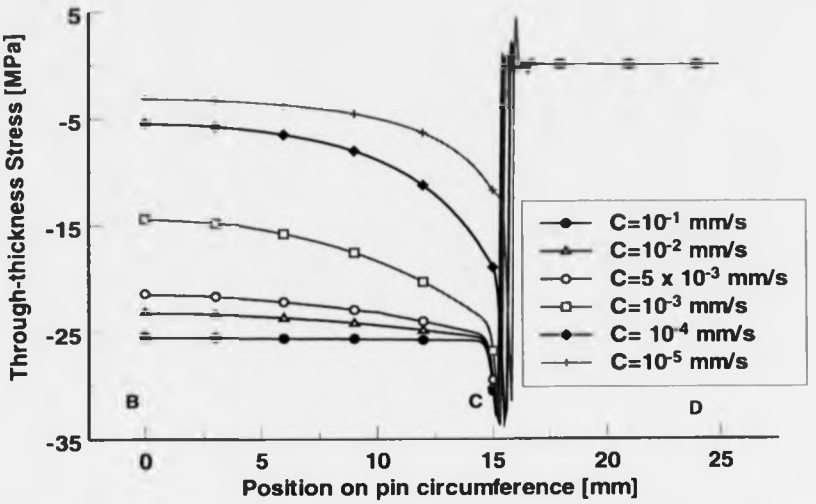

Figure 5.21: Through-thickness stress distribution at the pin-tape interface.

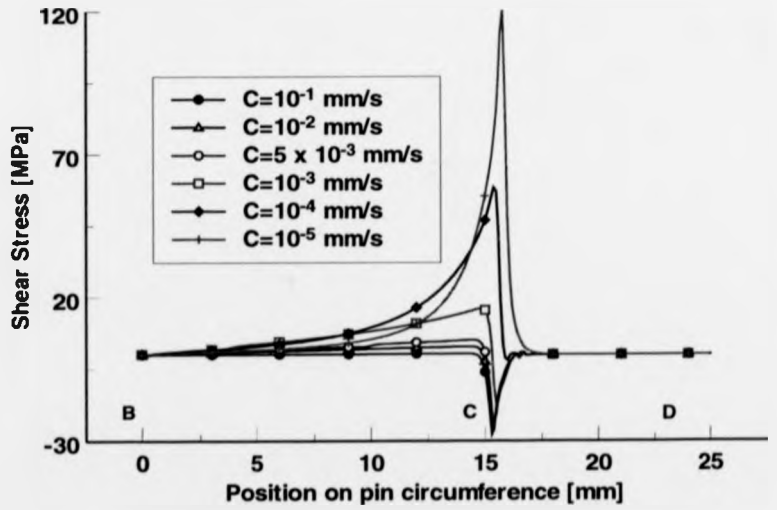

Figure 5.22: Shear stress distribution at the pin-tape interface.

A further model variable considered was the pin diameter, *D*. Figures 5.23 to 5.26 show the influence of the pin diameter on the stress distribution. The length of the tape was varied according to the pin diameter to reduce computational time. The maximum absolute value of the stresses in Figures 5.23 to 5.25 increase exponentially with decreasing pin diameter. In the case of shear stresses shown in Figure 5.26, the peak value is likely to be the result of the mathematical singularity present at C.

It is to be noted that for practical reasons, established after the FE analysis, the minimum pin diameter has been set to 30 mm. Load carrying capacities in Figure 4.13 for single layer straps having a pin diameter from 25 to 150 mm do confirm that the stress concentrations causing failure increase in severity as the pin diameter is reduced.

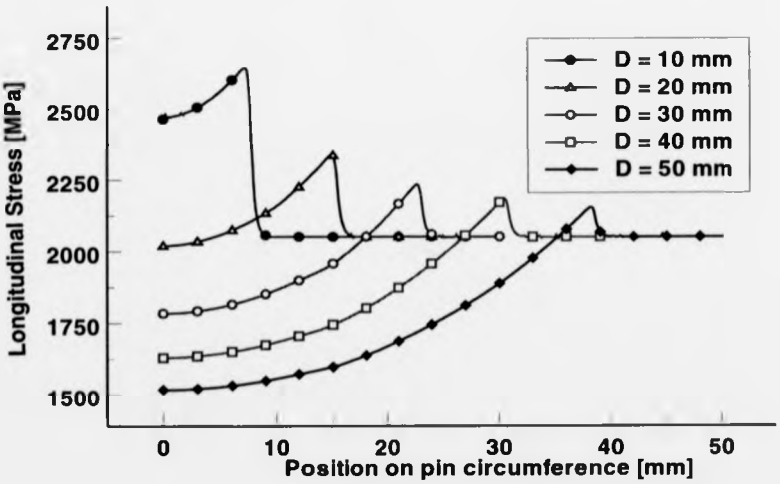

Figure 5.23: Longitudinal stress distribution at the tape's outer surface.

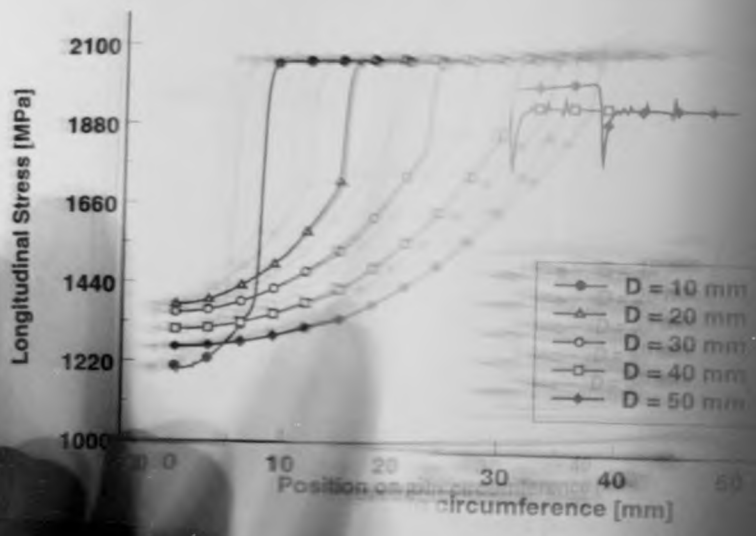

pin-tape interface.

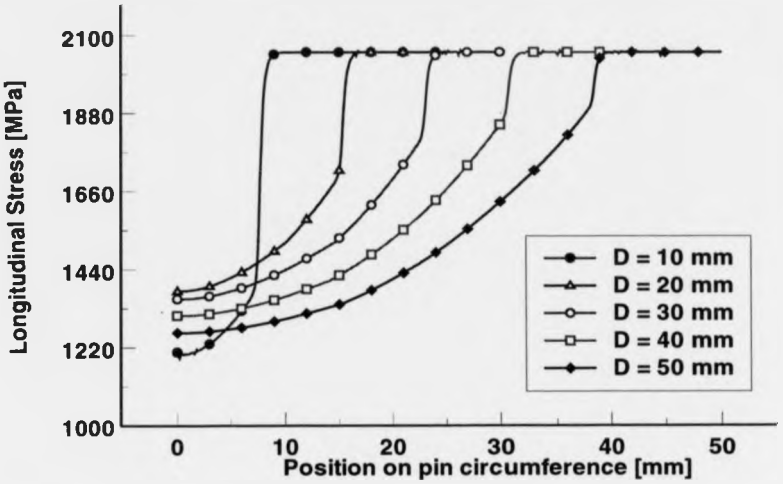

Figure 5.24: Longitudinal stress distribution at the pin-tape interface.

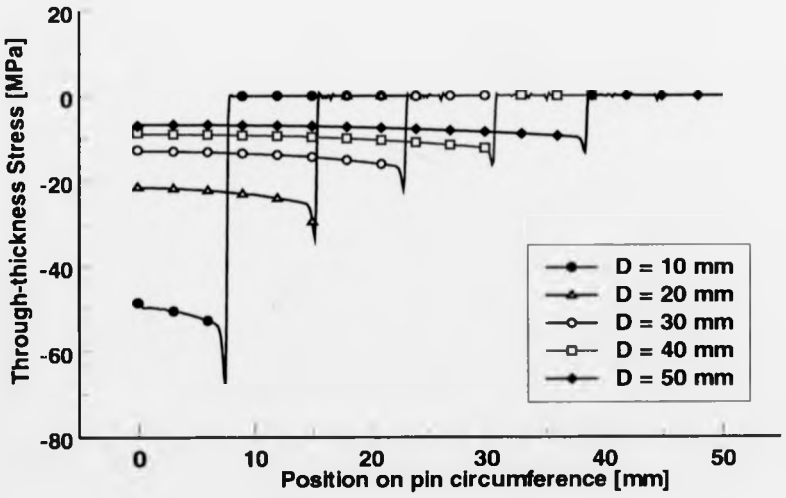

Figure 5.25: Through-thickness stress distribution at the pin-tape interface.

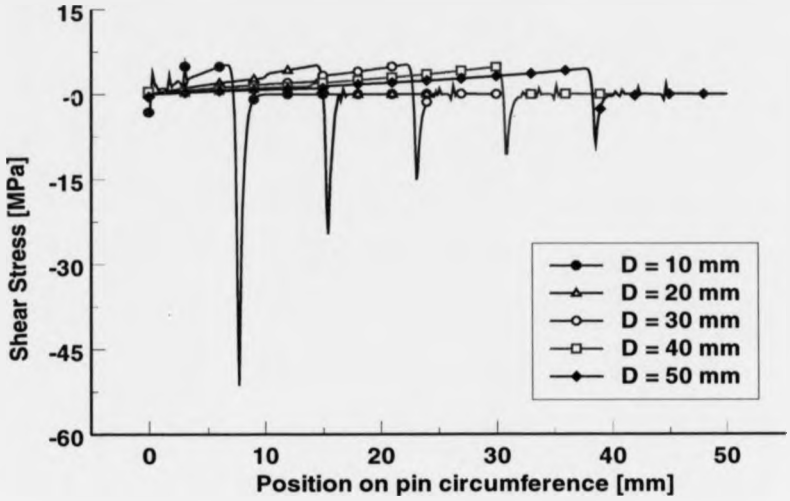

Figure 5.26: Shear stress distribution at the pin-tape interface.

The three modelling variables investigated provide an insight into the behaviour of a prepreg tape wrapped around a circular pin. The models, as presented, cannot be used for any strength prediction due to the presence of a mathematical singularity at the point where the two contacting bodies first touch. The through-thickness direct and the shear stress components are specifically influenced by the singularity and this leads to unrealistically high stresses. Furthermore the convergence tolerance of 0.1 used allows a maximum residual force in the analysis to be 10% of the maximum reaction force. This tolerance in combination with the orthotropic material properties results in transverse and shear stresses of questionable accuracy. Furthermore, it has been established that the error in any stress component derived from FE analysis (Mottram and Shaw1996) is 5 % of the maximum stress component. This indicates that if a stress component causing failure in a material is an order of magnitude less than the maximum case, then the error in this stress can be 50 %, and as such it is not useful in predicting failure.

An important conclusion from this parametric study is the possibility of creating a more uniform stress distribution by the combination of frictional effects with a gradual change in the radius of curvature of the pin.

5.5 Laminated pin-loaded strap

5.5.1 Classical modelling

The subsequent analysis considers the load transfer into a laminated pin-loaded strap assuming a perfect fit between strap and pin and a perfectly lubricated interface. Hence, zero shear stress at the pin strap interface is assumed ($\mu = 0$). An analytical formulation was developed by Conen (1966) to describe the stress concentrations in the load transfer region of straps made from glass fibre reinforced epoxy. The model assumes that the pin-loaded strap behaves like a thick walled pressure vessel for which Timoshenko and Goodier (1970) provide the Lamé equations a solution based on a two dimensional plane stress assumption. Equations (5.8) and (5.9) describe the tangential and the radial stress components, σ_1 and σ_2 respectively, in an isotropic cylinder subjected to internal pressure, p_i, per unit width.

$$\sigma_1 = \frac{p_i \times r_i^2}{r_o^2 - r_i^2} \times \left(1 - \frac{r_o^2}{r_i^2}\right) \tag{5.8}$$

$$\sigma_2 = \frac{p_i \times r_i^2}{r_o^2 - r_i^2} \times \left(1 + \frac{r_o^2}{r_i^2}\right) \tag{5.9}$$

The transfer of the load F ($2F_A$), into the pin is assumed to be uniformly distributed. Neglecting any frictional effects results in a constant internal pressure of

$$p_i = \frac{F}{2 \times r_i} \quad \text{per unit width.} \tag{5.10}$$

The generalised Hooke's law comprising the effects of symmetry in an orthotropic material can be described in terms of compliance as

$$\begin{vmatrix} \varepsilon_1 \\ \varepsilon_2 \\ \varepsilon_3 \\ \gamma_{23} \\ \gamma_{13} \\ \gamma_{12} \end{vmatrix} = \begin{vmatrix} S_{11} & S_{12} & S_{13} & 0 & 0 & 0 \\ S_{12} & S_{22} & S_{23} & 0 & 0 & 0 \\ S_{13} & S_{23} & S_{33} & 0 & 0 & 0 \\ 0 & 0 & 0 & S_{44} & 0 & 0 \\ 0 & 0 & 0 & 0 & S_{55} & 0 \\ 0 & 0 & 0 & 0 & 0 & S_{66} \end{vmatrix} \begin{vmatrix} \sigma_1 \\ \sigma_2 \\ \sigma_3 \\ \tau_{23} \\ \tau_{13} \\ \tau_{12} \end{vmatrix} \tag{5.11}$$

Where compliances S_{ij} are given in Tsai (1988). Conen (1966) measured strains in a number of locations through-the-thickness of laminated pin-loaded GFRP straps. He showed a good agreement, with a maximum error of 11% between the measured data and anticipated theoretical values using Equations (5.8) to (5.11).

When their laminated pin-loaded straps failed, Conen (1966) and Hütter (1966) observed extensive longitudinal splitting in the transverse direction. The damage mainly occurred at the interface between the strap and the steel pin. The splitting, which is responsible for the premature failure of a strap, was attributed to Poisson's ratio effects. These effects are dominated by the compressive stresses at the pin-strap interface (see Section 5.5.2 for further details). Hence they suggested the use of a restraining fixture in

the load transfer region to prevent positive transverse direct strains. Hütter (1966) found from experiments an increase in the tensile capacity in the range of 14% (r_o / r_i = 1.4) to 35% (r_o / r_i = 2.4) using such restraining end fixtures.

In addition, Conen (1966) developed a design criterion for laminated GFRP straps which contain the restraining fixture. He determined the stress in the transverse direction, σ_2 , from the boundary condition given by Equation (5.12) and Equations (5.8) to (5.11). Substituting for the three principal stress components resulted in Equation (5.13) that give the critical stress, σ_{UStrap} , in the free length of the strap at which a maximum allowable longitudinal strain, ε_U, occurs in the load transfer zone. The author tried to derive Equation (5.13) using MATHCAD. The resulting expression differed due to possible simplifications in the model development made by Conen (1966). Since the maximum error, within the investigated range, was less than 2%. the simplified analysis by Conen (1966) was found to be acceptable

$$\varepsilon_3 = \frac{\sigma_3}{E_3} - \left(\nu_{13} \times \frac{\sigma_1}{E_1} + \nu_{23} \times \frac{\sigma_2}{E_2} \right) = 0 \tag{5.12}$$

$$\sigma_{UStrap} = \frac{\varepsilon_U \times \left(\frac{r_o}{r_i} + 1 \right)}{\left[\left(\frac{r_o}{r_i} \right)^2 + 1 \right] \times \frac{1 - \nu_{13} \times \nu_{31}}{E_1} + \left[\left(\frac{r_o}{r_i} \right)^2 - 1 \right] \times \frac{\nu_{31} \times \nu_{23} + \nu_{21}}{E_2}} \tag{5.13}$$

In Equation (5.13) ν_{ij} denote the Poisson ratios with the first index, i, indicating the direction of the applied load and the second index, j, the direction of the resulting deformation. σ_{UStrap} normalised by the measured tensile strength of the material is presented in Figure 5.27 for a range of r_o / r_i from 1.01 to 1.2. The classical model

clearly overestimates the strength of laminated pin-loaded straps made from CFRP compared to the measured strengths described in Section 4.4.1.

The three stress components in Equations (5.8), (5.9) and (5.12) are used in the interactive failure criterion described by Knaust (1988). He derived Equation (5.14) from the general failure criterion for anisotropic materials described by Gol'denblatt and Kopnov (1965).

$$\frac{\sigma_1^2}{X_1^2}+\frac{\sigma_2^2}{X_2^2}+\frac{\sigma_3^2}{X_3^2}-\frac{\sigma_1\times\sigma_2}{X_1\times X_2}-\frac{\sigma_1\times\sigma_3}{X_1\times X_3}-\frac{\sigma_3\times\sigma_2}{X_3\times X_2}+\frac{3\times(\tau_{12}^2+\tau_{13}^2+\tau_{23}^2)}{S^2}=1 \qquad (5.14)$$

Substituting for the three direct stress components in Equation (5.14) results in a critical internal pressure, p_i, which fulfils Equation (5.14). The corresponding stress in the free length of the strap is normalised with the materials tensile strength. This stress ratio versus the radius ratio r_o / r_i is also given in Figure 5.27. This interactive failure criterion clearly underestimates the strength of laminated pin-loaded straps made from CFRP when r_o / r_i > 1.04. The difference is nearly three times when the radius ratio is 1.20. It is therefore concluded that this model does not accurately predict the resistance.

Mansfield (1983) also considered the problem of load transfer into laminated pin-loaded straps. He assumed the pin to be rigid with a surface capable of transmitting only normal stresses. He showed that the maximum stresses vary markedly with the ratio of the longitudinal to transverse modulus of the composite material. He derived Equation (5.15) to define stress concentration factors, k, for the hoop stress, σ_l, at the pin-strap interface.

$$k = \alpha \times (B - A) + D \tag{5.15}$$

where

$$\alpha = \sqrt{\frac{E_1}{E_3}}$$

$$A = -\frac{(\omega - 1) \times \left[\alpha^2 - \alpha + (\alpha^2 - \nu_{13}) \times (\omega^{\alpha-1} - 1)\right]}{\alpha \times \left[(\alpha - 1) \times (1 - \omega^{-\alpha-1}) + (\alpha + 1) \times (\omega^{\alpha-1} - 1)\right]}$$

$$B = -A \times \left(\frac{\alpha + 1}{\alpha - 1}\right) - \frac{(\omega - 1) \times (\alpha^2 - \nu_{13})}{\alpha \times (\alpha - 1)}$$

$$D = 1 - \omega - A - B$$

$$\omega = \frac{r_o}{r_i}$$

The inverse of the stress concentration factor, k, against the radius ratio is given in Figure 5.27. It is seen that the models by Conen (1966) and Mansfield (1983) give similar results which are non-conservative.

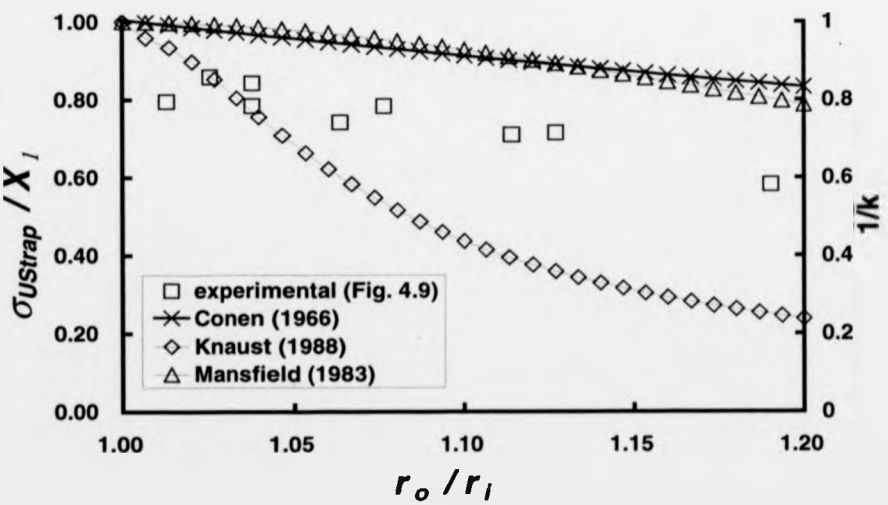

Figure 5.27: Theoretical and measured efficiency of the load transfer of laminated pin-loaded strap made from Tape IV-1.

5.5.2 FE modelling

A finite element analysis was carried out on a laminated pin-loaded strap to determine stress concentrations and to compare their positions to the failure locations found in the tests described in Section 4.4.1. The pin diameter was 20 mm and the radius ratio was 1.3. The circular steel pin was assumed to be a rigid body with a friction coefficient, μ, of 0.2. A relative sliding velocity, C, of 10^{-4} mm/s was used in analysis. A quarter-plane symmetry model was used for the CFRP strap as indicated in Figure 5.28. It had appropriate boundary conditions, to ensure zero displacement in x-direction at the plane of symmetry. To fulfil the symmetry requirement, the load on the strap was simulated by a fixed displacement in the y-direction. The strap was modelled using six elements across the thickness. The elements were four-noded, isoparametric quadrilateral elements with reduced integration. These elements are suitable for contact problems with orthotropic material properties. One of the element edges was selected as a reference axis for the orthotropic material behaviour.

The longitudinal, through-thickness direct and the shear stress components are shown in Figure 5.28. The bending deformation (shown magnified in the Figure 5.28), combined with variation in the length of innermost and outermost fibres are responsible for the occurrence of the premature failure in the load transfer region (C). The failure location in the experiments is consistent with the stress concentrations determined by the FE model, and this is seen by comparing Figures 1.2 and 5.28. The numerical prediction for the strength was not performed since it is not promising using this particular model due to the presence of a mathematical singularity at the point were the two contacting bodies first touch. Similar findings were reported by Graff and Springer (1991a) and Werne (1994) where different techniques were investigated to overcome the local disturbance.

A promising approach was the use of a so-called 'softened contact' option where a smooth stress distribution was obtained by placing truss elements between the pin and strap. The truss elements extended beyond the point where the strap leaves the pin. The truss stiffness was varied in this region to introduce a gradient in the influence of the friction. Graff and Springer (1991a) used this softened contact option successfully in combination with a purpose made finite element software Graff and Springer (1991b). The code allows a strength prediction of laminated pin-loaded straps to an accuracy of about 15-20%.

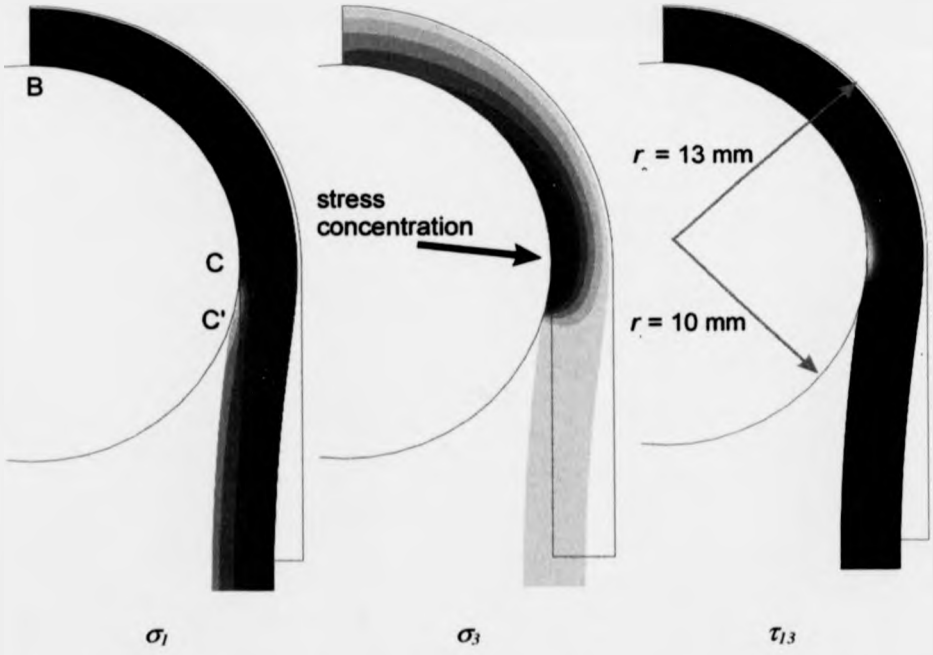

Figure 5.28: Longitudinal, through-thickness and shear stress component with magnified displacements in laminated pin loaded straps.

The longitudinal, through-thickness and shear stress distributions at the pin-tape interface are given in Figures 5.29, 5.30 and 5.31, respectively, for two coefficients of friction. In addition to the friction effects represented in the graphs, the effects of the mathematical singularity are present in the increased contact area (C to C'). Despite the possible errors in the stress recovery procedure outlined in Section 5.4.2 the through-thickness and the shear stress components are critical in terms of causing failure of the strap if compared with the longitudinal stress component.

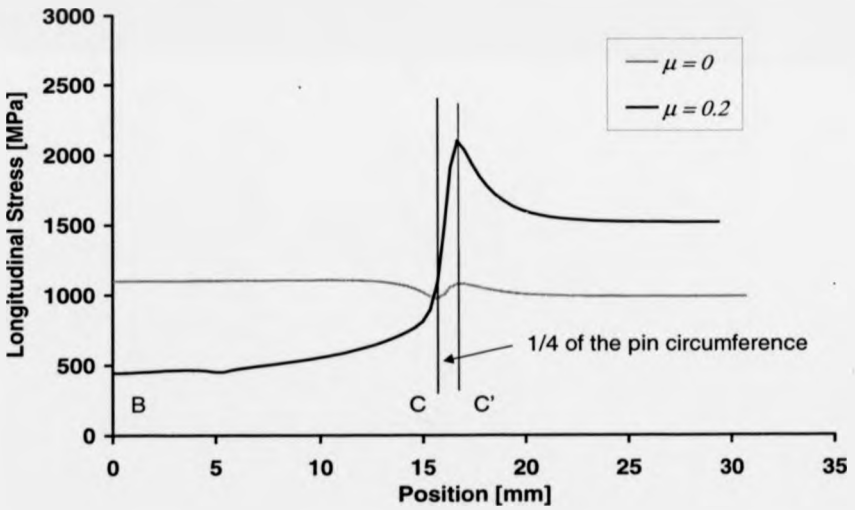

Figure 5.29: Longitudinal stress component at the pin-strap interface.

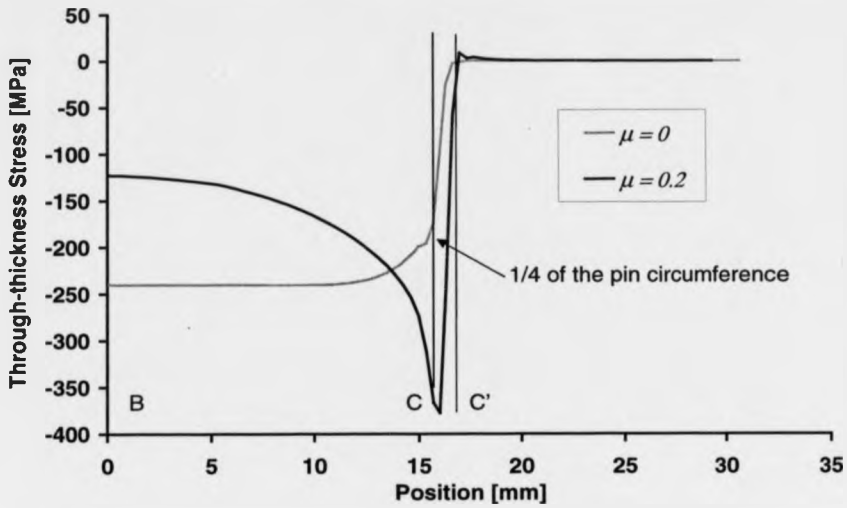

Figure 5.30: Through thickness stress component at the pin-strap interface.

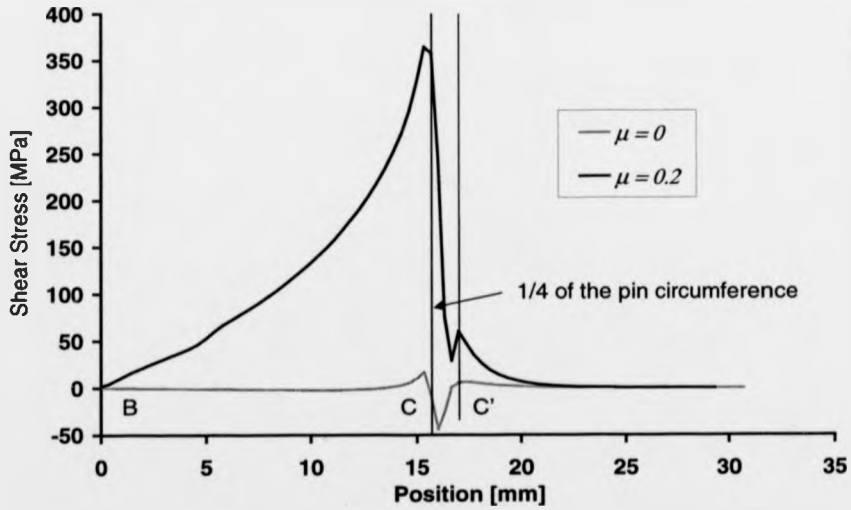

Figure 5.31: Shear stress component at the pin-strap interface.

6 FUTURE DEVELOPMENT AND APPLICATIONS

6.1 Review and Further Developments

Non-laminated pin loaded straps could provide an economic solution to a large number of applications where structural elements are under sustained tensile loading conditions. The project has successfully demonstrated the feasibility of the general principle. A number of proposals for new applications of the system are presented in Section 6.2. EMPA has now an international patent for the concept of non-laminated strap elements because the organisation sees a large commercial potential in structural engineering applications of composites.

The thermoplastic matrix tape with a quality standard of the Tape IV material has the scope to provide cost effective solutions for stiffening and strengthening problems. Research and development is still needed before the system can be commercialised. This work is listed later in the section

A driving force for the investigation of non-laminated pin-loaded strap elements was the development of a shear strengthening method based on post-tensioned external stirrups. The concept of non-laminated pin-loaded straps, as developed in this study, has been expanded to the use of non cylindrical 'pins', allowing a concrete structure to be strengthened as shown in Figure 6.1. Details of this work will be published elsewhere

since it is the combined effort of a group of researchers at EMPA. A conventional reinforced concrete beam was specifically designed to investigate the shear enhancement due to the external post-tensioned CFRP straps. The beam shown in Figure 6.1 was strengthened with non-laminated straps using semi-elliptical steel pads instead of the cylindrical pins. The prepreg tape was threaded through holes in the concrete slab and wrapped around the pads. The final layer was anchored using the fusion bonding process developed by the author. The top pad was lifted with a jacking system to tension the strap to approximately 60 % of its capacity. The prestressing force in a strap was locked-off by a shim placed between the pad and the concrete.

Figure 6.1: Shear strengthened concrete beam.

The unreinforced control specimen, tested in four-point bending, failed in shear at a load on each jack of F = 310 kN after tensile rupture of a steel stirrup. The beam, strengthened with twelve external straps of 200 mm spacing in the shear span of

1100 mm, failed by yielding of the longitudinal reinforcement bars at F = 420 kN. As a result, four straps were removed from the damaged beam to double the spacing of the external stirrups in the shear span to 400 mm. The second test on the damaged beam resulted in tensile failure of one strap in the pad region, followed by a shear failure of the beam at F = 410 kN. The shear failure in the beam occurred where the failed strap was located. The failed beam is shown in Figure 6.2.

These initial tests provided valuable information on the practicality of the system. The preliminary results suggest that the shear strength of a reinforced concrete beam can be significantly enhanced by using external non-laminated straps as strengthening elements.

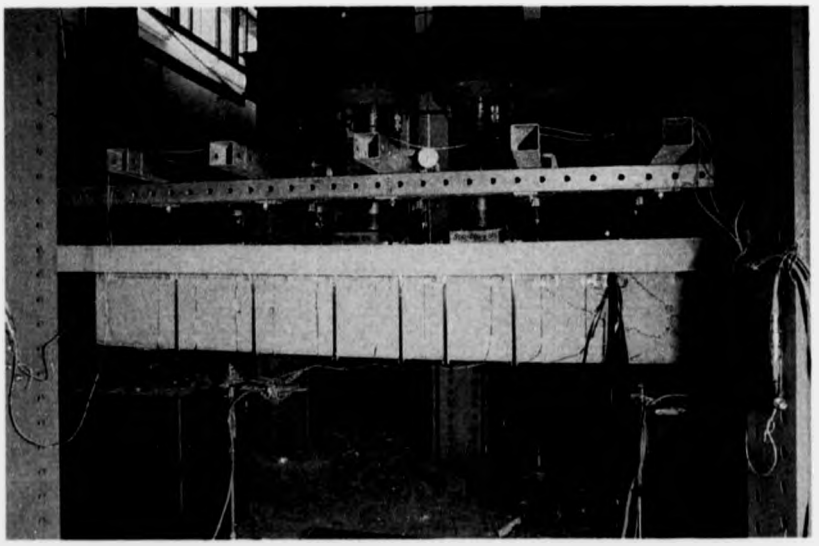

Figure 6.2: Shear failure in a concrete beam.

Future research on non-laminated straps should address in more detail the various topics introduced in this study. Despite the considerable effort made to characterise the longitudinal tensile properties of the prepreg tapes, reliable and more cost effective methods have to be developed for quality control purposes to ensure the reliability of non-laminated straps.

A key issue still to be investigated is the limitations of the principle of non-laminated straps. The limitations include the maximum number of layers in a strap maintaining the required load transfer efficiency. It is not feasible to give an efficiency value because this will be application dependant. A measure for the efficiency could be the tensile load carrying capacity per layer in a strap. The requirements in terms of efficiency are, however, dependent on various factors, such as strength or stiffness requirements of the tendon, length and manufacturing constraints. These factors have to be determined for each application and will include the overall cost of the system.

The load carrying capacity per layer in a strap is believed to be dependant on the frictional properties of the prepreg tape itself. Furthermore it may be influenced by variable frictional properties within the strap. An appropriate method for the characterisation of the frictional properties has therefore to be developed. The standard DIN 53375 was found not to be appropriate because of the low contact stress. The concept shown in Figure 6.3 would allow friction measurements at contact stress levels occurring in pin-loaded straps. The frictional properties could be determined by a single layer of prepreg wrapped around a cylindrical pin fixed to a torsional testing machine. The prepreg could be tensioned to a predefined value to control the normal forces acting on the interface between the prepreg and the pin. Monitoring the loads in each leg of the

strap and the torque applied to the pin would provide the information required to determine the frictional properties. The concept shown in Figure 6.3 will provide the frictional properties for the pin/CFRP combination. For any other combination, the other friction partner would need to be adhesively bonded to the pin surface.

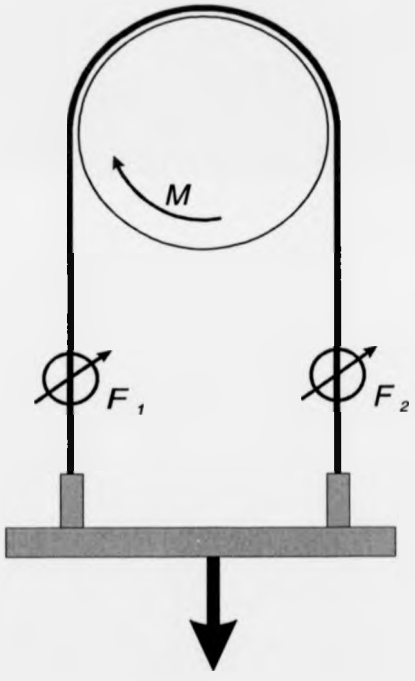

Figure 6.3: Proposed concept for friction measurements.

Further consideration should be given to the long-term performance of non-laminated pin-loaded straps. The preliminary creep results presented in Section 4.5 question the reliability of the fusion bonded joint. Moreover, the shear modulus of the polyamide matrix starts to decrease at temperatures around 20°C, depending on the humidity content in the matrix. Further creep tests must therefore be a priority, and they must be

performed outside the controlled laboratory, where higher temperatures and humidities occur. Twelve units of the test rig shown schematically in Figure 6.4 are currently being built and will be used for continuous outdoor weathering tests over the next few years. Each rig has a 100 kN tensile load carrying capacity and will allow continuous deformation measurements on the strap using a data acquisition system. The outdoor environment will incorporate the influence of temperature and humidity but also possible deterioration of the frictional properties due to moisture ingress. The concept of the test rig and the deformation measurement device was designed by the author and detailed by engineers at EMPA.

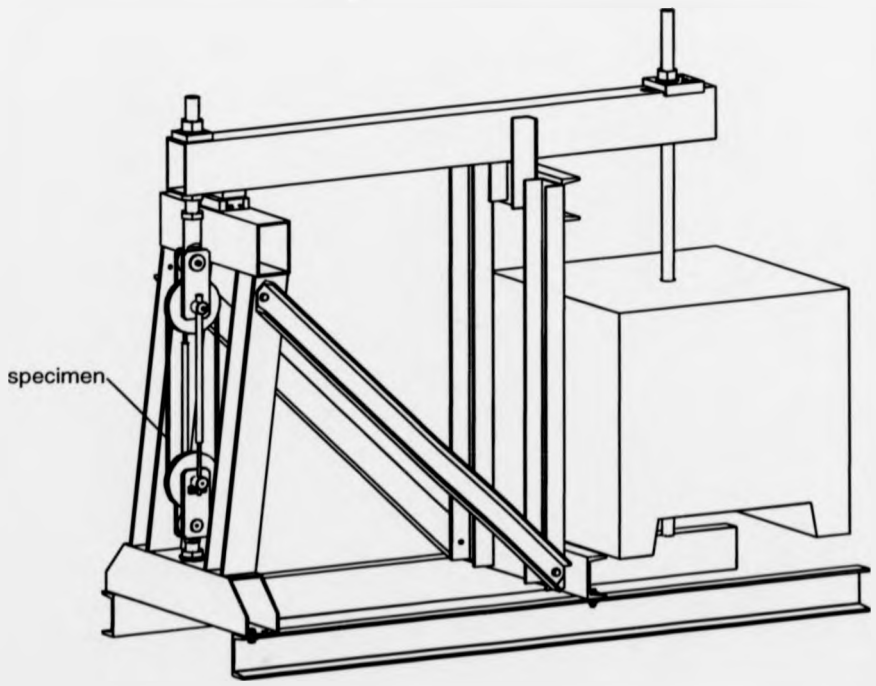

Figure 6.4: Creep test rig for outdoor weathering tests.

The fatigue properties of the prepreg itself are not considered to be an important issue, although fatigue loading on non-laminated straps may lead to a gradual unwrapping process and therefore to overloading of the end anchorage of the final layer. The result would be the failure of the strap since the final layer is providing the normal force for the load transfer by friction. Hence, the fatigue properties should be investigated. Furthermore, the relaxation behaviour of non-laminated strap elements ought to be determined.

The feasibility of non-laminated pin-loaded straps has been demonstrated using high quality prepreg tape with a polyamide matrix. The mechanical properties of this matrix material will unfortunately limit the range of possible applications. The susceptibility of the polyamide to creep at temperatures above the glass transition temperature, T_g, of 40° C, may require straps to be made from CFRP based on a different matrix material. The work presented has shown that the tape material must be of high quality , having excellent surface finish and parallel continuous fibres aligned with the longitudinal axis of the tape. The options for other thermoplastic matrices will therefore be limited to those where processing will maintain the required quality of the tape material.

A further aspect to investigate is the end-anchorage of the final layer. A plastic clamping device, as shown schematically in Figure 6.5, may provide sufficient capacity to anchor a single layer of prepreg tape. Such a device could be bolted to the surrounding structure and be produced in large quantities by injection moulding. This simple load transferring device is seen by the author as a cost effective method to produce non-laminated strap elements.

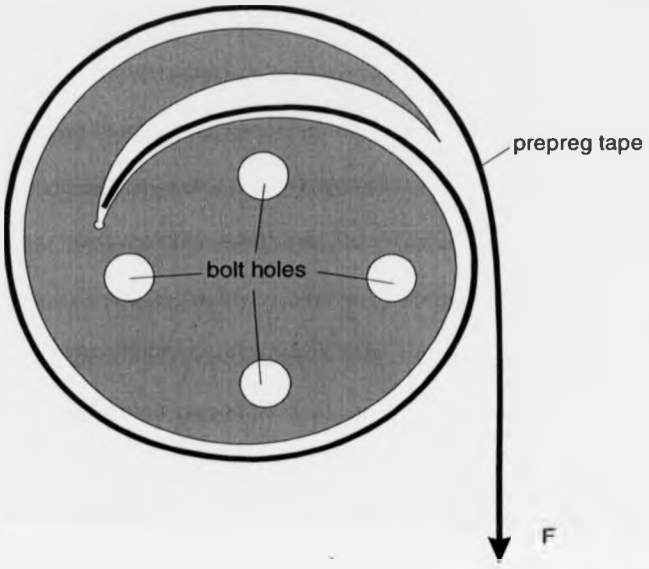

Figure 6.5: Clamping device for anchorage purposes.

6.2 Further applications

A promising application for non-laminated pin-loaded straps could be permanent rock anchors in the tunnelling industry. The stress corrosion resistance of CFRP would provide a reliable product with a superior life expectancy compared to current products based on steel or glass fibre reinforced polymers. The challenge for this particular application is the development of a procedure to fabricate the end-anchorage which is not accessible.

Another application for non-laminated pin loaded straps is currently under investigation in an ongoing collaborative research project with the University of Manitoba, Canada. Highway and railway bridges made from sawn timber beams have been in service for more than 40 years. The main goal of this research project is the development of a

strengthening technique to upgrade these bridges to increased loading conditions. The oil based impregnation of the timber prevents the use of any bonded reinforcement. Hence, a proposed solution is the use of non-laminated pin-loaded straps as external post tensioning cables. Screening tests on strengthened timber beams have been performed at the structural testing facility at the University of Manitoba. A typical test specimen from the programme is shown in Figure 6.6

Figure 6.6: Timber beam strengthened with non-laminated pin-loaded straps.

The possibility to produce the non-laminated pin-loaded strap on site in various configurations, in terms of length and anchorage design, will allow different tailor made strengthening options to be developed over the next decade.

Such a possibility is shown schematically in Figure 6.7. The figure shows an alternative method for flexural strengthening of a reinforced concrete T-beam, whereby a non-laminated pin-loaded strap is placed horizontally on the tension face of the beam.

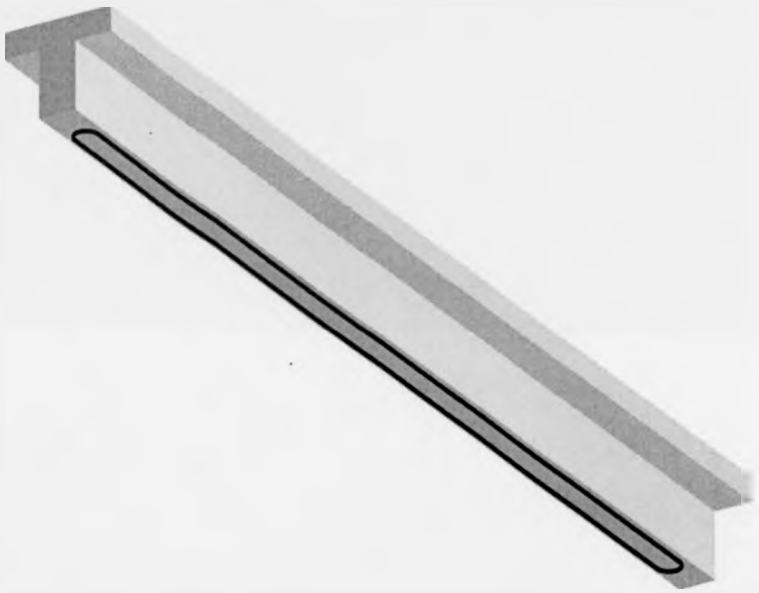

Figure 6.7: Flexural strengthening application.

The concept of non-laminated pin-loaded straps is not limited to civil engineering applications. Figure 6.8 shows a design of a composite connection rod for a combustion engine or a pump. The tensile loads between the two bearings are carried by a component with similar features as a pin-loaded strap element. This component could be replaced by a non-laminated design providing the potential for a low inertia rod at competitive cost.

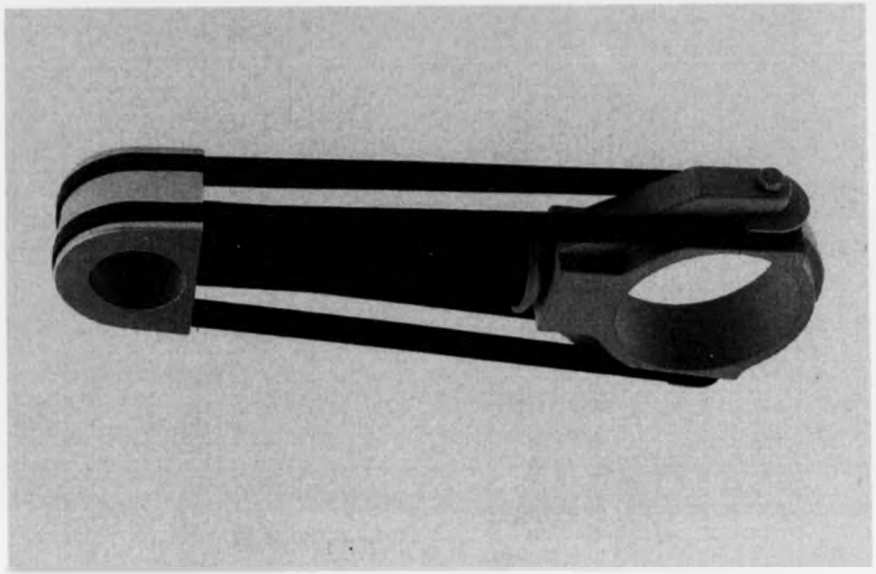

Figure 6.8: Composite connection rod.

7 CONCLUSIONS AND RECOMMENDATIONS

7.1 Conclusions

The focus of this research has been the feasibility of a novel load transfer concept for a CFRP tendon system using non-laminated pin-loaded straps. The principle is based on a number of non-laminated layers formed from a single, continuous, thin, thermoplastic matrix. Such a system enables the individual layers to move relative to each other. Undesirable stress concentrations are, therefore, reduced compared to a laminated system because this structural form has greater flexibility and a more uniform strain distribution is achieved in all the layers.

The material development, results from experimental investigation and the analytical modelling can be concluded as:

7.1.1 Material development

One objective of the research was the development of an appropriate material for non-laminated pin-loaded straps since no commercially available material was suitable in terms of quality or cost. The findings concerning the material development can be concluded as:

- commercially available prepreg tape materials were found to be inappropriate because of uneven surface texture and edge contours, extensive width tolerances and poor impregnation quality.
- aqueous powder impregnation of rovings using PA 12 particles was selected to produce tape material at high production rates to reduce the cost.
- specific modification to the existing facility of Sulzer Innotec Ltd. resulted in prepreg tape of high quality, suitable to show the feasibility of non-laminated pin-loaded straps.
- the measured longitudinal tensile properties, determined using different anchorage methods, were found to be lower than expected from the Rule of Mixture equation.
- a successful process was developed to produce specimens to characterise thermoplastic tape material in transverse and in-plane shear direction.
- the developed fusion bonding process resulted in a joint efficiency of 99% using a single lap-joint configuration.

7.1.2 Pin-loaded strap elements

The performance of laminated and non-laminated pin-loaded straps with different end anchorage systems can be concluded as:

- a successful process was developed to manufacture laminated straps for research purposes.
- the efficiency of the load transfer in laminated straps decreases considerably with increasing radius ratio.

- A minimum pin diameter of 30 mm was selected since no significant influence on the load carrying capacity of a single layer strap could be determined when the pin diameter was varied from 25 to 150 mm.
- the relative displacement between individual layers was visualised to show the principle of non-laminated pin-loaded straps. As the prepreg tape material, developed with Sulzer become available, the feasibility was shown successfully by strain measurements on individual layers. The innermost layer of a 10 layer specimen experienced a strain increase of 9% compared to the outermost layer.
- it was found that non-laminated straps, where the final layer was anchored to the surrounding structure using the clamping device developed to measure the longitudinal properties of the prepreg tape, were superior to straps with a fusion bonded anchorage, where the final layer is anchored to the strap itself. Hence, indicating that failure was dependent on the anchorage method. It was expected, however, that failure of a strap was governed by the stress in the pin region. This expectation was underlined by observations during testing where the progressive type of failure initiated in the pin region. The reason for the contradictory results is unclear.
- non-laminated straps attained a higher load carrying capacity compared to equivalent laminated straps. A maximum increase of 29% was found with straps with a clamped end anchorage consisting of 15 layers.
- the occurred creep failure questions the reliability of the fusion bonded anchorage system, although the circumstances were such that the result is not conclusive and further investigations are required.

7.1.3 Analytical modelling

Analytical modelling was carried out to gain an insight of the stress distributions in the pin region. The main findings of this research are summarised as follows:

- if contact and friction is to be considered in a finite element model using MARC K6.3, the analyst is required to provide the relative sliding velocity, a numerical parameter which defines the stick-slip transition. No accurate value for this parameter is known.
- the influence of the relative sliding velocity was established by a sensitivity study where the friction coefficient and the sliding velocity was varied. The stress distribution was found to be highly dependent on the sliding velocity.
- the failure location in the experiments is consistent with the stress concentrations determined by the finite element model. Furthermore, a material and geometric discontinuity is present in the same location. Hence, failure prediction was not performed.
- the classical modelling carried out confirms the general trends of the stress distributions acquired by finite element modelling and strain measurements.
- classical failure criteria developed for laminated straps are non-conservative. The same classical modelling used in combination with an interactive failure criteria underestimates the strength of laminated straps considerably.

7.2 Recommendations for further work

From the experimental investigations and the stress analysis, the following aspects are required to be investigated to make the concept of non-laminated pin-loaded straps exploitable:

- the limitations of the principle such as the maximum and the optimum number of layers in a non-laminated strap have to be investigated experimentally. The option of using variable coefficients of friction within one strap by placing polymeric films between layers of tape should be considered in this investigation.
- the reason for the higher load carrying capacity of non-laminated straps with a clamped end anchorage compared to the fusion bonded one, needs to be investigated further. The experimental observations suggest that failure was initiated in the pin region.
- for safety reasons and the efficient use of the material the long term performance of non-laminated straps has to be investigated by creep and relaxation tests. Such tests have to be performed in a realistic environment, depending on the application. The degradation of the frictional properties due to the presence of lubricating substances should be included in the experimental program.
- the load transfer in pin-loaded straps can be optimised by using a non-circular pin. This optimisation requires a reliable classical or finite element model, which includes the influence of friction, to determine the stress distributions in the pin region.
- a classical or finite element model to predict failure of laminated and non-laminated pin-loaded straps will be needed.

REFERENCES

Anon (1998a). Thermosets continue to dominate thermoplastics, *Advanced Composites*, November 1998, pp. 11.

Anon (1998b). Advancing Composites, *High Performance Composites*, Vol. 6. No. 6, November-December 1998, pp. 10.

Arias, M. (1998). *Experimentelle Untersuchung des Kontinuierlichen und gepulsten Widerstandsschweissen als Fügeverfahren zur Herstellung von Faserverbundbauteilen mit thermoplastischer Matrix*, PhD thesis, Mechanical Engineering Department, Swiss Federal Institut of Technology ETHZ, Zuerich, Switzerland, 1998.

Augustin, G. (1989). *Herstellung und Charakterisierung von hochgefüllten, unidirektional faserverstärkten thermoplastischen Polymeren*, PhD thesis, Department of Material Science, Technical University of Berlin, Germany.

Bauersfeld, D. W. (1984). *Composite graphite/epoxy tensile element*, Report 2404, United States Army, Belvoir Research & Development Center, Fort Belvoir, Virginia 22060, USA, May 1984, pp. 1-62.

Bieling, U. (1983). *Ermittlung mechanischer und thermischer Eigenschaften kohlenstoffaserverstärkter Kunststoffe*, PhD thesis, Department of Mechanical Engineering, University of Aachen RWTH, 1983.

Bresson, J. (1971). Nouvelles recherches et application concernant l'utilisation des collages dans les structures. *Béton plaqué*, Annales I. T. B. T. P. No. 278, Série Béton, Béton armé No. 116, 1971.

Bunsell, A.R. and Somer, A. (1992). The tensile and fatigue behaviour of carbon fibres *Plastics, Rubber and Composites Processing* and Applications Vol. 18 No.4, 1992, pp. 263-267

Callister, W. D. (1996). *Materials Science and Engineering* An Introduction, 4th Edition, John Wiley & Sons, 1996

Chabrier, G., Moine, G., Maurion, R. and Szabo, R. (1986). Process for Manufacturing Profiled Strips in Fibre-Loaded Thermoplastic Resin, Installation for the Implementation thereof and Profiled Strips Obtained, *United States Patent 4,626,306*, December 2 1986.

Chajes, M. J., Januszka, T. F., Mertz, D. R., Thomson, T. A- and Finch, W. W. (1995). RC Beams with Externally Applied Composite Fabrics, *American Concrete Institute Structural Journal*, Vol. 92 No. 3, May-June 1995, pp. 295-303.

Clarke, J. (1993). The need for durable reinforcement. in J. L. Clarke (Ed), *Alternative Materials for the Reinforcement and Prestressing of Concrete*, Blackie Academic and Professional, 1993, pp.1-33.

Collins, M. P., Mitchell, D., Adebar, P. and Vecchio, F. J. (1996). A General Shear Design Method, *American Concrete Institute Structural Journal*, Vol. 93, No. 1, Jan.-Feb. 1996, pp. 36-45.

Conen, H. (1966). Deformation und Versagen von GFK-Strangschlaufen, *Kunststoffe* Vol. 56 No. 9, 1966, pp. 629-681.

Cook, R. D., Malkus, D. S. and Plesha, M. E. (1989). *Concepts and Applications of Finite Element Analysis*, 3rd Edition, Wiley, New York.

Deuring, M. (1993). Verstärken von Stahlbeton mit gespannten Faserverbund-werkstoffen, *EMPA Research-Report No. 224*, Dübendorf, Switzerland, 1993.

Donnet, J. B. and Bansal, R. C. (1990). Carbon Fibers, in M. Lewin (Ed) *International Fiber Science and Technology Series*, Second Edition, New York, USA, 1990.

Drimoussis, E. and Cheng, R. (1994). Shear Strengthening of Concrete Girders using Carbon Fiber Reinforced Plastic Sheets. *Structural Engineering Report* No. 205, University of Alberta, Canada, October 1994.

Dubbel (1995), *Taschenbuch für den Maschinenbau*, 18th Edition Springer Verlag, ISBN 3-540-57650-9

Dunker, K. F. and Rabbat, B. G. (1993). Why America's Bridges Are Crumbling, *Scientific American*, March 1993, pp. 18.

Fiberite (1989). *Beispiel eines modernen Faserverbundwerkstoffes: APC-2*, Aromatic Polymer Composite, ICI Fiberite Europe GmbH, November 1989.

Frank, A. and Biederbick, K. (1984). *Kunststoff-Kompendium*: Kunststoffaufbau, Polymerisation, Kunststoffverarbeitung, -eigenschaften, -anwendung, Würzburg, Germany, 1984.

Gerritse, A., (1990). ARAPREE, an non-metallic tendon, Technical Contribution to the Conference on Durable Reinforcement for Aggressive Environment, Luton, British Cement Association, November 1990, pp. 3-28.

Gol'denblatt, I. I. and Kopnov, V. A. (1965). Strength of Glass-Reinforced Plastics in the Complex Stress State, *Polymer Mechanics*, Vol. 1 No. 2, 1965, pp. 70-78.

Graff, E. and Springer G. S. (1991). Design of Composite Straps, *Composite Structures*, Vol. 17, 1991, pp. 187-211.

Graff, E. and Springer G. S. (1991). Stress Analysis of Thick, Curved Composite Laminates, *Computers & Structures*, Vol. 38, 1991, pp. 41-55.

Grafil (1996). *Grafil Standard Modulus Carbon Fibers*, Grafil Inc., Coventry, England, 1996.

Guckenberger, H., Kupfer, H. and Daschner, F. (1985). Versuche zur Ermüdungsbeanspruchung der Schubbewehrung von Stahlbetonträgern, *Deutscher Ausschuss für Stahlbeton*, Heft 359, 1985, pp.1-92.

Guigon, M., Oberlin, A. and Desarmot, G. (1984). Microtexture and Structure of Some High Tensile Strength, PAN-Base Carbon Fibres, *Fibre Science and Technology* Vol. 20, 1984, pp. 55-72.

Hamilton, H. R., Breen, J. E. and Al-Rashid, N. I. (1995). *Stay Cable Survey*, Phil M. Ferguson Structural Engineering Laboratory, Department of Civil Engineering, Bureau of Engineering Research, The University of Texas at Austin, USA, February 15, 1995.

Hartness, J. T. (1988). Thermoplastic powder technology for advanced composite systems, *Journal of Thermoplastic Composite Materials*, Vol. 1, 1988, pp. 210-220.

Herbsleb, G. and Theiler, F. (1989). Stress corrosion cracking of austenitic chromium-nickel stainless steels at ambient temperature. *Werkstoffe und Korrosion* 40, 1989, pp. 467-480.

Hercules (1989). *Product Data Hercules Carbon Fiber Type AS4*, Hercules Inc., Magna UT, USA, 1989.

Hoechst (1996). *Fortron Polymere Werkstoffe*, Hoechst High Chem, Hoechst AG, Frankfurt, Germany, 1996.

Huels (1996). *Properties of unreinforced VESTOSINT*, Chemische Werke Hüls AG, Marl, Germany.

Hull, D. (1981). *An introduction to composite materials*, Cambridge solid state science series, Cambridge University Press, 1981.

Hutchinson, R., Abdelrahman, A. and Rizkalla, S. (1997). Shear Strengthening Using CFRP Sheets for a Prestressed Concrete Highway Bridge in Manitoba, Canada, in U. Meier and R. Betti (Eds), *Recent Advances in Bridge Engineering, US-Canada-Europe Workshop on Bridge Engineering*, Zürich, Switzerland, July 11-15 1997, pp. 99-106.

Hütter, U. (1966). Probleme der Krafteinleitung in Glasfaser-Kunststoff-Bauteile, *Kunststoffe* Vol. 56 No. 9, 1966, pp. 843-846.

Kempe, G. (1997). Duroplastische und Thermoplastische Faserverbundwerkstoffe-Vorteile-Eigenschaften-Verarbeitung und Anwendungsgebiet beider Werkstoffgruppen, in H. Zepf (Ed), *Faserverbundwerkstoffe mit thermoplastischer Matrix*, Kontakt und Studium, Band 529, 1997, pp. 44-74.

Knaust, U. (1988). Zur Analyse und Optimierung von Faserverbund-Leichtbauteilen, *Fortschritt-Berichte VDI*, Reihe 20 No.11, October 1988, Düsseldorf, Germany, pp. 1-136

Kohan, M. I. (Ed) (1995). *Nylon Plastics Handbook*, Carl Hanser Munich, 1995.

Krüger, R. and Beckmann, H. (1985). Gasoline Engine Components Made of CFRP, in G. Bartelds and R. J. Schliekelmann (Eds), Progress in Advanced Materials and Processes, Proceedings 6th International European Chapter Conference of SAMPE, Scheveningen, The Netherlands, May 28-30, 1985, pp. 223-236.

Mansfield, E. H. (1983). Load Transfer from a Pin to a Wound Fibre Composite Strip, *Journal of Composite Materials*, Vol. 17, September, 1983.

MARC (1996). *Seminar on the Simulation of Contact Problems*, Milton Keynes, England, February 21, 1996.

MARC (1997). *Volume A: Theory and User Information*, MARC Analysis Research Corporation, Palo Alto, USA, August 1997.

Mc Crum, N. G., Buckley, C. P. and Bucknall C. B. (1988). *Principles of Polymer Engineering*, Oxford Science Publications, 1988.

Meier, U., Meier, H. and Kim, P. (1998). *Anchorage device for high performance composite cables*, United States Patent 5,713,169, February 3 1998

Meier, U, and Betti, R. (Eds) (1997). *Recent Advances in Bridge Engineering*, Proceedings from US-Canada-Europe Workshop on Bridge Engineering, Zürich, Switzerland, July 11-15 1997.

Meier, U. (1987). Brückensanierungen mit Hochleistungs-Faserverbund-Werkstoffen, *Material und Technik*, No. 4, 1987, pp. 125-128.

Meier, U. (1996). *Grundlagen zum Bemessen von Kunststoffbauteilen*, Skript ETH-Vorlesung 39-605, Swiss Federal Institute of Technology ETHZ, Zürich Switzerland, 1997.

Meier, U. (1997). Repair Using Advanced Composites, in *Composite Construction - Conventional and Innovative*, Proceedings International IABSE Conference, Innsbruck, Austria, September 16-18 1997. pp. 113-124.

Meier, U. and Winistoerfer, A. (1995). Retrofitting of structures through external bonding of CFRP sheets. in L. Taerwe (Ed), *Non-Metallic (FRP) Reinforcement for Concrete Structures*, 2nd International RILEM symposium (FRPRCS-2), Ghent, Belgium, August 23-25 1995, pp 465 - 472.

Meier, U. and Winistoerfer, A. (1998). *Multilayer Traction Element in the Form of a Loop*, European Patent 0 815 329, January 7 1998.

Michaeli, W. and Wegener, M. (1989). *Einführung in die Technologie der Faserverbundwerkstoffe*, Carl Hanser Munich, 1989.

Mottram, J. T. (1998). Bonded Connections, in J. T. Mottram and G. J. Turvey (Eds), *State-of-the-art review on design, testing, analysis and applications of polymeric composite connections*, COST C1 EUR 18172 EN, pp. 56-70.

Mottram, J. T. and Shaw, C. T. (1996). *Using Finite Elements in Mechanical Design*, McGraw-Hill Europe, 1996.

Neitzel, M. and Breuer, U. (1997). *Die Verarbeitungstechnik der Faser-Kunststoff-Verbunde*, Munich, Germany, 1997.

Niemann, R. C., Gonczy, J. D., Mataya, K. F. and Smelser, P. (1978). An Epoxy Fibreglass Tension Member Support for Superconducting Magnets, *Advances in Cryogenic Engineering*, Vol. 24, 1978, pp. 283-289.

O'Connor, J. (1987). Reinforced Plastic, *United States Patent 4,680,224*, July 14 1987.

O'Connor, J. E., Geibel, J. F. and Beever, W. H. (1988). *Reinforced Plastic*, United States Patent 4,792,481, December 20 1988.

Puck, A. and Schürmann, H. (1982). Die Zug/Druck-Torsionsprüfung an rohrförmigen Probekörpern, *Kunststoffe*, Vol. 72, 1982, pp. 554-561.

Rasche, M. (1987). Niederdruckplasma, Vorbehandlung zur Verbesserung der Adhäsionseigenschaften, in E. Schindel (Ed.), *Kleben: Grundlagen, Technologie, Anwendung*, 1. Fachseminar am Technikum Rapperswil, May 12-14, 1987, pp. 261-283.

Ruhnau, J. and Kupfer, H. (1985). Vorgespannte Schubbewehrung, *Deutscher Ausschuss für Stahlbeton*, Heft 359, 1985, pp.93-142.

Schindel, E. (1988). Strukturelles Kleben und Dichten, Band 1: Grundlagen des strukturellen Klebens und Dichtens, Klebstoffarten, Kleb und Dichttechnik, Hinterwaldner Verlag, Munich, Germany, 1988.

Singkofer, R. and Mehn, R. (1996). Advanced Thermoplastic Composites based on Knitted Fabrics with Weft Insertion-Economical Application in Highly Loaded Vehicle Components, in U.Meier (Ed), *Success of Materials by Combination*, Proceedings 17th International SAMPE Europe Conference, Basel, Switzerland, May 38-30, 1996, pp.273-286.

Taylor, G. J. (1981). *Method of Impregnating a Fibrous Textile Material with a Plastic Resin*, United States Patent 4,292,105, September 29 1981.

Timoshenko, S. P. and Goodier, N. J. (1988). *Theory of Elasticity*, 2nd Edition, McGraw-Hill, New York.

Toray (1997). *Torayca Technical Reference Manual*, Toray Industries Inc., Tokyo, Japan, 1997.

Tsai, S. W. (1988). *Composites Design*, 4th Edition, Think Composites: Dayton, Paris, and Tokyo.

Victrex (1998). *Typische Eigenschaften von Victrex PEEK*, Victrex Europa GmbH, Hofheim, Germany, 1998.

Vodermayer, A. M. (1992). *Herstellung von unidirektional kohlefaserverstärkten Thermoplasten durch Polymerpulverimprägnierung mittels einer wässrigen Dispersion*, PhD thesis, Department of Material Science, Technical University of Berlin, Germany.

Vodermayer, A. M., Kaerger, J. C. and Hinrichsen, G. (1993). Manufacture of high performance fibre reinforced thermoplastics by aqueous powder impregnation, *Composites Manufacturing*, Vol. 4 No. 3, 1993, pp.123-132.

Weintz, K. F., Basci, M. I. and Uber, J. M. (1994). SHOOT Dewar support strap design and performance, *Cryogenics*, Vol. 34 No. 5, 1994, pp. 357-360.

Werne, D. (1994). *Experimental and Analytical Investigation of Strength of Composite Straps*, Report No. 94-18, Department of Lightweight Structures, University of Stockholm, Kungl. Tekniska Högskolan, 10044 Stockholm, Sweden, 1994.

Werner,E. (1997). Powder-Based Prepreg Fabric: What, How, Why, *Evolving Technologies for the Competitive Edge*, Proceedings 42nd International SAMPE Symposium, Anaheim, USA, May 4-8, 1997, pp.706-719.

Winistoerfer, A. (1998). Anchorage Systems, in J. T. Mottram and G. J. Turvey (Eds), *State-of-the-art review on design, testing, analysis and applications of polymeric composite connections*, COST C1 EUR 18172 EN, pp. 50-55.

Winistörfer, A. and Mottram, T. (1997). The Future of Pin-Loaded Straps in Civil Engineering Applications, in U. Meier and R. Betti (Eds.), *Recent Advances in Bridge Engineering, US-Canada-Europe Workshop on Bridge Engineering*, Zürich, Switzerland, July 11-15 1997, pp. 115-120.

Wise, R. (1992). Approaching total joining technology for carbon fibre reinforced thermoplastics, Reprint 418/1/92 *TWI Bulletin 1*, January/February 1992.

Young, R. J. and Lovell, P. A. (1991). *Introduction to Polymers*, 2nd Edition, Chapman and Hall, 1991.

Zepf, H. (Ed) (1997). *Faserverbundwerkstoffe mit thermoplastischer Matrix*, Kontakt und Studium, Band 529, 1997.

Zhong, Z. H. (1993). *Finite Element Procedures for Contact-Impact Problems*, Oxford University Press, New York, 1993.

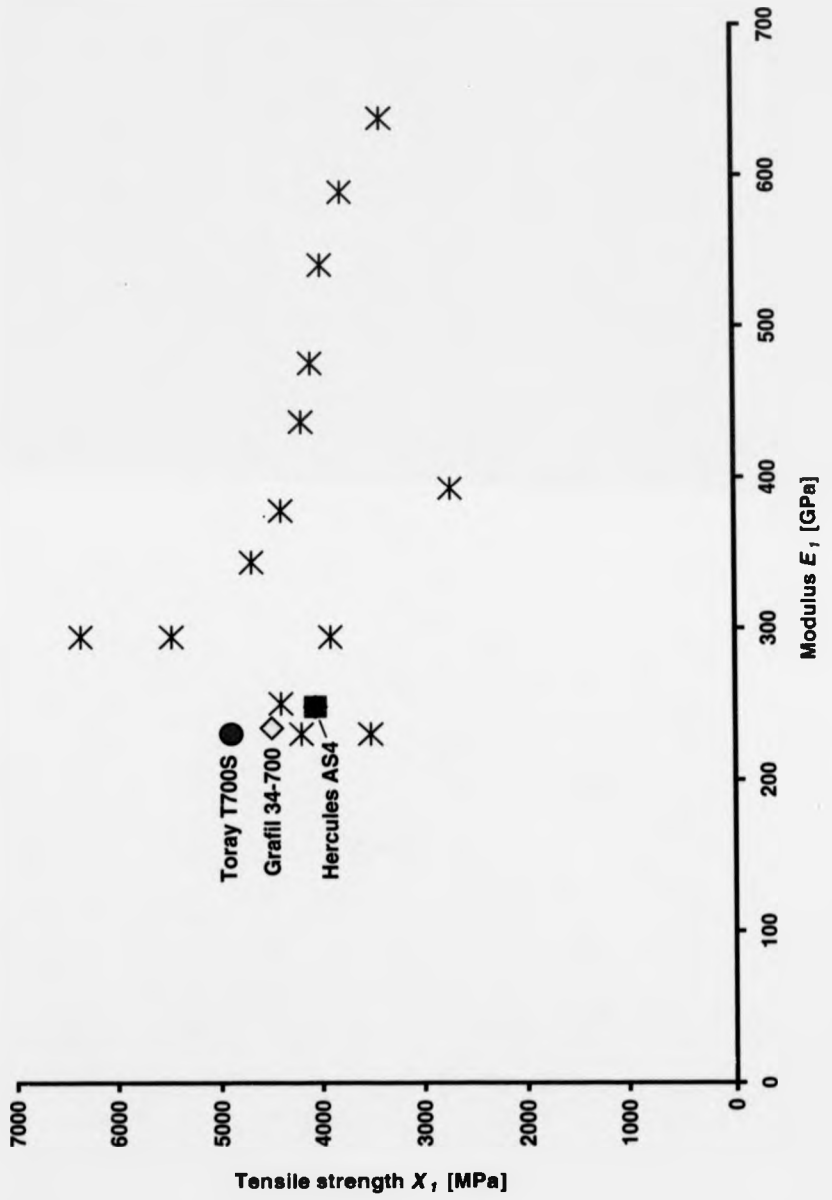

Tensile strength, X_1, versus modulus, E_1, of the different carbon fibres used in this research project in comparison with the Torayca product line.

Table B1: Load carrying capacities of different tape materials

Specimen	Tape I	Tape II	Tape III	Tape IV-1	Tape IV-2	Tape IV-3
	ICI	Baycomp	TU-Berlin	Sulzer	Sulzer	Sulzer
1	1941	1815	2077	1820	1725	1869
2	1695	1695	2021	1856	1830	1979
3	1740	1740	2136	1877	1722	1915
4	1903	1903	2053	1718	1605	1874
5	1998	1733	1975	1825	1669	1976
6	1797	1797	2079	1900	1980	1585
7	1816			1887	1894	1862
8				1792	1789	1900
9				1783	1856	1740
10				1848	1802	1861
Mean	1841	1780	2057	1831	1787	1856
s	110	75	55	55	111	117
C.O.V.	5.98	4.19	2.67	3.02	6.21	6.29

Table B2: Mechanical properties of the Tape IV-3 material.

Tape IV-3	Capacity	Strain	thickness	width	Stress	Stiffness
	[N]	[%]	[mm]	[mm]	[MPa]	[GPa]
1	1868.80	1.89	0.14	5.90	2262.47	119.71
2	1978.90	1.94	0.14	5.90	2395.76	123.49
3	1914.90	1.86	0.14	5.90	2318.28	124.64
4	1873.90	1.90	0.14	5.90	2268.64	119.40
5	1976.30	1.92	0.14	5.90	2392.62	124.62
6	1584.60	1.71	0.14	5.90	1918.40	112.19
7	1862.40	1.86	0.14	5.90	2254.72	121.22
8	1899.50	1.93	0.14	5.90	2299.64	119.15
9	1739.50	1.74	0.14	5.90	2105.93	121.03
10	1861.10	1.86	0.14	5.90	2253.15	121.14
Mean	1855.99	1.86			2246.96	120.66
s	116.77	0.08			141.37	3.60
C.O.V.	6.29	4.17			6.29	2.98

Table B3: Frictional properties of Tape II material

	steel / CFRP	CFRP / CFRP	Teflon / CFRP	Wrightlon / CFRP			
weight	μ	μ	μ	weight	μ	weight	μ
[kg]	[-]	[-]	[-]	[kg]	[-]	[kg]	[-]
5.78	0.18	0.26	0.11	5.78	0.48	20.78	0.45
5.78	0.18	0.26	0.1	5.78	0.50	20.78	0.45
5.78	0.19	0.26	0.10	5.78	0.48	25.78	0.43
10.78	0.19	0.25	0.11	5.78	0.51	25.78	0.44
10.78	0.18	0.25	0.10	5.78	0.50	25.78	0.43
10.78	0.17	0.25	0.10	10.78	0.50	25.78	0.46
15.78	0.18	0.25	0.10	10.78	0.46	25.78	0.46
15.78	0.17	0.25	0.09	10.78	0.49	30.78	0.44
15.78	0.17	0.25	0.10	10.78	0.50	30.78	0.51
20.78	0.17	0.24	0.11	10.78	0.50	30.78	0.44
20.78	0.18	0.25	0.11	15.78	0.46	30.78	0.50
20.78	0.18	0.24	0.10	15.78	0.47	30.78	0.51
25.78	0.18	0.25	0.11	15.78	0.48	30.78	0.53
25.78	0.17	0.25	0.09	15.78	0.49	30.78	0.52
25.78	0.17	0.24	0.09	15.78	0.50	30.78	0.53
30.78	0.16	0.25	0.11	20.78	0.43	30.78	0.54
30.78	0.17	0.24	0.10	20.78	0.43		
30.78	0.17	0.24	0.09	20.78	0.47		

Table B4: Lap shear capacities of Tape IV-1 at different welding temperatures.

Specimen	175°C	180°C	185°C	190°C	195°C
1	1661	1569	1696	1606	1583
2	1457	1595	1489	1588	1587
3	1557	1554	1618	1516	1528
4	1610	1607	1581	1606	1474
5	1595	1482	1655	1526	1622
6	1501	1557	1471	1554	1626
Mean	1563	1561	1585	1566	1570
s	75	44	90	40	59
C.O.V.	4.78	2.82	5.68	2.54	3.76

Table B5. Lap shear capacities of Tape IV-3 material with different joint configurations.

Specimen	as received	PA-12 film
1	1185	1779
2	1069	1766
3	1158	1829
4	1174	1997
5	1230	1761
6	1370	1915
Mean	1198	1841
s	99	96
C.O.V.	8.31	5.19

Table B6.1: Load carrying capacities of laminated pin-loaded straps of Tape IV-1 material.

F_U [N]	D = 30 mm	D = 50 mm	D = 150 mm
5 layers	10541	13338	15526
	13030	14579	14694
	15411	14694	13875
	14669	14746	14118
	14234	14490	
		14272	
Mean	13577	14353	14554
s	1904	525	734
C.O.V.	14.03	3.66	5.04

Table B6.2: Load carrying capacities of laminated pin-loaded straps of Tape IV-1 material.

	D = 30 mm	D = 50 mm	D = 150 mm
F_U [N]	24320	31130	30874
10 layers	24333	27750	32461
	25446	28160	30976
	28211	26829	32410
	28416	29542	30464
Mean	26145	28682	31437
s	2033	1681	932
C.O.V.	7.78	5.86	2.96

Table B6.3: Load carrying capacities of laminated pin-loaded straps of Tape IV-1 material.

	D = 30 mm	D = 50 mm	D = 150 mm
F_U [N]	33280	42522	46080
15 layers	32384	36685	46541
	31462	40909	47258
	32461	36250	44595
	30054	38400	46899
Mean	31928	38953	46275
s	1230	2707	1035
C.O.V.	3.85	6.95	2.24

Table B7.1: Load carrying capacities of one leg of a single layer of tape wrapped around steel pins of different diameter.

F_U [kN]	D = 25 mm	D = 30 mm	D = 35 mm	D = 40 mm	D = 50 mm	D = 150 mm
Tape II	1.16	1.27	1.11	1.42	1.40	1.78
as received	1.11	1.35	1.15	1.41	1.24	1.75
	1.19	1.27	1.22	1.61	1.51	1.74
	1.27	1.22	1.19	1.47	1.53	1.79
	1.24	1.31	1.25	1.58	1.41	1.63
	1.22	1.16	1.21	1.71	1.57	1.65
	1.34	1.16	1.20	1.57	1.45	1.61
	1.22	1.37	1.24	1.34	1.59	1.85
	1.31	1.34	1.26	1.53	1.37	1.69
	1.30	1.26	1.35	1.55	1.42	1.55
Mean	1.23	1.27	1.22	1.52	1.45	1.70
s	0.07	0.07	0.07	0.11	0.10	0.09
C.O.V.	5.76	5.72	5.35	7.24	7.24	5.56

Table B7.2: Load carrying capacities of one leg of a single layer of tape wrapped around steel pins of different diameter (Teflon film was placed between the pin and the tape).

F_U [kN]	D = 25 mm	D = 30 mm	D = 35 mm	D = 40 mm	D = 50 mm	D = 150 mm
Tape II	1.26	1.36	1.46	1.61	1.73	1.64
Teflon	1.46	1.41	1.36	1.51	1.61	1.66
film	1.41	1.49	1.62	1.64	1.58	1.72
	1.40	1.31	1.36	1.53	1.59	1.66
	1.48	1.48	1.35	1.71	1.67	1.55
	1.32	1.48	1.37	1.61	1.55	1.64
	1.41	1.48	1.64	1.55	1.50	1.59
	1.43	1.52	1.57	1.64	1.58	1.42
	1.43	1.36	1.37	1.69	1.60	1.63
	1.43	1.45	1.55	1.48	1.49	1.71
Mean	1.40	1.43	1.46	1.60	1.59	1.62
s	0.06	0.07	0.12	0.08	0.07	0.09
C.O.V.	4.60	5.02	8.01	4.92	4.44	5.42

Table B7.3: Load carrying capacities of one leg of a single layer of tape wrapped around steel pins of different diameter.

F_U [kN]	D = 30 mm	D = 50 mm	D = 150 mm
Tape IV-2	1.44	1.55	1.44
as received	1.47	1.68	1.47
	1.39	1.57	1.39
	1.43	1.56	1.43
	1.45	1.47	1.45
	1.48	1.59	1.48
	1.48	1.41	1.48
	1.49	1.60	1.49
	1.38	1.49	1.38
	1.66	1.24	1.63
	1.40		1.40
			1.40
Mean	1.46	1.52	1.46
s	0.08	0.12	0.07
C.O.V.	5.20	8.16	4.77

Table B8: Tensile capacity of Tape IV-3 non-laminated pin-loaded straps with a fusion bonded end anchorage.

welded	3 layers	5 layers	7 layers	10 layers	15 layers	20 layers
F_U [N]	6989	12493				
	7181	11072				
	6067	12544				
	6547	13030	20122	29491	36147	48845
	7078	13082	16602	29286	39322	53146
	7374	13414	18662	30029	36557	50432
Mean	6873	12606	18462	29602	37342	50807
s	481	828	1769	383	1727	2175
C.O.V.	7.00	6.57	9.58	1.30	4.62	4.28

Table B9: Tensile capacity of Tape IV-3 non-laminated pin-loaded straps with a clamped end anchorage.

clamped	3 layers	5 layers	7 layers	10 layers	15 layers	20 layers
F_U [N]	7887	13363	21414	28493	41574	57344
	7846	12493	19430	29696	41318	51482
	8102	11807	22477	30925	41728	55091
Mean	7945	12554	21107	29705	41540	54639
s	138	780	1546	1216	207	2957
C.O.V.	1.73	6.21	7.33	4.09	0.50	5.41